

AD-A126 938

A COMPARISON OF THE TUBE-SIDE PERFORMANCE OF ENHANCED  
HEAT TRANSFER TUBING FOR NAVAL CONDENSERS(U) NAVAL  
POSTGRADUATE SCHOOL MONTEREY CA R K ALEXANDER DEC 82

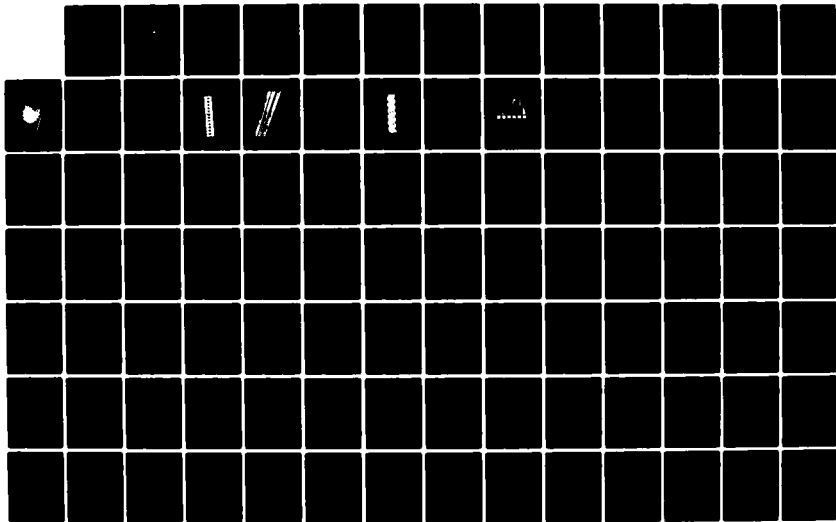
1/2

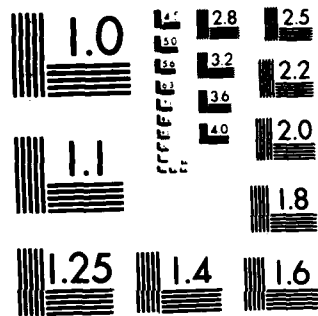
UNCLASSIFIED

NPS69-82-008

F/G 20/13

NL





MICROCOPY RESOLUTION TEST CHART  
NATIONAL BUREAU OF STANDARDS-1963-A

ADA 126938

NPS69-82-008

2

# NAVAL POSTGRADUATE SCHOOL

Monterey, California



DTIC  
SELECTE  
APR 18 1983  
S D  
H

## THESIS

A COMPARISON OF THE TUBE-SIDE  
PERFORMANCE OF ENHANCED HEAT TRANSFER  
TUBING FOR NAVAL CONDENSERS

by

Ronald Keith Alexander

December 1982

Thesis Advisor:

P. J. Marto

Approved for public release; distribution unlimited.

Prepared for:  
David Taylor Naval Ship Research  
and Development Center  
Bethesda, Maryland

DTIC FILE COPY

88 04 18 006

Naval Postgraduate School  
Monterey, California

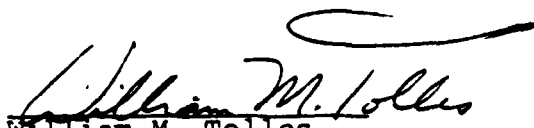
Rear Admiral John J. Ekelund  
Superintendent

David A. Schradly  
Provost

This thesis is prepared in conjunction with research supported in part by David Taylor Ship Research and Development Center under N00167-WR2-0114.

Reproduction of all or part of this report is authorized.

Released as a  
Technical Report by:

  
William M. Tolles  
Dean of Research

UNCLASSIFIED

SECURITY CLASSIFICATION OF THIS PAGE (When Data Entered)

REPORT DOCUMENTATION PAGE		READ INSTRUCTIONS BEFORE COMPLETING FORM
1. REPORT NUMBER NPS69-82-008	2. GOVT ACCESSION NO. AD A126 731	3. RECIPIENT'S CATALOG NUMBER
4. TITLE (and Subtitle) A Comparison of the Tube-Side Performance of Enhanced Heat Transfer Tubing for Naval Condensers		5. TYPE OF REPORT & PERIOD COVERED Master's Thesis
		6. PERFORMING ORG. REPORT NUMBER
7. AUTHOR(s) Ronald Keith Alexander		8. CONTRACT OR GRANT NUMBER(s)
9. PERFORMING ORGANIZATION NAME AND ADDRESS Naval Postgraduate School Monterey, California 93940		10. PROGRAM ELEMENT PROJECT TASK AREA & WORK UNIT NUMBERS N00167-WR2-0114
11. CONTROLLING OFFICE NAME AND ADDRESS David Taylor Naval Ship Research and Development Center Bethesda, Maryland		12. REPORT DATE December 1982
		13. NUMBER OF PAGES 122
14. MONITORING AGENCY NAME & ADDRESS (if different from Controlling Office)		15. SECURITY CLASS. (of this report) Unclassified
		15a. DECLASSIFICATION/DOWNGRADING SCHEDULE
16. DISTRIBUTION STATEMENT (of this Report) Approved for public release; distribution unlimited.		
17. DISTRIBUTION STATEMENT (of the abstract entered in Block 20, if different from Report)		
18. SUPPLEMENTARY NOTES		
19. KEY WORDS (Continue on reverse side if necessary and identify by block number) Heat Transfer Coefficients Friction Factors Augmentation		
20. ABSTRACT (Continue on reverse side if necessary and identify by block number) → The data of several investigators conducting research in the area of enhanced heat transfer in internally ribbed and spirally corrugated tubes is compiled and examined to determine the effects of the geometric characteristics of enhanced tubing on flow resistance and heat transfer. The data are compared to determine if there are any relations, either new or previously published, which can be of use to the designer to predict the friction →		

DD FORM 1473 JAN 73

EDITION OF 1 NOV 69 IS OBSOLETE  
S/N 0102-014-6001

UNCLASSIFIED

SECURITY CLASSIFICATION OF THIS PAGE (When Data Entered)

UNCLASSIFIED

SECURITY CLASSIFICATION OF THIS PAGE (When Data Entered)

#20 - ABSTRACT - (CONTINUED)

factor and heat transfer coefficient for a specified enhanced tube.

Empirical relations are recommended for friction factor and heat transfer coefficient for single-start and multiple-start spirally corrugated tubes based on the law of the wall similarity analysis and a heat transfer similarity analysis. The empirical relations are compared to experimental data for single-start and multiple-start corrugated tubes with pitch-to-groove ratios greater than 10 and dimensionless groove depths less than 0.05. The recommended relations correlate with the experimental data for heat transfer coefficient within  $\pm 15\%$  for 94% of the specified tubes.



Accession For	
NTIS GRA&I	<input checked="" type="checkbox"/>
DTIC TAB	<input type="checkbox"/>
Unannounced	<input type="checkbox"/>
Justification	
By _____	
Distribution/	
Availability Codes	
Avail and/or	
Dist	Special
A	

DD Form 1473  
S/N 0102-014-6601  
Jan 13

UNCLASSIFIED

SECURITY CLASSIFICATION OF THIS PAGE (When Data Entered)

Approved for public release; distribution unlimited.

A Comparison of the Tube-Side  
Performance of Enhanced Heat Transfer  
Tubing for Naval Condensers

by

Ronald Keith Alexander  
Lieutenant Commander, United States Navy  
B.S.M.E., Purdue University, 1971

Submitted in partial fulfillment of the  
requirements for the degree of

MASTER OF SCIENCE IN MECHANICAL ENGINEERING

from the

NAVAL POSTGRADUATE SCHOOL

December 1982

Author:

Ronald Keith Alexander

Approved by:

J. J. Marto

Thesis Advisor

Matthew Kelleher

Second Reader

J. J. Marto

Chairman, Department of Mechanical Engineering

William M. Jolley

Dean of Science and Engineering

## ABSTRACT

The data of several investigators conducting research in the area of enhanced heat transfer in internally ribbed and spirally corrugated tubes is compiled and examined to determine the effects of the geometric characteristics of enhanced tubing on flow resistance and heat transfer. The data are compared to determine if there are any relations, either new or previously published, which can be of use to the designer to predict the friction factor and heat transfer coefficient for a specified enhanced tube.

Empirical relations are recommended for friction factor and heat transfer coefficient for single-start and multiple-start spirally corrugated tubes based on the law of the wall similarity analysis and a heat transfer similarity analysis. The empirical relations are compared to experimental data for single-start and multiple-start corrugated tubes with pitch-to-groove ratios greater than 10 and dimensionless groove depths less than 0.05. The recommended relations correlate with the experimental data for heat transfer coefficient within  $\pm 15\%$  for 94% of the specified tubes.

TABLE OF CONTENTS

I.	INTRODUCTION -----	10
	A. BACKGROUND INFORMATION -----	10
	B. PARAMETRIC ANALYSIS -----	20
	C. GOALS OF THIS WORK -----	22
II.	FRICTION FACTOR -----	26
	A. GENERAL -----	26
	B. INTERNALLY RIBBED TUBES -----	27
	1. Empirical Relations -----	27
	2. Determination of the Effect of the Relevant Parameters -----	32
	3. Comparison of Empirical Relations to Existing Data -----	37
	4. Summary -----	39
	C. SPIRALLY CORRUGATED TUBES -----	40
	1. Empirical Relations -----	40
	2. Determination of the Effects of the Relevant Parameters -----	47
	3. Comparison of Empirical Relations to Existing Data -----	56
	4. Summary -----	65
III.	HEAT TRANSFER COEFFICIENT -----	76
	A. GENERAL -----	76
	1. Analytical Basis -----	76
	2. Background Analysis -----	76
	B. INTERNALLY RIBBED TUBES -----	77

1. Empirical Relations -----	77
2. Determination of Effect of Relevant Parameters -----	81
3. Comparison of Empirical Relations to Existing Data -----	91
4. Summary -----	98
C. SPIRALLY CORRUGATED TUBES -----	100
1. Empirical Relations -----	100
2. Determination of the Effect of Relevant Parameters -----	102
3. Comparison of Empirical Relations to Existing Data -----	108
4. Summary -----	111
IV. CONCLUSION AND RECOMMENDATIONS -----	114
A. CONCLUSION -----	114
B. RECOMMENDATIONS -----	117
LIST OF REFERENCES -----	119
INITIAL DISTRIBUTION LIST -----	122

## NOMENCLATURE

A	-	heat transfer area
$A(e^+)$	-	friction factor correlating parameter, equations (5) and (6)
$B(e^+)$	-	heat transfer correlating parameter, equation (18)
$D_i$	-	maximum inner diameter
e	-	groove depth (rib height)
$e/D_i$	-	dimensionless groove depth (rib height)
$e^+$	-	roughness Reynolds number, $e^+ = (e/D_i) Re \sqrt{f/2}$
f	-	Fanning friction factor
G	-	mass velocity
$g(e^+, Pr)$	-	heat transfer correlating parameter, equation (18)
$g^+$	-	heat transfer correlating parameter, equation (28)
$g(e^+, Pr, \alpha)$	-	heat transfer correlating parameter, equation (20)
j	-	empirical exponent, equations (20) and (22)
$k_s$	-	representative roughness element height
L	-	tube length
$l$	-	lead of groove (rib)
m	-	operand for equation (8)
N	-	Number of groove (rib) starts in enhanced tube
Nu	-	Nusselt number
Pr	-	Prandtl number
p	-	groove (rib) pitch
$p/D_i$	-	dimensionless pitch
$p/e$	-	pitch-to-groove ratio

- R - tube radius
- Re - Reynolds number
- r - operand for equation (8)
- St - Stanton number
- T - Temperature

#### GREEK SYMBOLS

- $\alpha$  - helix angle defined by equation (1)
- $\theta$  - severity factor defined by equation (10)
- $\rho$  - fluid density
- $\mu$  - fluid dynamic viscosity
- $\gamma$  - heat transfer correlating parameter, equation (27)
- $\epsilon$  - eddy diffusivity

#### SUBSCRIPTS

- b - bulk
- c - centerline
- H - heat
- i - inner
- m - momentum
- w - wall

### ACKNOWLEDGMENTS

The author wishes to express his appreciation to Dr. Paul J. Marto for his advice, guidance, and enthusiastic support towards the completion of this thesis.

The author must also express his most sincere gratitude to his wife, Joanne, for her untiring patience with the long hours and many frustrations inherent in such an endeavor.

## I. INTRODUCTION

### A. BACKGROUND INFORMATION

In recent years there has been an increasing awareness of the benefits to be derived from the augmentation of heat transfer in naval condensers. Augmented heat transfer will permit condensers to be designed smaller and with greater efficiency. The smaller size and increased efficiency will result not only in reduced capital costs, but also in decreased operating expenses.

Bergles [1] compiled a comprehensive summary of existing works covering various heat transfer augmentation techniques. These various techniques are divided into two broad classes: active techniques and passive techniques. Active techniques include surface vibration, electro-static fields, etc. Passive techniques include roughened surfaces, fins, internal swirl devices, etc.

For condenser applications, a prominent heat transfer augmentation technique is the use of tubes with either internal ribs or spiral corrugations. Carnavos [2] conducted experiments on 8 tubes having internal spiral ribs. Figure 1 is a photograph of the type of tube studied. The experiments were conducted using water, air, and a 50/50% ethylene glycol/water solution in a counter-flow heat exchanger apparatus. Gee and Webb [3] also conducted experiments on the type of tube shown in Figure 1, but with tubes of a larger diameter.

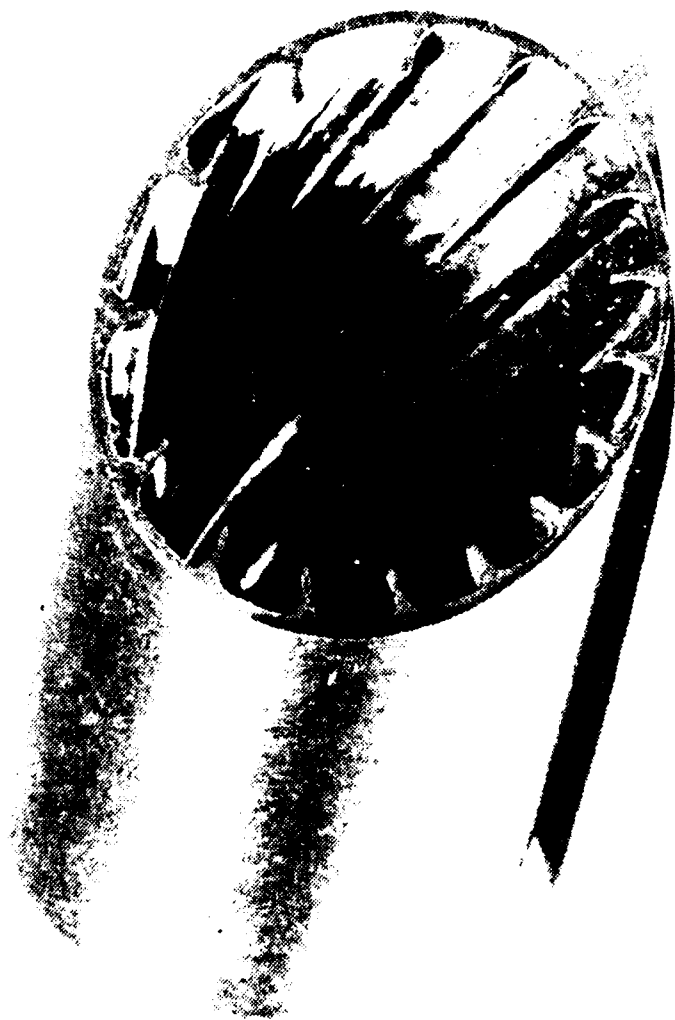
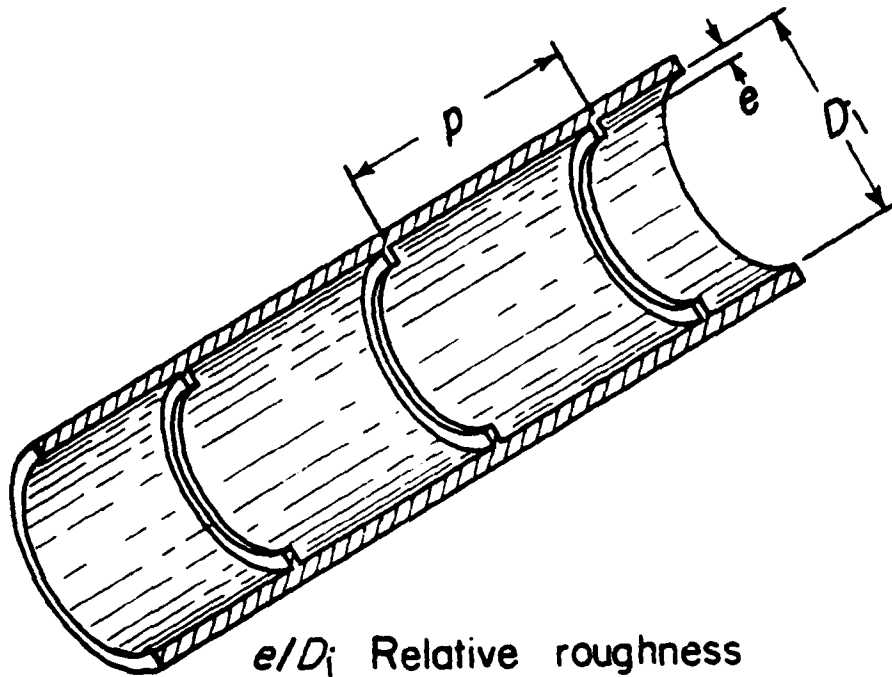


FIGURE 1 - Photograph of lens to be employed in experimentally induced  
collapse of tubes. From [3].

Their experiments were conducted with air as the working fluid. Webb, et al [4] also used air as the working fluid in their investigation of 5 tubes enhanced by the addition of internal transverse ribs of the type shown in Figure 2. Han, et al [5] also conducted experiments with repeated-rib roughness, but with the repeated ribs mounted on a flat plate.

Mehta and Rao [6] and Gupta and Rao [7] have reported on heat exchanger tubes enhanced by the mechanical rolling of a spiral groove along the length of the tube. The general configuration of this type of spirally corrugated tube is shown in Figure 3. The tests were conducted using water, 40% glycol, and dilute aqueous solutions of 0.3%, 0.5%, and 0.75% by weight of sodium carboxy methyl cellulose and 1.0% potassium alginate. Data reduction techniques accounted for the property dependence in the flow resistance and heat transfer calculations.

LaRue [8] reported on spirally fluted tubes manufactured by General Atomic Company. The General Atomic tube is made by first impressing the desired fluting onto a narrow strip of metal, and then rolling the fluted strip into a tube, while welding the seam. Figure 4 is a photograph showing three tubes made by this process. The three tubes in Figure 4 are labeled with the helix angle value for the tube. The tests of LaRue [8] were conducted with water as the working fluid, for heat transfer in both the radially inward and radially outward



$e/D_i$  Relative roughness  
 $p/e$  Relative rib spacing

FIGURE 2 Illustration of repeated-rib roughened enhanced tube, showing characteristic dimensions. From [4].



FIGURE 3 Photograph of a spirally corrugated enhanced tube.

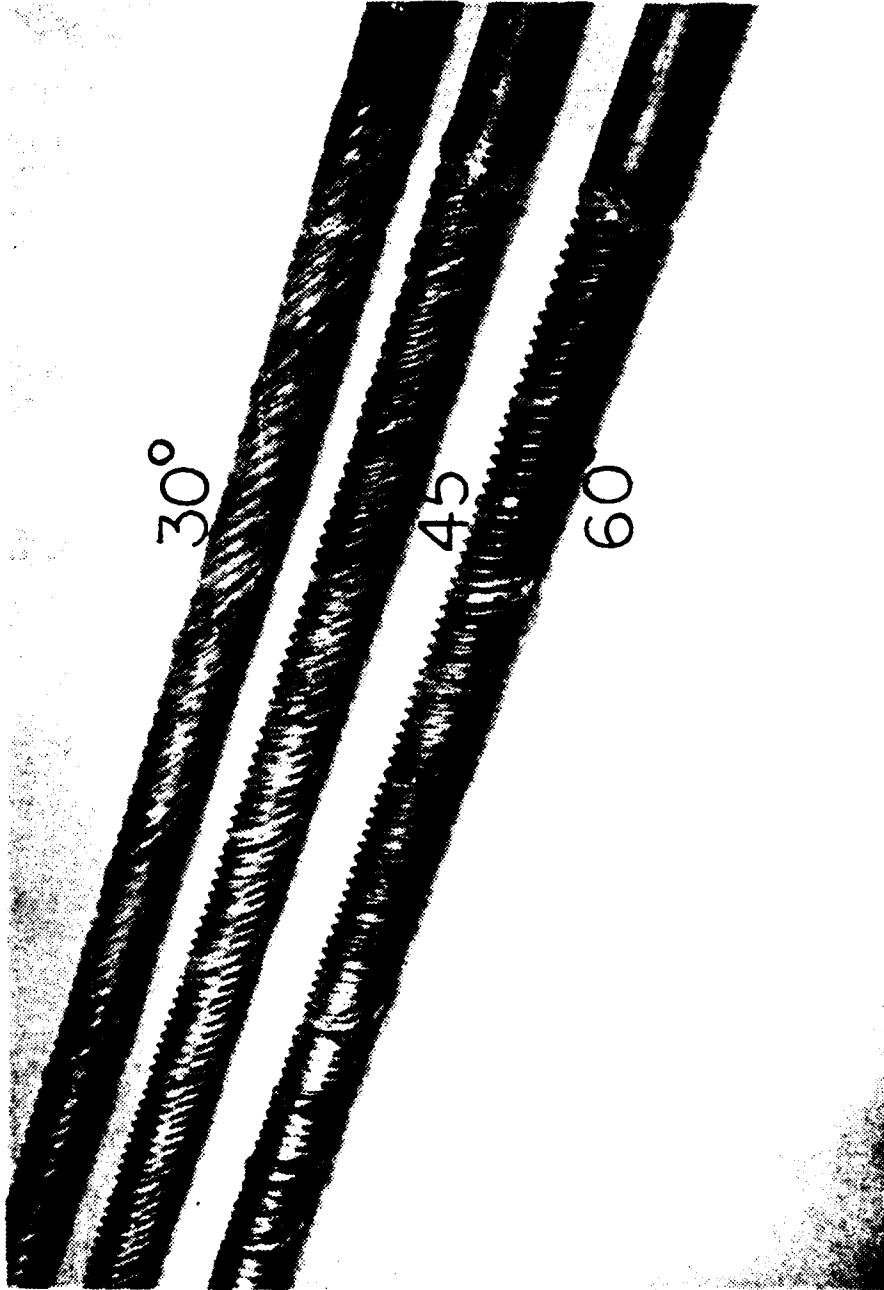


FIGURE 4 Photograph of tubes manufactured by General Atomic Company, showing three different helix angles.

directions. Bergles [9] provides a summary of studies conducted for spirally corrugated tubes manufactured by Turbo-tec Products by a process of twisting a smooth tube until the desired spiral is obtained. Figure 5 is a photograph of the Turbotec tube.

Catchpole and Drew [10] and Cunningham and Milne [11] conducted similar experiments on spirally corrugated tubes. Both teams of investigators studied tubes manufactured by Yorkshire Imperial Metals, of the United Kingdom which are similar in appearance to the tube shown in Figure 3.

Withers [12,13] reported on tubes manufactured by the Wolverine Division of United Oil Products. These tubes are listed by the trade names of Korodense (Figure 6.a) and Turbo-chil (Figure 6.b). Withers [12,13] conducted his experiments with a water-to-water heat exchanger.

Marto, et al [14] report on the results of experiments conducted on General Atomic, Turbotec, and Korodense tubes. The experiments were conducted in a condensing application with water as the working fluid.

All of the above cited works report on experiments conducted with the enhanced tubes mounted horizontally. Newson and Hodgson [15] report on a variety of tubes (Figure 7) for condenser application with the tubes mounted vertically.

Li, et al [16] conducted experiments on 20 spirally corrugated tubes of the type shown in Figure 3. Additionally, three tubes were specially manufactured of clear plastic



FIGURE 5 Photograph of a Turbotec spirally corrugated tube.

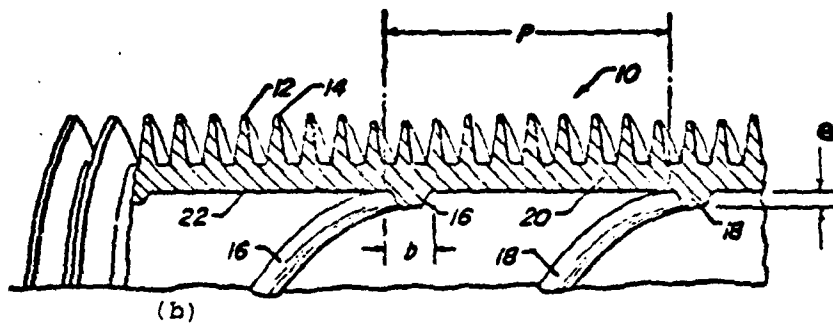
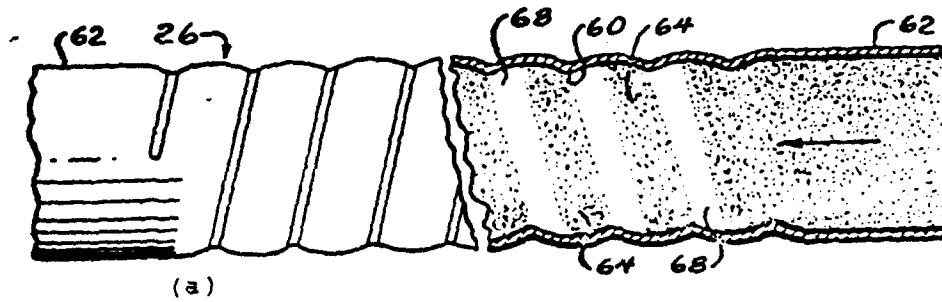


FIGURE 6 Illustrations of a.) Korodense and b.) Turbo-chil enhanced tubes manufactured by Wolverine.

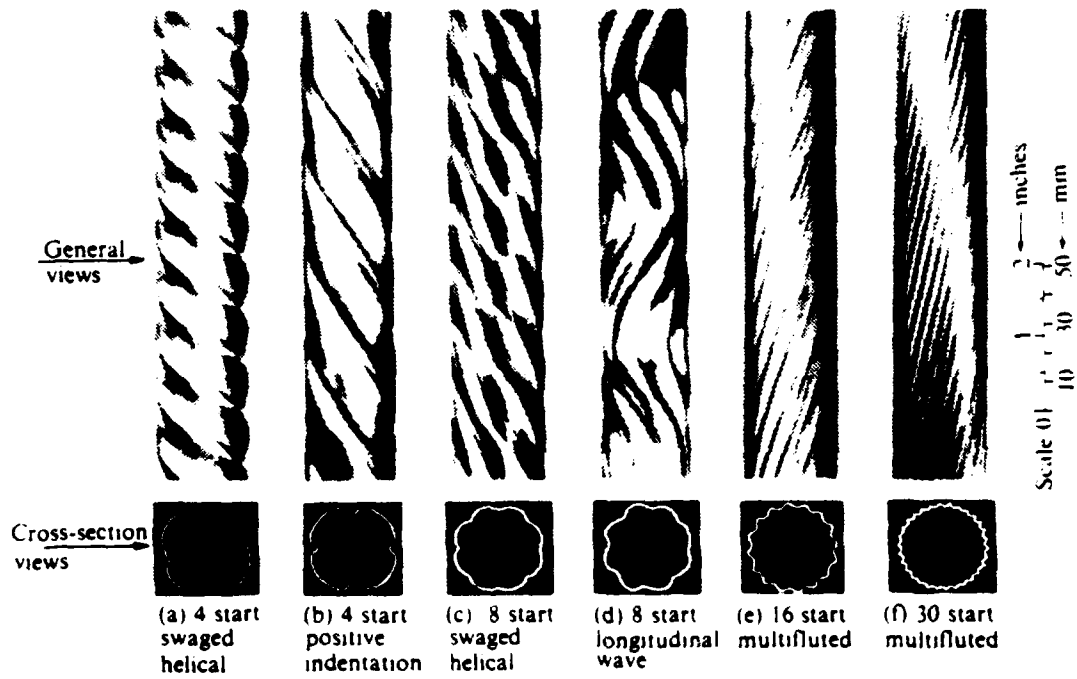


FIGURE 7 Photograph of enhanced tubes studied by Newson and Hodson [15].

to aid in the study of flow patterns in corrugated tubes. The heat transfer experiments were conducted with the tubes in a horizontal mounting, while the flow visualization studies were conducted with the tubes mounted vertically.

#### B. PARAMETRIC ANALYSIS

Figure 8 illustrates the three geometric characteristics commonly associated with enhanced heat transfer tubing. The groove pitch,  $p$ , is defined as the longitudinal distance between successive grooves (ribs) in the tube. The groove (rib) depth is defined as the radially inward depth of the groove, in the case of spirally corrugated tubes, or the height of the internal rib in the case of internally ribbed tubes. The diameter,  $D_i$ , is defined as the maximum inner diameter of the enhanced tube. (NOTE: Figure 8 is an illustration for the Korodense tube, but the general geometric characteristics are common to all tubes.)

The three geometric characteristics of the enhanced tubes have been combined by several researchers into three dimensionless parameters defined as the dimensionless groove depth (rib height),  $e/D_i$ , the pitch-to-groove ratio,  $p/e$ , and the dimensionless pitch,  $p/D_i$ . Since the dimensionless pitch,  $p/D_i$ , is a combination of the dimensionless groove depth and the pitch-to-groove ratio, it will not be considered as a parameter for the remainder of this work.

An additional geometric characteristic that has been employed by several researchers, is the helix angle,  $\alpha$ . The

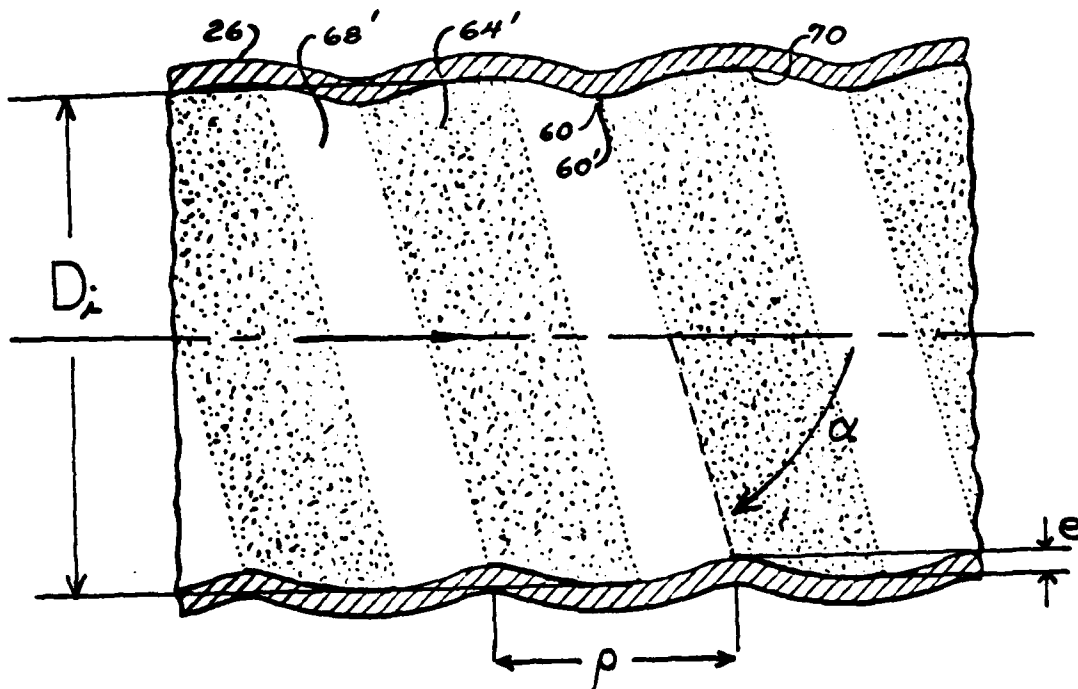


FIGURE 8 Illustration of cross-section of a Korodense spirally corrugated tube, showing geometric characteristics. From [22].

helix angle is defined as the angle formed by the line of the longitudinal axis and a line drawn tangent to the groove (rib). The helix angle is calculated by equation (1) in which  $N$  represents the number of individual groove (rib) starts in the enhanced tube.

$$\tan \alpha = \frac{\pi D_i}{N p} \quad (1)$$

As seen in equation (1), the helix angle for a tube may be varied by changing the number of groove (rib) starts while maintaining the groove pitch constant.

For the particular case of transverse ribs, the helix angle is fixed at 90 degrees. The pitch is then defined as the longitudinal distance between successive ribs as shown in Figure 2.

For purposes of consistency and correlation, a family of tubes is defined as a set of enhanced tubes in which 2 of the 3 geometric parameters ( $e/D_i, p/e, \alpha$ ) are held constant while the remaining parameter is varied. Figures 9 and 10 illustrate the range of parameters encountered in the literature cited in this work, from which families of tubes can be assembled for analysis.

### C. GOALS OF THIS WORK

As seen in Figures 1 through 10, there has been a wide variety of enhanced heat transfer tubes investigated. The various studies have been conducted not only with a variety

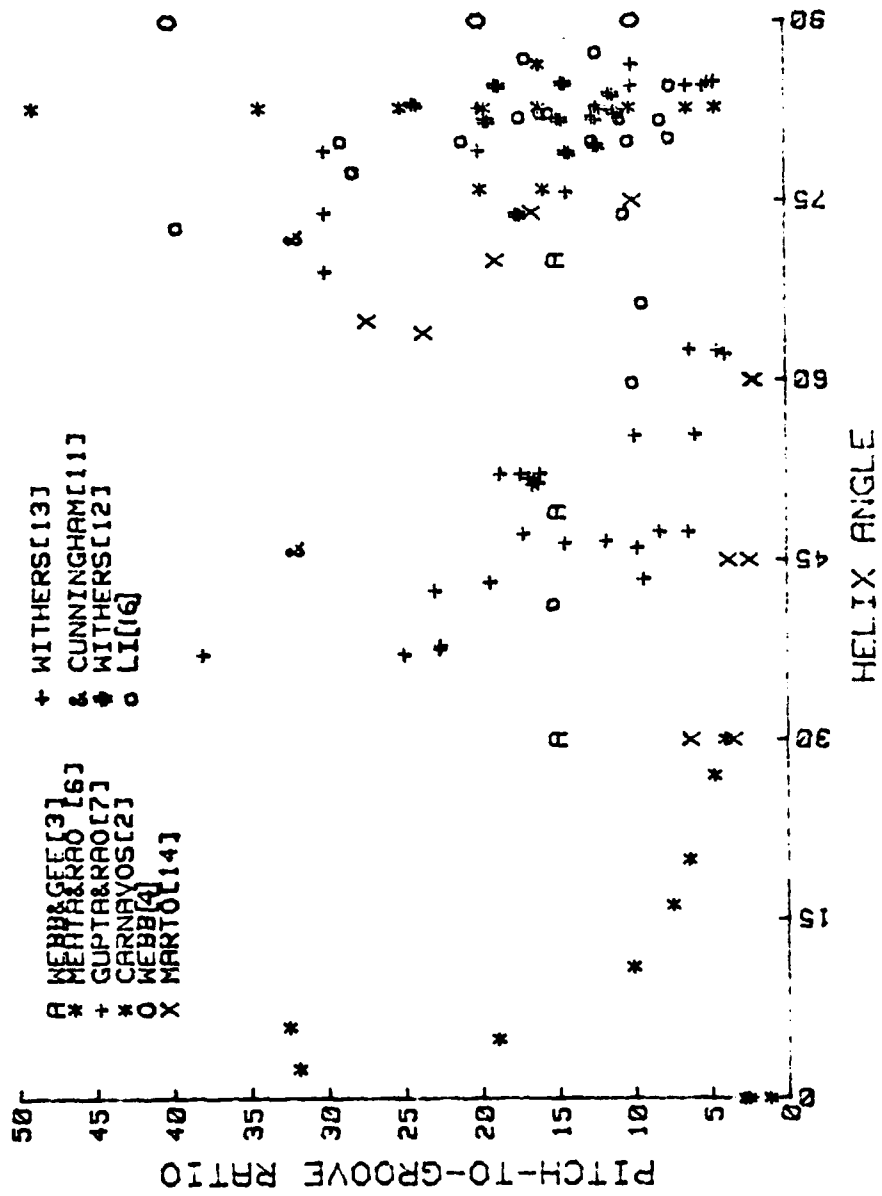


FIGURE 9 Pitch-to-groove ratio vs. helix angle for the enhanced tubes studied in this work.



of working fluids, but also with many different configurations and operating conditions. What remains to be accomplished is to analyze the existing data for flow resistance and heat transfer in order to establish a common denominator, or set of parameters, that will allow comparison of several different tube geometries by the same standards.

This analysis should provide empirical relations, either new or previously published, with which a designer may accurately predict tube-side friction factor and heat transfer coefficient for a family of tubes without the necessity of experimentation.

The purpose of this thesis then was to:

- 1) compile and present data from several authors on the tube-side flow resistance and heat transfer performance of several types of enhanced heat transfer tubing, and
- 2) determine reliable and consistent relations for the designer to accurately predict tube-side friction factor and heat transfer coefficient for specified tube geometries.

## II. FRICTION FACTOR

### A. GENERAL

Nikuradse [17] in his investigation of sand-grain roughness developed a relation based on the law of the wall similarity for friction factor as a function of the relative roughness,  $k_s/R$  where  $R$  is the tube radius and  $k_s$  is the representative height of the roughness element:

$$f = [2 \log(R/k_s) + 1.74]^{-2} \quad (2)$$

Equation 2 is the relation that is valid for the completely rough regime, where the roughness Reynolds number ( $e^+ = (e/D_i) \text{Re} \sqrt{f/2}$ ), is greater than 70. In the transition region ( $5 < e^+ < 70$ ) Schlichting [18] developed equation (3) also using a law of the wall similarity analysis:

$$B(e^+) = 2 \sqrt{f/2} - 2.5 \text{Ln}(R/k_s) + 3.75 \quad (3)$$

Nikuradse's [17] experiments show that for the completely rough regime, ( $e^+ > 70$ ),  $B(e^+)$  attains a constant value of 8.48. When equation (2) is substituted into equation (3), it is found that  $B(e^+)$  equals 8.67. The close agreement between the experimental data and equation (3) indicates that a relation of the form of equation (3) may be applicable throughout the range of roughness types encountered, if sufficient data are available to determine  $B(e^+)$ .

Dipprey and Sabersky [19] also conducted experiments on roughened tubes in which the roughness elements were of a close-packed granular type. The results of their experiments confirm the validity and applicability of the law of the wall similarity analysis for determining friction factor as a function of the roughness of the tube.

## B. INTERNALLY RIBBED TUBES

### 1. Empirical Relations

Webb, et al [4] conducted experiments on 5 tubes enhanced by the addition of internal ribs placed transverse to the longitudinal axis of the tube (see Figure 2). For this type of tube the helix angle is fixed at 90 degrees. Table I shows the range of geometric characteristics for the tubes studied.

TABLE I  
Webb, et al [4] Tubes

Tube	$e/D_i$	$p/e$	$\theta \times 10^4$	$\alpha$ ( $^\circ$ )
01/10	0.01	10	10	90
02/10	0.02	10	20	90
04/10	0.04	10	40	90
02/20	0.02	20	20	90
02/40	0.02	40	20	90

Following a law of the wall similarity analysis similar to that of Dipprey and Sabersky [19] Webb, et al

[4] developed an empirical relation for friction factor as a function of the dimensionless rib height and the pitch-to-groove ratio, for the fully rough region,  $e^+ > 35$ :

$$\sqrt{2/f} = 2.5 \ln(D_i/2e) - 3.75 + 0.95(p/e)^{0.53} \quad (4)$$

Comparison of equation (4) to equation (3) shows that  $B(e^+)$  for the repeated-rib type tube is determined to be  $0.95(p/e)^{0.53}$ . It is noted in equation (4) that the helix angle is not a correlating parameter. The functional dependence on helix angle could not be determined by Webb, et al [4] since all the tubes studied had helix angles of 90 degrees. Equation (4) was derived from data on tubes with a dimensionless rib height from 0.01 to 0.04, and a pitch-to-groove ratio from 10 to 40.

Gee and Webb [3] from their experiments with 3 internally, spirally ribbed tubes of the type shown in Figure 1 also arrived at an empirical relation similar in form to equation (3). Equation (5) is the relation recommended by Gee and Webb [3] for friction factor as a function of the dimensionless rib height and helix angle (for  $5 < e^+ < 45$ ):

$$B(e^+, \alpha) = [\sqrt{2/f} + 2.5 \ln(2e/D_i) + 3.75] (\alpha/50)^{0.16} \quad (5)$$

Figure 11 from [3] shows graphically the correlation for  $B(e^+, \alpha)$ . Using the friction factor data of [3], a

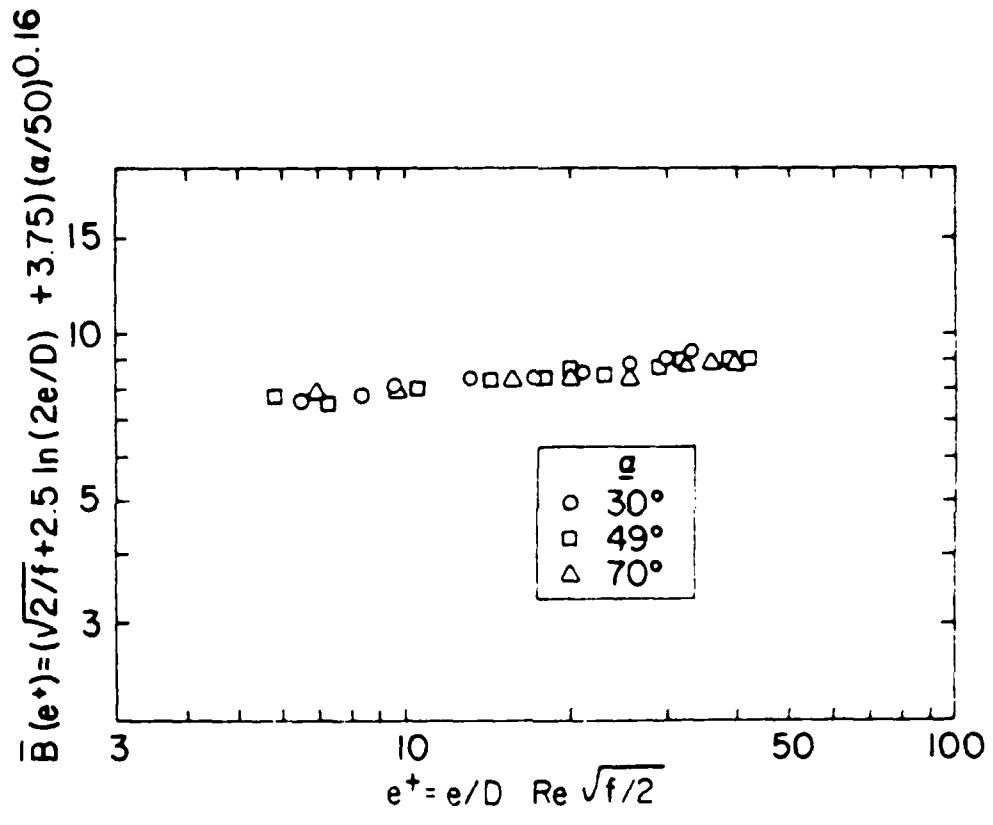


FIGURE 11 Correlation of friction data using Nikuradse's [17] similarity law. From [3].

specific relation for  $B(e^+, \alpha)$  can be formulated by linear regression analysis:

$$B(e^+, \alpha) = 7.735 + 0.029(e^+) \quad (6)$$

As seen in Figure 11, an average value of 8.26 for  $B(e^+, \alpha)$  is also appropriate, which is in very close agreement with the value of 8.48 recommended by Nikuradse [17] for the fully rough region. Note in equation (5) that the pitch-to-groove ratio is not a correlating parameter. The tubes studied by Gee and Webb [3] were of constant pitch-to-groove ratio, prohibiting the determination of a functional relation to the pitch-to-groove ratio (see Table II).

TABLE II  
Gee and Webb [3] Tubes

Tube	$e/D_i$	$p/e$	$\vartheta \times 10^4$	$\alpha$ (°)
1	0.01	15	6.67	70
2	0.01	15	6.67	49
3	0.01	15	6.67	30

Carnavos [2] from his studies of internally, spirally ribbed tubes also of the type shown in Figure 1 recommends equation (7) as an empirical relation for friction factor as a function of the tube geometric characteristics:

$$f = 0.046 / [Re^{0.2} (Afa/Afn)^{0.5} (\sec \alpha)^{0.75}] \quad (7)$$

where Afa is defined as the actual free flow area of the ribbed tube and Afn is defined as the nominal free flow area, based on the tube diameter as if the ribs were not present. Equation (7) is reported as valid in the Reynolds number range of 10,000 to 100,000. The range of values for the geometric characteristics for the Carnavos [2] tubes is shown in Table III.

TABLE III  
Carnavos [2] Tubes

Tube	$e/D_i$	$p/e$	$\theta \times 10^4$	$\alpha$ (°)
15	0.153	32.55	47	6.00
20	0.141	31.9	44.2	2.5
21	0.118	18.98	62.2	5.0
22	0.100	10.1	99	11.0
24	0.084	6.42	130.9	20.0
30	0.045	7.5	59.9	16.3
32	0.042	4.05	103.8	30.0
34	0.034	4.76	71.4	27.0

Withers [13] investigated several Turbo-chil tubes as shown in Figure 6.b. These tubes are basically internally ribbed tubes with the addition of external fins to provide

double augmentation. Note however that the ribs of the Turbo-chil tubes are semi-circular in appearance rather than rectangular as the type of tube shown in Figure 1. From his studies with the Turbo-chil tube, Withers [13] recommended equation (8) as an empirical relation for friction factor as a function of the tube geometry:

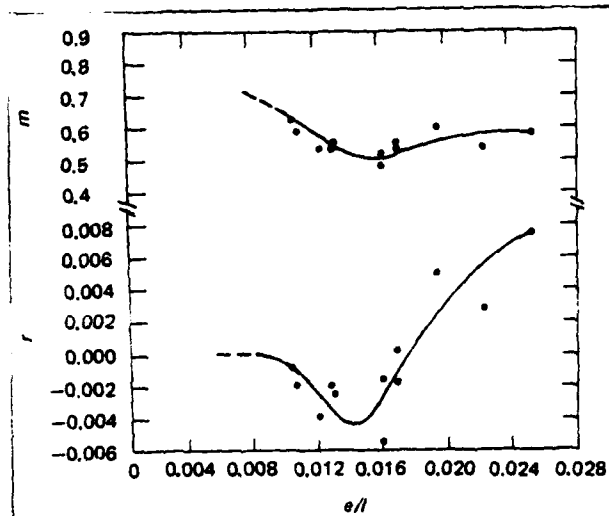
$$\sqrt{2/f} = 2.46 \ln[r + (7/Re)^m] \quad (8)$$

The operands  $r$  and  $m$  in equation (8) are related to the rib height,  $e$ , and the lead of the internal rib,  $\lambda$ . The lead,  $\lambda$ , is defined as the axial distance for one 360 degree turn of the rib. (For single start tubes, the lead,  $\lambda$ , is the pitch,  $p$ .) Figure 12 shows the operands  $r$  and  $m$  versus the ratio  $e/\lambda$  for the cases of  $p/D_i < 0.36$  and  $p/D_i > 0.36$  [13].

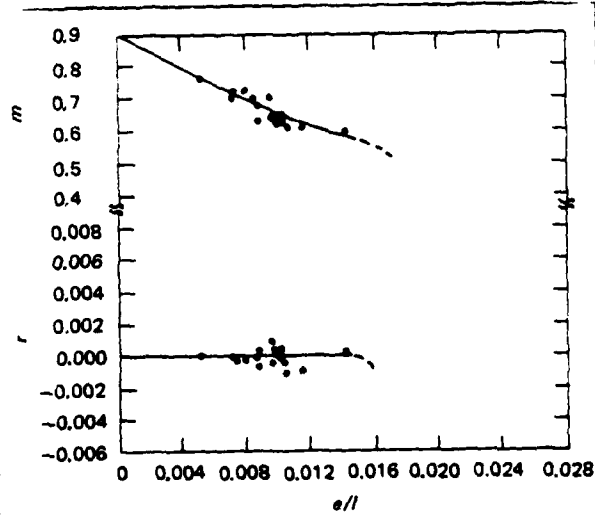
Equation (8) is reported as valid in the Reynolds number range of 10,000 to 120,000. The helix angle range covered by the studies of Withers [13] was from 37 degrees to 62 degrees. The complete range of values for the geometric characteristics of these tubes is shown in Table IV.

## 2. Determination of the Effect of the Relevant Parameters

Of the data studied so far for internally, spirally ribbed tubes and repeated-rib roughened tubes, only the data of Gee and Webb [3] provide data on a family of tubes with constant dimensionless rib height and constant pitch-to-groove



(a) Operand for friction factor equation versus geometric aspect ratio  $e/l$  for multiple-helix internal ridging (5- to 12-start) with  $p/d_i < 0.36$ .



(b) Operands for friction factor equation versus geometric aspect ratio  $e/l$  for multiple-helix internal ridging (5- to 12-start) with  $p/d_i > 0.36$ .

FIGURE 12 Operands for equation (8). From [13]

TABLE IV  
Withers [13] Tubes

Tube	$e/D_i$	$p/e$	$\theta \times 10^4$	$\alpha$ (°)
12	0.0218	38	5.74	37.2
30	0.0282	17.2	16.4	47.2
22	0.0288	19.4	14.95	43.2
27	0.0297	22.6	13.12	37.9
28	0.0332	25.0	13.26	37.2
31	0.0334	14.5	23.72	46.4
29	0.0360	22.68	15.9	37.6
38	0.0315	11.78	26.7	46.6
37	0.0348	8.3	41.98	47.4
40	0.0312	9.72	32.11	46.0
41	0.0376	6.42	58.6	47.4
9	0.0355	9.35	37.9	43.4
21	0.0249	22.99	10.81	42.5
19	0.0246	16.78	14.65	51.8
44	0.0366	9.9	37.12	55.4
43	0.0366	5.92	62.07	55.5
42	0.0419	3.95	105.9	62.2
46	0.0367	4.48	81.88	62.4
45	0.026	6.27	41.5	62.6
13	0.0217	18.69	11.6	52.2
32	0.0234	17.36	13.5	52.2
25	0.0253	16.58	15.15	51.3
24	0.0252	16.1	15.65	52.3
23	0.0251	16.47	15.24	51.7
26	0.0258	16.18	15.92	51.5

ratio. Their experiments were conducted on 3 tubes with a constant dimensionless rib height of 0.01 and a constant pitch-to-groove ratio of 15 (see Table II). The 3 different helix angles of the tubes (30, 49 and 70 degrees) were a result of varying the number of individual rib starts (see equation (1)). Figure 13 shows the Fanning friction factor data of Gee and Webb [3] plotted as a function of helix angle (see also Table V). The friction factors shown are for an arbitrary Reynolds number of 40,000 which is a reasonable value for naval condensers. Figure 13 clearly shows a direct relation between friction factor and helix angle for the family of tubes studied by Gee and Webb [3]. Also shown on Figure 13 is

TABLE V

Friction Factors and Stanton Number for  
Gee and Webb [3] Tubes at  $Re = 40K$

Tube	Ref #	$e/D_i$	$p/e$	$\alpha$ (°)	$f$	$St$
1	3	0.01	15	70	0.011	0.0042
2	3	0.01	15	49	0.0091	0.0040
3	3	0.01	15	30	0.0082	0.0033

the Fanning friction factor for a smooth tube at the same Reynolds number. As helix angle increases, the friction factor increases, most probably due to the increased turbulence resulting from the rib becoming more aligned to the transverse direction (perpendicular to the flow).

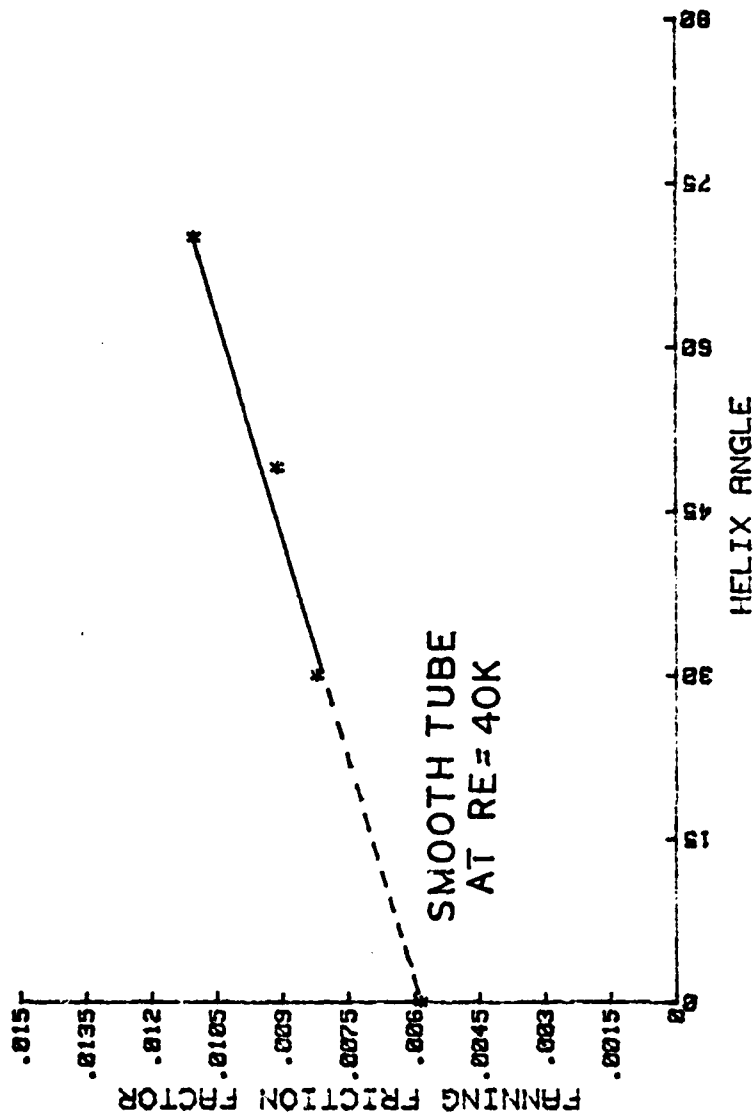


FIGURE 13 Fanning friction factor as a function of helix angle for constant dimensionless rib height of 0.02 and constant pitch-to-groove ratio of 15. From Gee and Webb [3].

Figure 14 plots friction factor data from Webb, et al [4] at an arbitrary Reynolds number of 40,000 as a function of the pitch-to-groove ratio for constant dimensionless rib height of 0.02 and a constant helix angle of 90 degrees. Figure 14 shows that as  $p/e$  increases, the friction factor decreases. The decrease in friction factor may be attributed to the increased distance between the ribs which allows the fluid to remain in contact with the smooth portion of the tube for a longer time before the rib introduces turbulence.

### 3. Comparison of Empirical Relations to Existing Data

Equation (4) from Webb, et al [4] was used to calculate friction factors for the tubes studied by Gee and Webb [3], at a Reynolds number of 40,000. For a constant pitch-to-groove ratio of 15 and a constant dimensionless rib height of 0.01, equation (4) predicts a constant friction factor of 0.0199 for all the tubes. This friction factor is in obvious conflict with the experimental data (see Table V). The constant friction factor is also contrary to the friction factor trend shown in Figure 13.

Equation (5) from Gee and Webb [3] was then used to calculate friction factors for the tubes of Webb, et al [4]. For a constant dimensionless rib height of 0.02, and a constant helix angle of 90 degrees, equation (5) predicts a constant friction factor of 0.0143. This friction factor is contrary to the experimental data of Webb, et al [4] and contrary to the friction factor trend shown in Figure 14.

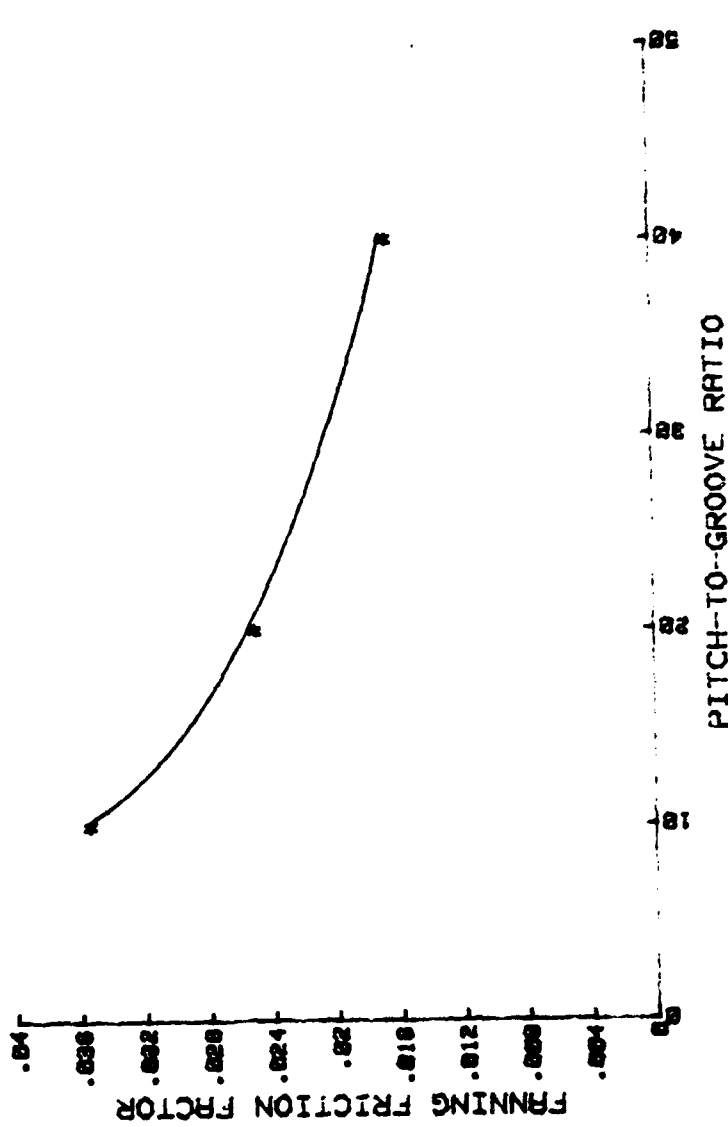


FIGURE 14 Fanning friction factor as a function of pitch-to-groove ratio for constant dimensionless rib height of 0.02 and constant helix angle of 90 degrees. From Webb, et al [4].

A comparison of the experimental data of Carnavos [2] to the predicted friction factors of equations (4) and (5) showed large disagreement (as large as a factor of 4) but did not produce any further information. Equation (7) from Carnavos [2] could not be used in a comparison of data from Webb, et al [4] since the helix angle of 90 degrees for the repeated-rib roughened tubes will produce a zero friction factor due to the helix angle term in equation (7). The data of Gee and Webb [3] were however compared to the friction factors predicted by equation (7). The areas  $A_{fa}$  and  $A_{fn}$  for the internally, spirally ribbed tubes were calculated and used in equation (7) to calculate friction factors of 0.0049, 0.0040, and 0.0024 for the 30 degree, 49 degree, and 70 degree tubes respectively. These predicted values of friction factor are in wide contrast to the trend shown in Figure 13.

Equation (8) could not be used for a comparison with the data of Gee and Webb [3], Webb, et al [4] and Carnavos [2] due to the inability to determine or calculate with any reliability the operands  $r$  and  $m$  for the various tubes.

#### 4. Summary

The law of the wall similarity analysis technique for determining friction factor as a function of the geometric characteristics of an enhanced tube is a widely recognized and potentially powerful method for the assessment of flow resistance of internally, spirally ribbed tubes and repeated-rib tubes. The reader is cautioned, however, that the

analysis must account not only for the effect of the roughness Reynolds number, but also for the effects of the helix angle and the pitch-to-groove ratio.

Equations (4), (5), and (7) do not sufficiently accommodate variations in the geometric parameters to permit their application to geometries other than those tubes for which the relations were derived. Insufficient data for several families of tubes also precludes a thorough investigation of the effects of each of the relevant parameters (dimensionless rib height, pitch-to-groove ratio, and helix angle) and the valid application of the law of the wall similarity analysis.

Equation (8) does not provide a universally applicable relation unless the operands  $r$  and  $m$  are known for a particular tube, or a method is established to calculate  $r$  and  $m$  from geometric characteristics for a specified tube geometry.

### C. SPIRALLY CORRUGATED TUBES

#### 1. Empirical Relations

Mehta and Rao [6] in their investigation of 11 single-start spirally corrugated tubes of the type shown in Figure 3, recommend equation (9) as an empirical relation for the friction factor as a function of the Reynolds number and a dimensionless geometric parameter,  $\theta$ :

$$f = 0.079e^{-92\theta}/\text{Re} (0.25e^{-215\theta}) \quad (9)$$

Equation (9) represents the Blasius relation for friction factor modified by the dimensionless parameter,  $\theta$ , the severity factor, which is defined below:

$$\theta = e^2/pD_i \quad (10)$$

Equation (9) is reported as valid in the Reynolds number range of 10,000 to 80,000 and for a range of severity factor from 0 to  $200 \times 10^{-4}$ . The range of values of the helix angle, severity factor, and other geometric characteristics for the tubes studied by Mehta and Rao [6] are tabulated in Table VII.

TABLE VI

Friction Factor and Stanton Number for  
Webb, et al [4] Tubes at Re = 40K

Tube	Ref #	$e/D_i$	$p/e$	$\alpha$ (°)	$f$	St
01/10	4	0.01	10	90	0.0234	0.00282
02/10	4	0.02	10	90	0.0354	0.0029
04/10	4	0.04	10	90	0.0598	0.00304
02/20	4	0.02	20	90	0.025	0.00255
02/40	4	0.02	40	90	0.0165	0.00218

Gupta and Rao [7] from their experiments with 12 single-start tubes also recommend an empirical relation based on the severity factor:

TABLE VII  
Mehta and Rao [6] Tubes

Tube	$e/D_i$	$p/e$	$\theta \times 10^4$	$\alpha$ (°)
2	0.0082	48.85	1.74	82.76
3	0.0117	34.14	3.43	82.76
4	0.0159	25.0	6.43	82.78
5	0.0204	19.54	10.48	82.77
6	0.0248	16.04	15.5	82.78
7	0.0395	10.1	39.0	82.77
8	0.0629	6.35	99.1	82.76
9	0.0886	4.50	195.5	82.76
10	0.0496	15.78	31.6	76.0
11	0.0124	16.06	7.8	86.37
12	0.0394	19.87	20.6	76.0

$$f = 0.079e^{-79.5\theta} / \text{Re}^{(0.25e^{-210\theta})} \quad (11)$$

Equation (11) is reported as valid in the Reynolds number range of 10,000 to 60,000 and over a severity factor range of 0 to  $135 \times 10^{-4}$ . The complete range of values for the helix angle, severity factor, and other geometric characteristics for the tubes studied by Gupta and Rao [7] are tabulated in Table VIII.

The spirally corrugated tubes studied by Mehta and Rao [6] and Gupta and Rao [7] were all of the type shown in

TABLE VIII  
Gupta and Rao [7] Tubes

Tube	$e/D_i$	$p/e$	$\theta \times 10^4$	$\alpha$ (°)
2	0.02	30.0	6.7	79.3
3	0.02	20.0	10.0	82.7
4	0.03	30.0	10.0	74.0
5	0.04	30.0	13.4	69.1
6	0.03	20.0	15.0	79.2
7	0.02	10.0	20.0	86.4
8	0.03	10.0	30.0	84.6
9	0.056	14.3	39.1	75.7
10	0.046	6.4	71.6	84.6
11	0.056	5.3	106.0	84.6
12	0.056	5.0	113.0	84.9
13	0.061	4.6	135.0	84.9

Figure 3. The range of values for the dimensionless groove depth, pitch-to-groove ratio, helix angle and severity factor are on the same order for the two sets of tubes (see Tables VII and VIII). The only difference in the tubes was the tube diameter. The tubes of Mehta and Rao [6] had diameters on the order of 16mm, while the tubes of Gupta and Rao [7] had diameters on the order of 25mm. The groove depths of the two sets of tubes however resulted in the similarity of values for the dimensionless parameters.

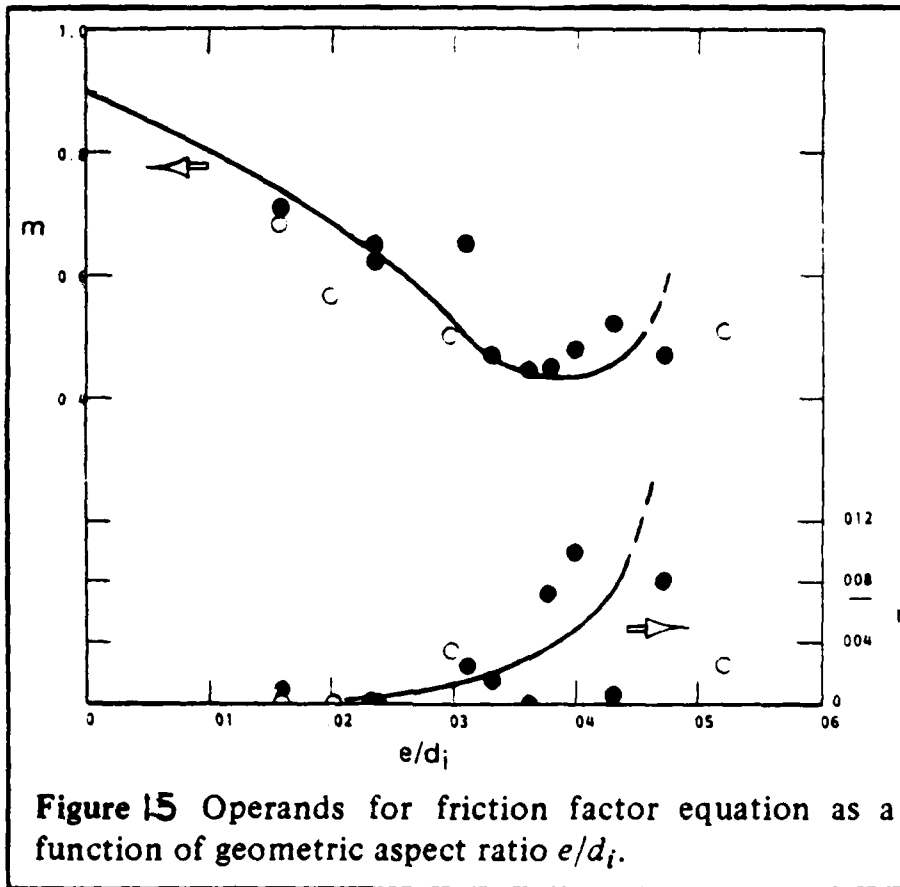
Withers [12] in his investigation of several single-start Korodense tubes (Figure 6.a) recommends equation (12) as the empirical relation for the friction factor as a function of the tube geometry:

$$\sqrt{2/f} = 2.46 \ln[r + (7/Re)^m] \quad (12)$$

The operands  $r$  and  $m$  are related to the dimensionless groove depth and were experimentally determined for each tube studied. Figure 15 is reproduced from [12] and shows the operands  $r$  and  $m$  versus the dimensionless groove depth for single-start tubes. The range of values for helix angle, severity factor, and the other geometric characteristics are shown in Table IX. Equation (12) is reported as valid in the Reynolds number range of  $Re > 10,000$ .

Li, et al [16] from their investigation of 20 single-start and multiple-start tubes, recommend equation (13) as an empirical relation that explicitly relates friction factor to the helix angle, dimensionless groove depth, pitch-to-groove ratio, and Reynolds number:

$$\begin{aligned} \sqrt{2/f} = & 3.42 \ln\left(\frac{D_i}{2e}\right) - 4.64 \\ & + 1.25(e/D_i)^{-0.057} (p/e)^{0.5} \left(\frac{\alpha}{90}\right)^{1.14} \\ & \times \exp\left[\frac{(\ln Re - 9.62)^2}{1000(p/e)^{-1.38}}\right] \end{aligned} \quad (13)$$



Equation (13) is reported as valid for the Reynolds number range of 10,000 to 80,000. The range of values for helix angle, severity factor, and the other geometric characteristics for the single-start and multiple-start tubes are shown in Table X. (The multiple-start tubes are indicated by \*).

TABLE IX  
Withers [12] Tubes

Tube	$e/D_i$	$p/e$	$\theta \times 10^4$	$\alpha$ ( $^\circ$ )
1100	0.0311	14.7	21.15	81.7
5	0.0522	17.5	29.9	73.8
1	0.0236	19.5	12.13	81.7
2	0.0236	19.5	12.13	91.7
20	0.0363	12.4	29.22	81.8
33	0.0473	12.3	38.5	79.5
2300	0.0159	24.1	6.59	83.0
2100	0.0159	18.8	8.47	84.6
7	0.0331	12.1	27.27	82.7
6	0.0379	11.0	37.52	82.4
14	0.0431	14.2	30.34	78.9
9	0.0298	11.3	26.34	83.8
15	0.0399	11.0	36.35	82.1

Cunningham and Milne [11] investigated 2 multiple-start tubes also of the type shown in Figure 3 to determine

the effect of helix angle on the friction factor and heat transfer coefficient of spirally corrugated tubes. As seen in Table XI the tubes studied had a constant dimensionless groove depth of 0.018 and a constant pitch-to-groove ratio of 32. The 6-start tube had a helix angle of 46 degrees, and the 2-start tube had a helix angle of 72 degrees (see equation (1)). No specific relation was recommended, however for friction factor as a function of helix angle.

## 2. Determination of the Effects of the Relevant Parameters

Tables XII, XIII, and XIV represent data from Mehta and Rao [6], Gupta and Rao [7], Cunningham and Milne [11], Withers [12,13], and Li, et al [16] arranged such that data for a family of tubes is presented in one tabulation.

Figures 16 through 20 are plots representing the tabular data of Tables XII, XIII, and XIV. Figures 16, 17, and 18 show friction factor as a function of helix angle and pitch-to-groove ratio for dimensionless groove depths of 0.02, 0.03, and 0.04 respectively. Two trends are evident in Figures 16, 17, and 18. Friction factor increases with increasing helix angle for constant pitch-to-groove ratio, and friction factor decreases with increasing pitch-to-groove ratio for constant dimensionless groove depth. Figures 19 and 20 show friction factor as a function of helix angle and dimensionless groove depth for pitch-to-groove ratios of 10 and 20 respectively. Two trends are also evident in Figures 19 and 20. Friction factor increases with increasing helix

TABLE X

Li, et al [16] Tubes

Tube	$e/D_i$	p/e	$\theta \times 10^4$	$\alpha$ (°)
1	0.019	29.12	6.53	80.0
2	0.0433	12.79	33.86	80.0
3	0.0533	10.44	50.83	80.0
4	0.026	21.25	12.26	80.0
5	0.025	39.73	6.16	72.9
6	0.026	16.16	16.15	82.4
7	0.027	15.63	17.2	82.4
8	0.025	28.41	8.65	77.5
9	0.024	17.52	13.71	82.0
10	0.025	28.28	8.74	77.5
11	0.041	10.96	37.49	81.9
12*(2)	0.042	10.75	39.14	73.9
13*(3)	0.048	9.57	49.72	66.5
14*(4)	0.045	10.23	43.53	59.88
15*(4)	0.058	15.5	37.1	41.4
16	0.01	17.14	5.78	86.9
17	0.07	7.79	88.62	80.3
18	0.055	8.33	65.6	81.8
19	0.01	12.5	9.16	87.4
20	0.038	7.69	49.76	84.6

\* indicates multi-start tubes

Number of starts in parentheses

TABLE XI  
Cunningham and Milne [11] Tubes

Tube	$e/D_i$	$p/e$	$\theta \times 10^4$	$\alpha$ (°)
6-start	0.018	32.0	5.6	46
2-start	0.018	32.0	5.6	72

TABLE XII  
Friction Factors and Stanton Numbers  
for Families of Tubes with Dimensionless  
Groove Depths = 0.02, at  $Re = 40K$

Tube	Ref #	$e/D_i$	$p/e$	$\alpha$ (°)	$f$	$St$
21	13	0.02	20	43	0.0088	0.00164
5	6	0.02	20	83	0.0095	0.00165
3	7	0.02	20	83	0.0090	0.00165
2100	12	0.02	20	85	0.0106	0.00164
1	12	0.02	20	82	0.0114	0.00155
2	12	0.02	20	82	0.0105	0.00149
6-start	11	0.02	30	46	0.0066	0.0012
2-start	11	0.02	30	72	0.0088	0.0016
1	16	0.02	30	80	0.0098	0.00157

TABLE XIII

Friction Factors and Stanton Numbers  
for Families of Tubes with Dimensionless  
Groove Depths = 0.03, at Re = 40K

Tube	Ref #	$e/D_i$	p/e	$\alpha$ (°)	f	St
40	13	0.03	10	46	0.0105	0.00193
9	12	0.03	10	84	0.0197	0.00164
27	13	0.03	20	38	0.0082	0.0016
22	13	0.03	20	43	0.0089	0.0017
6	7	0.03	20	79	0.0095	0.0018

TABLE XIV

Friction Factors and Stanton Numbers  
for Families of Tubes with Dimensionless  
Groove Depth = 0.04, at Re = 40K

Tube	Ref #	$e/D_i$	p/e	$\alpha$ (°)	f	St
41	13	0.04	5	47	0.01144	0.00214
43	13	0.04	5	55	0.0158	0.00248
42	13	0.04	5	62	0.0185	0.00277
46	13	0.04	5	62	0.017	0.00262
9	13	0.04	10	43	0.011	0.0020
44	13	0.04	10	55	0.0145	0.00227
12	16	0.04	10	74	0.025	0.0021
6	12	0.04	10	82	0.025	0.00146
11	16	0.04	10	82	0.027	0.0023
20	16	0.04	10	85	0.035	0.0026
29	13	0.04	20	38	0.0088	0.00167
12	6	0.04	20	76	0.0125	N/A

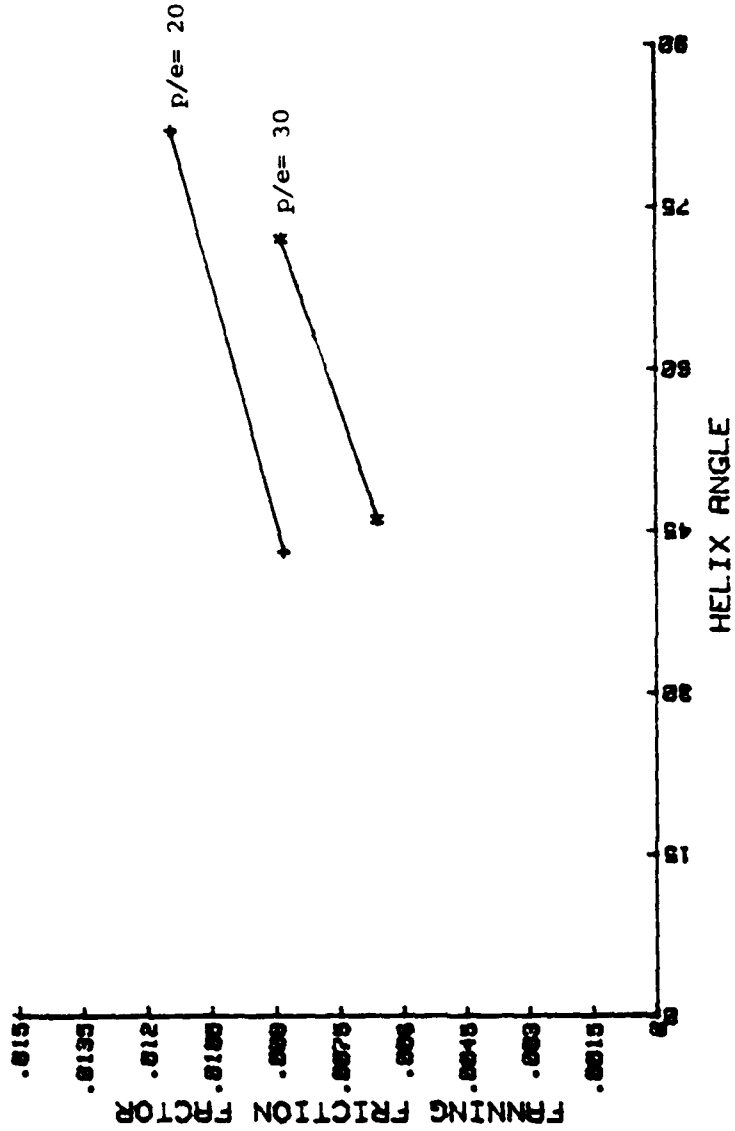


FIGURE 16 Fanning friction factor as a function of helix angle and pitch-to-groove ratio for constant dimensionless groove depth of 0.02.

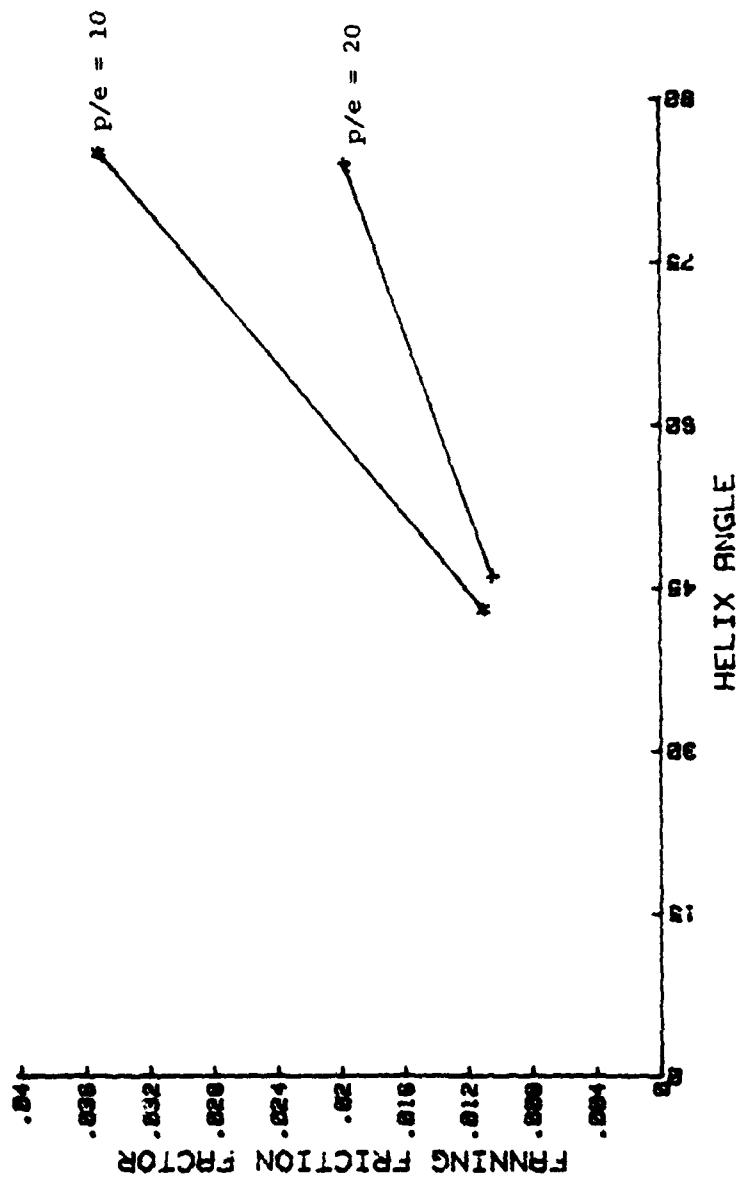


FIGURE 17 Fanning friction factor as a function of helix angle and pitch-to-groove ratio for constant dimensionless groove depth of 0.03

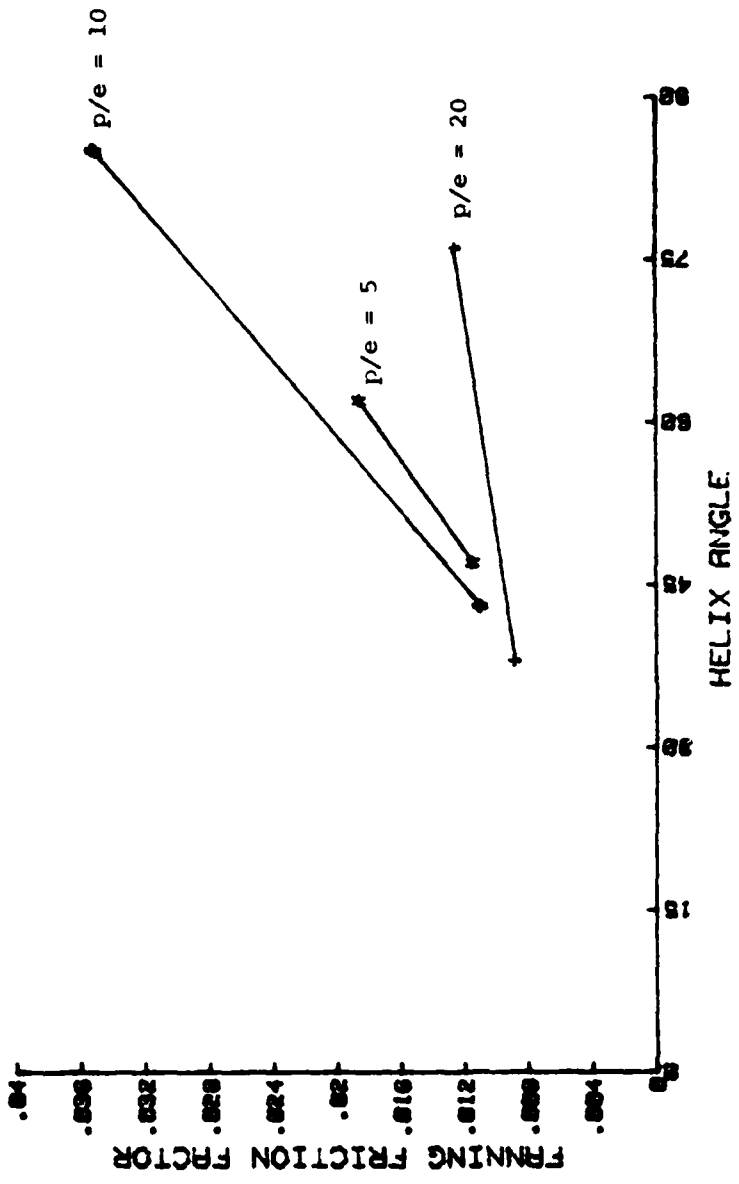


FIGURE 18 Fanning friction factor as a function of helix angle and pitch-to-groove ratio for constant dimensionless groove depth of 0.04

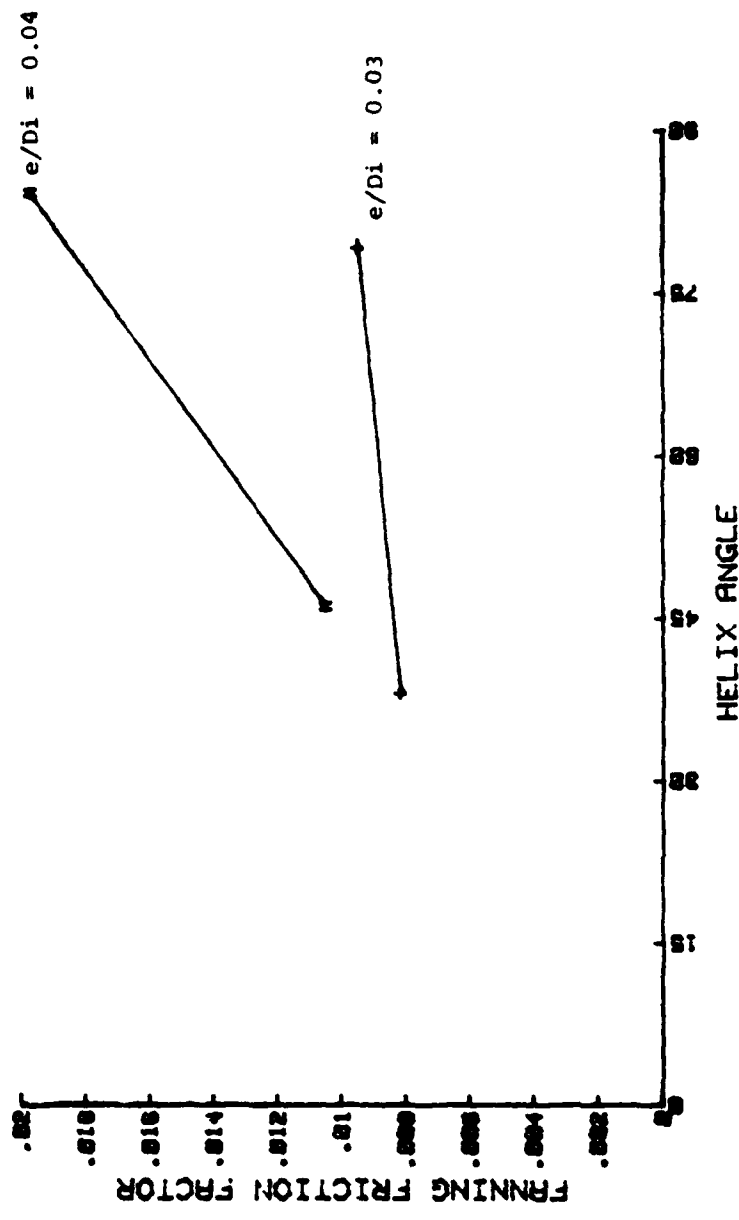


FIGURE 19 Fanning friction factor as a function of helix angle and dimensionless groove depth for constant pitch-to-groove ratio of 10.

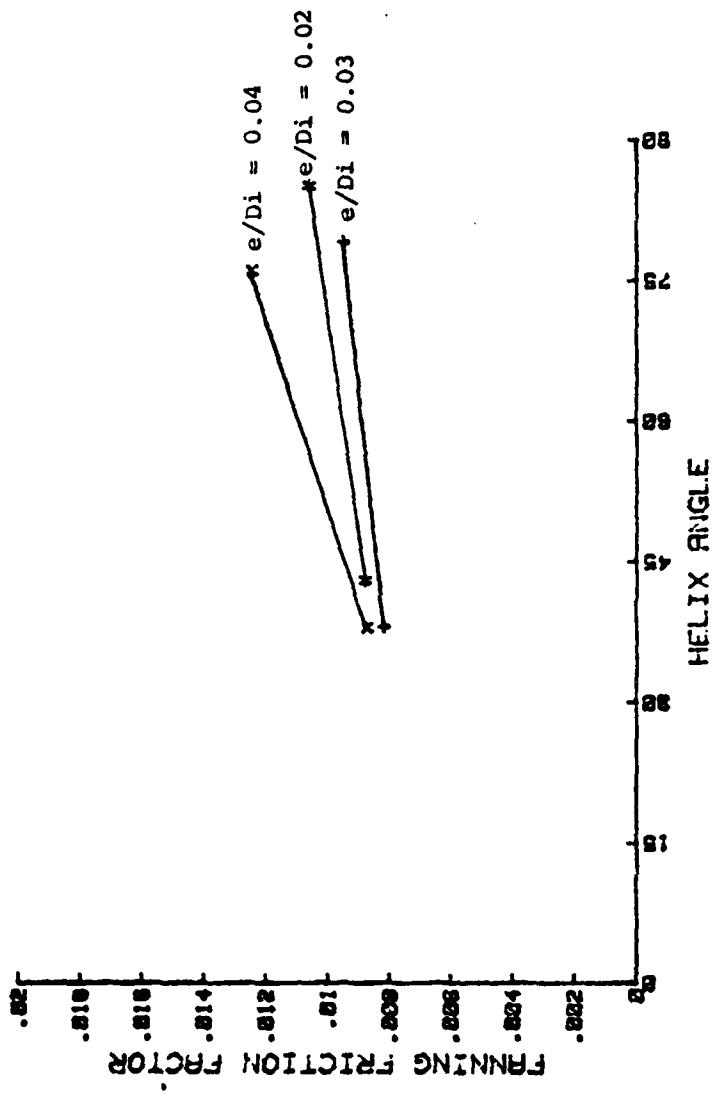


FIGURE 20 Fanning friction factor as a function of helix angle and dimensionless groove depth for constant pitch-to-groove ratio of 20.

angle for constant pitch-to-groove ratio and constant dimensionless groove depth, and friction factor increases with increasing dimensionless groove depth for a constant pitch-to-groove ratio. The trends noted above are in agreement with the trends for internally, spirally ribbed tubes shown in Figures 13 and 14.

The conclusion to be drawn from Figures 16 through 20 is that any general relation for friction factor as a function of the geometric characteristics of spirally corrugated enhanced tubes also should explicitly relate friction factor in terms of the dimensionless groove depth, pitch-to-groove ratio, and helix angle, as was demonstrated for internally, spirally ribbed tubes.

### 3. Comparison of Empirical Relations to Existing Data

Equations (9), (11), and (13) from Section II.C.1 above were examined to determine the applicability of each to a wide variety of tube geometries not specifically studied by the particular author(s).

Equation (12) from Withers [12] could not be used for comparison purposes, however due to the previously stated limitation of not being able to calculate or determine the operands  $r$  and  $m$  for the tubes of the other authors.

Equations (9) and (11) are presented graphically in Figure 21 (at an arbitrary Reynolds number of 40,000) with friction factor data taken from Mehta and Rao [6] and Gupta and Rao [7] shown as data points. As seen in Figure 21, the

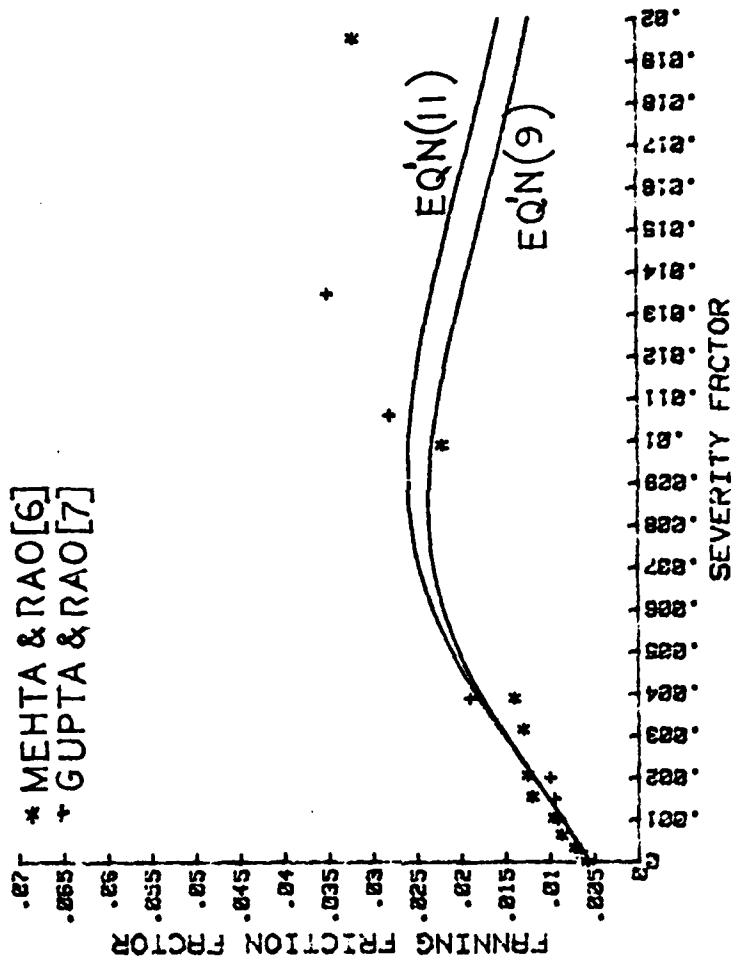


FIGURE 21 Comparison of experimental data from Mehta and Rao [6] and Gupta and Rao [7] to equations (9) and (11) at Re = 40K.

data points showing the experimentally obtained friction factors correlate well with the empirical relations for severity factors up to  $20 \times 10^{-4}$ . For severity factors in the range of  $20 \times 10^{-4}$  to  $40 \times 10^{-4}$ , the Mehta and Rao [6] data deviate from the predicted value by approximately 20%, though the Gupta and Rao [7] data show good agreement. For severity factors in the vicinity of  $100 \times 10^{-4}$ , good agreement is seen between the experimental data and the predicted values. For large values of severity factor ( $\theta > 100 \times 10^{-4}$ ) a wide variance is however noted. It should be noted that the values of severity factor greater than  $30 \times 10^{-4}$  correspond to enhanced tubes with dimensionless groove depths larger than 0.05 and/or pitch-to-groove ratios less than 10.

Figure 22 is another graphical representation of equations (9) and (11), with data points taken from Cunningham and Milne [11] shown for comparison. As seen in Table XI the tubes studied by Cunningham and Milne [11] have the same dimensionless groove depths and the same pitch-to-groove ratios. As shown by equation (10) constant geometric characteristics will result in a constant value of severity factor. Figure 22 shows different values for friction factor at a constant value of severity factor, contrary to the predictions of either equation (9) or equation (11). This difference in friction factor is attributed to the 2 different helix angles of the tubes. (The helix angle is a function of the number of individual groove starts as shown in equation (1).)

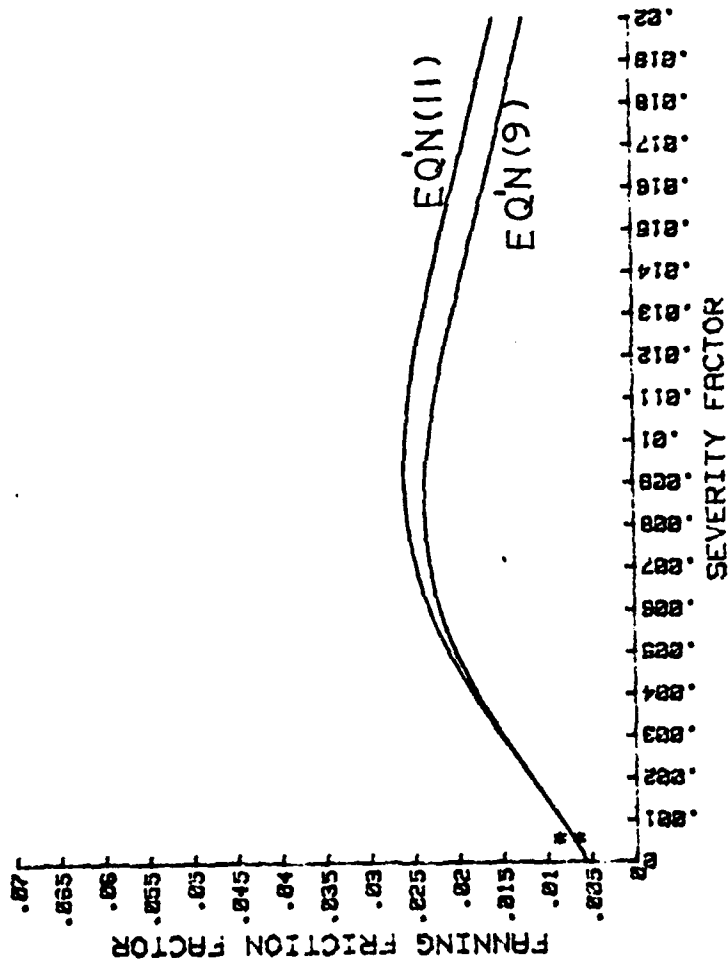


FIGURE 22 Comparison of experimental data from Cunninghamham and Milne [1] to equations (9) and (11) at  $Re = 40K$ .

Figure 23 shows data points representing friction factors for single-start tubes taken from Withers [12], compared to the predictions of equations (9) and (11). Although only a narrow range of severity factors is encountered in the Withers [12] data, there is very little agreement between the experimentally obtained friction factors and the predictions of equations (9) and (11). Equations (9) and (11) underpredict friction factor by as much as 35% even at moderate values of severity factor.

Figure 24 is a graphic comparison of the multiple-start tube data from Withers [13] to equations (9) and (11). As in previous comparisons, there is not a definitive correlation between the observed and predicted values for friction factor. This lack of correlation of the multiple-start tubes data to equations (9) and (11) should be expected however, since the tubes studied by Mehta and Rao [6] and Gupta and Rao [7] were all single-start tubes and equations (9) and (11) are recommended for single-start tubes.

Figure 25 compares data points from Li, et al [16] for single-start tubes to the friction factors predicted by equations (9) and (11). Figure 26 is a like comparison for the multiple-start tubes of Li, et al [16]. As seen in previous comparisons, equations (9) and (11) do not accurately predict friction factors at moderate to large values of severity factor. In all cases, the values of severity factor greater than  $30 \times 10^{-4}$  correspond to dimensionless groove

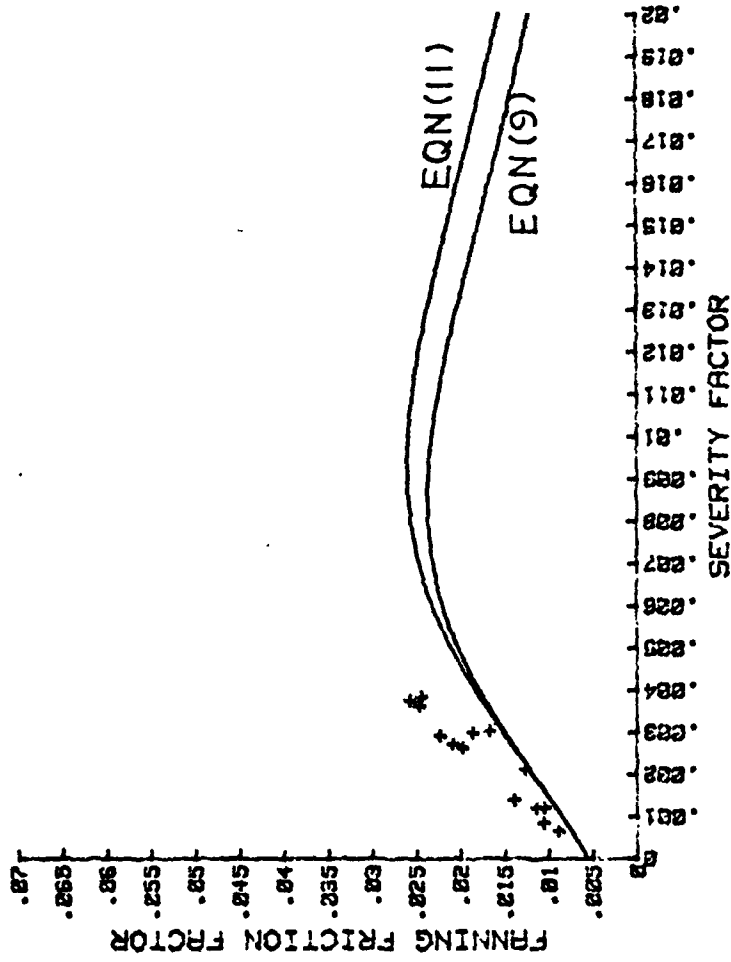


FIGURE 23 Comparison of experimental data from Withers [12] for single start tubes to equations(9) and (11) at  $Re = 40K$ .

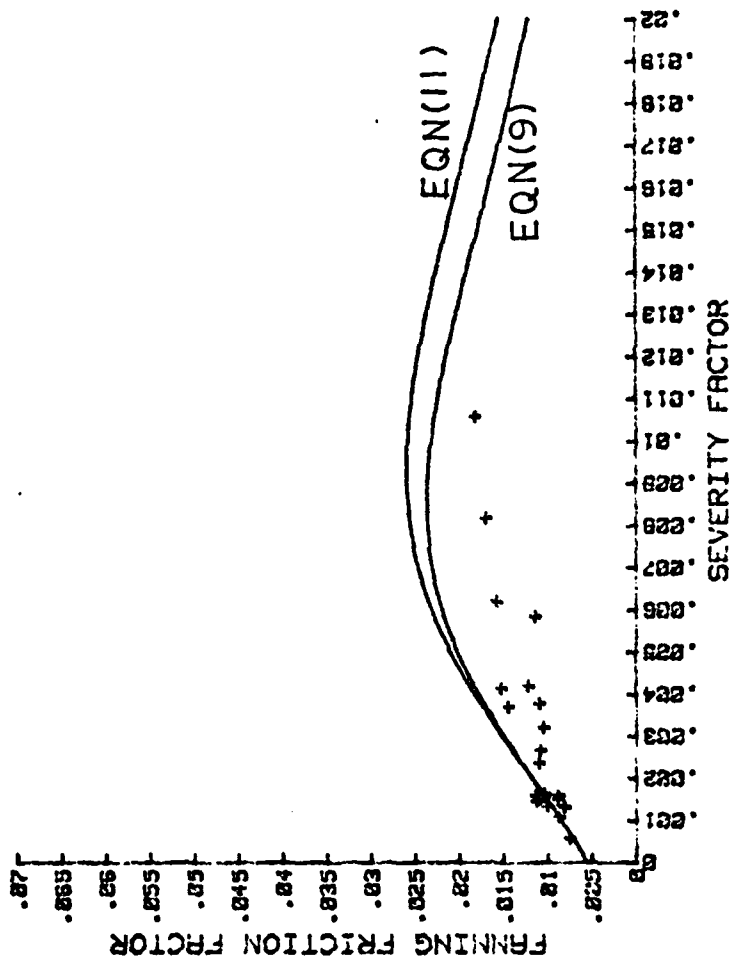


FIGURE 24 Comparison of experimental data from Withers [13] for multiple start tubes to equations (9) and 11) at  $Re = 40K$ .

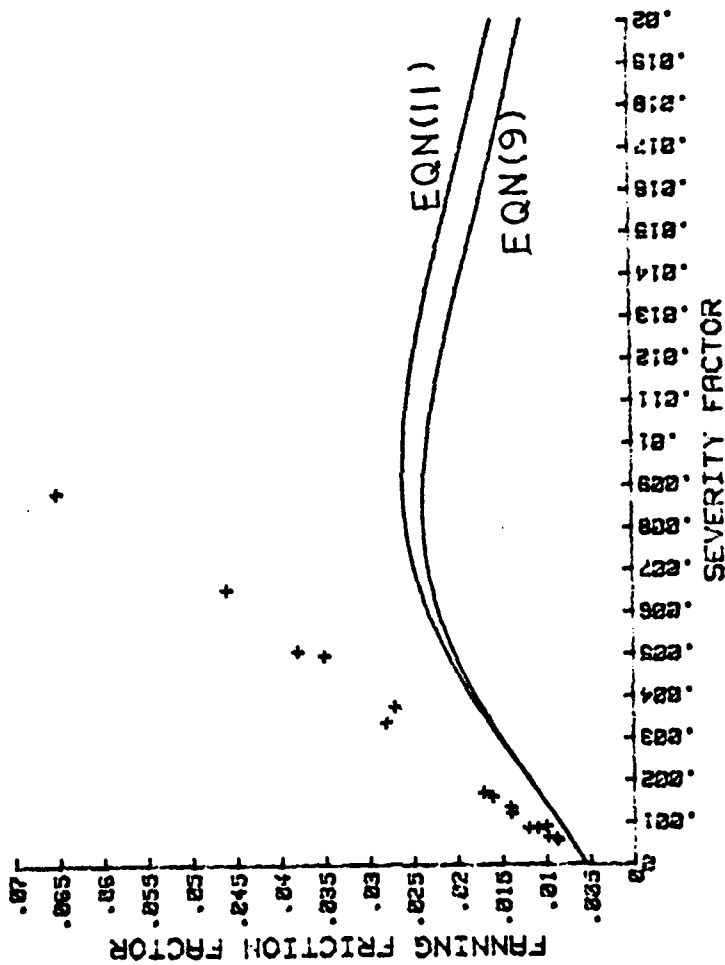


FIGURE 25 Comparison of experimental data from Li, et al [16] for single start tubes to equations (9) and (11) at  $Re = 40K$ .

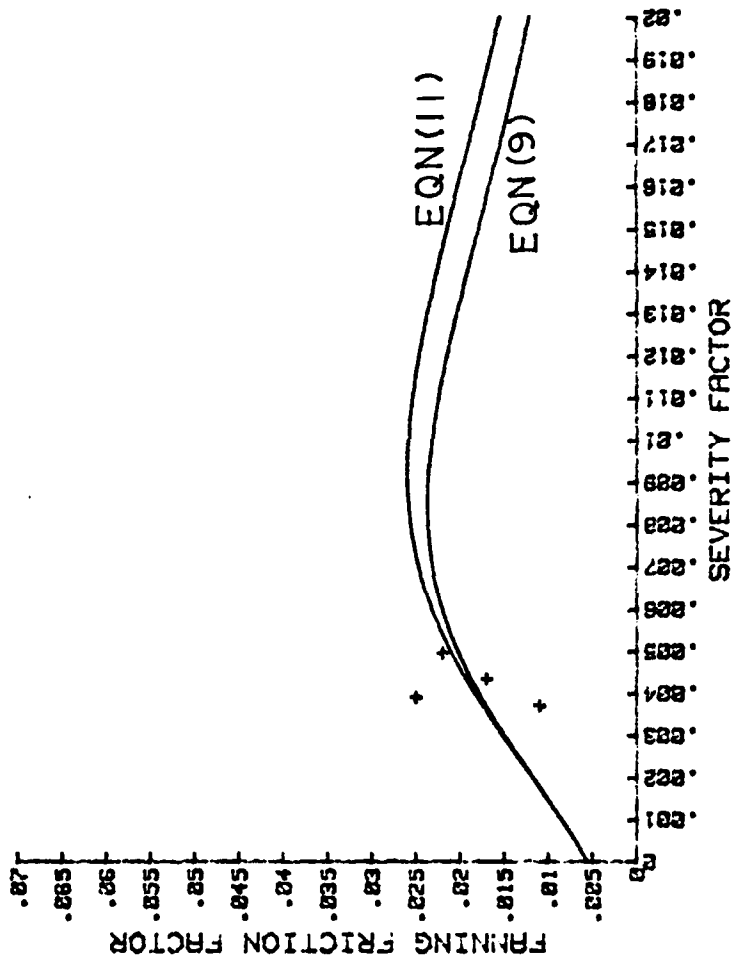


FIGURE 26 Comparison of experimental data from Li, et al [16] for multiple start tubes to equations (9) and (11) at  $Re = 40K$ .

depths greater than 0.05 and/or pitch-to-groove ratios less than 10.

Equation (13) was also examined as a possible applicable relation for friction factor as a function of the relevant geometric parameters of the spirally corrugated tubes. Figures 27 through 30 are point-by-point comparisons of experimentally obtained friction factors for single-start tubes with the predictions of equation (13). The data of Li, et al [16] (Figure 27) show very good agreement, except for those points representing tubes with dimensionless groove depths greater than 0.05 and/or pitch-to-groove ratios less than 10. The variation between the observed and predicted values in Figures 28 through 30 also represent data for the large dimensionless groove depths and/or low pitch-to-groove ratios.

#### 4. Summary

The law of the wall similarity analysis technique must be applied to spirally corrugated tubes with the same cautions applicable to internally, spirally ribbed tubes: i.e., the analysis must account for the effects of the helix angle, dimensionless groove depth, and pitch-to-groove ratio.

Equations (9) and (11) are useful in a narrow range of severity factor, but do not explicitly account for the relevant parameter effects as in a thorough law of the wall similarity analysis. The severity factor does not explicitly relate friction factor to the helix angle. The narrow range

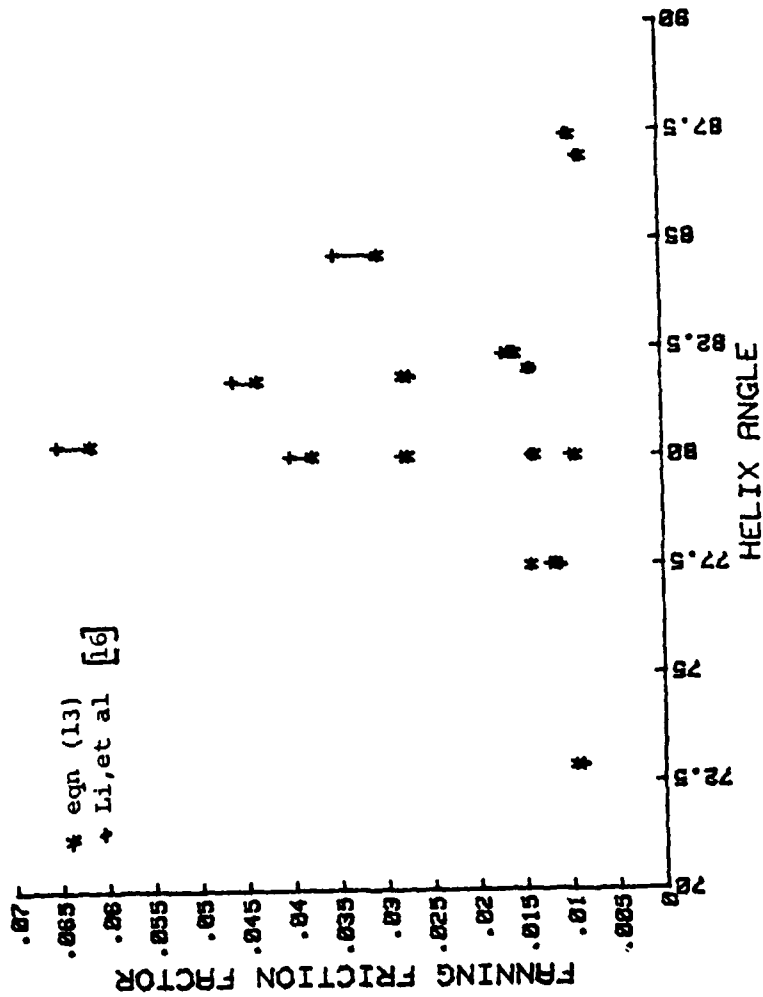


FIGURE 27 Point-by-point comparison of the experimental data of Li, et al [16] to the predictions of equation (13) at  $Re = 40K$ .

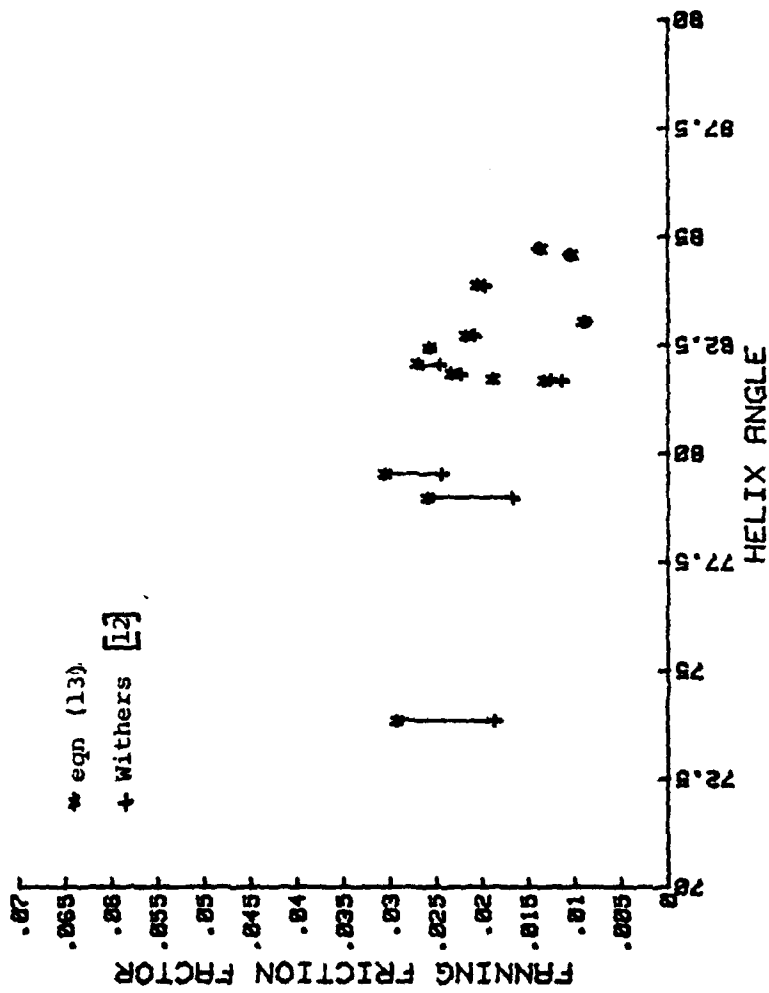


FIGURE 28 Point-by-point comparison of the experimental data of Withers [12] for single start tubes to the predictions of equation (13) at  $Re = 40K$ .

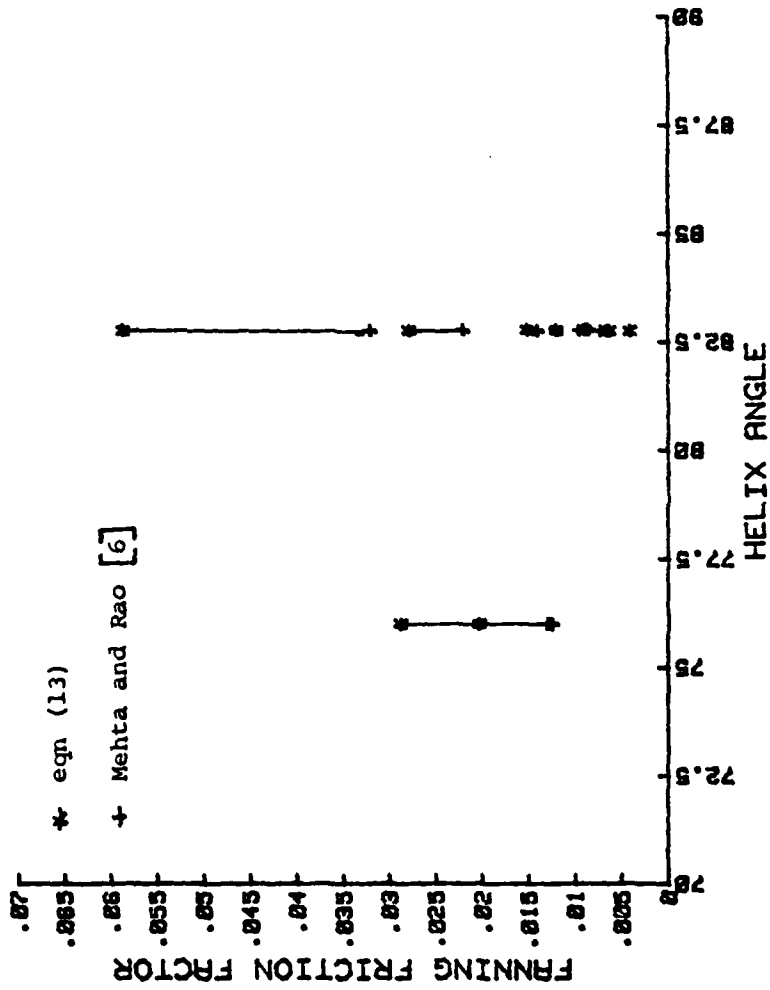


FIGURE 29 Point-by-point comparison of the experimental data of Mehta and Rao [6] to the predictions of equation (13) at  $Re = 40K$ .

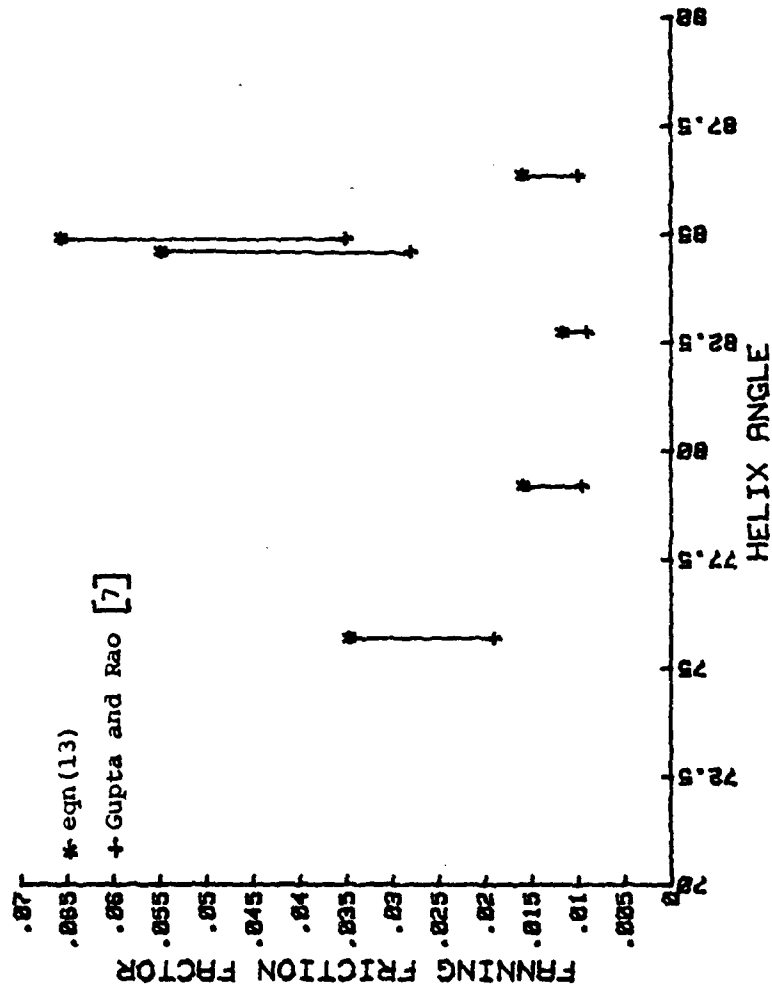


FIGURE 30 Point-by-point comparison of the experimental data of Gupta and Rao [7] to the predictions of equation (13) at  $Re = 40K$ .

of applicability of equations (9) and (11) limits their use as predictive equations for a wide variety of enhanced tubes.

As noted earlier, equation (12) though of a form similar to that expected from a similarity analysis, is limited in applicability due to the limitation of determining the operands  $r$  and  $m$ , without the benefit of a specific function relating the operands to the geometric characteristics of the tube.

Equation (13) does explicitly relate the friction factor to the relevant geometric parameters (dimensionless groove depth, pitch-to-groove ratio, helix angle). This equation is presented in modified form below:

$$\frac{\sqrt{2/f} + 3.42 \ln\left(\frac{2e}{D_i}\right) + 4.64}{1.25(e/D_i)^{-0.57} (p/e)^{0.5} \exp\left[\frac{(\ln Re - 9.62)^2}{1000 (p/e)^{-1.38}}\right]} = \left(\frac{\alpha}{90}\right)^{1.14} \quad (13)$$

Examination of equation (13) above shows that it will predict a decrease in friction factor for an increase in helix angle, for a constant dimensionless groove depth and constant pitch-to-groove ratio, at a constant Reynolds number. This predicted trend is contrary to the trend observed in the previous data (see Figures 16 through 20). This contrary trend suggests that the exponent of  $(\alpha/90)$  should be negative (as in equation (5)).

Figure 31 plots the natural logarithm of the left side of equation (13) as the ordinate with the natural logarithm of  $(\alpha/90)$  as the abscissa, for single-start tubes encountered in this work. The solid line of slope +1.14 represents the exponent of  $(\alpha/90)$  in equation (13). The scatter of data for the Li, et al [16] tubes and the limited range of abscissa values used to predict the slope of the exponent would indicate that the sign and magnitude of the  $(\alpha/90)$  exponent could be open to adjustment. The additional data points in Figure 31 from Mehta and Rao [6], Gupta and Rao [7], and Withers [12] further illustrate that the sign and magnitude of the exponent could be adjusted. The wide scatter of data also indicate that possibly the factors accounting for the effects of the dimensionless groove depth and pitch-to-groove ratio could be altered to bring the data to a closer grouping.

Figure 32 is a plot similar to Figure 31, but for the multiple-start tube data of Li, et al [16], Cunningham and Milne [11] and Withers [13]. As in Figure 31 the solid line represents the +1.14 slope in equation (13). Figure 32 shows that equation (13) will not predict friction factors for multiple-start tubes in its present form.

Figure 33 illustrates the friction factor data for all the spirally corrugated tubes (single-start and multiple-start). The solid line of slope -0.6 is a graphic estimate of the best fit slope for the data of Figure 33.

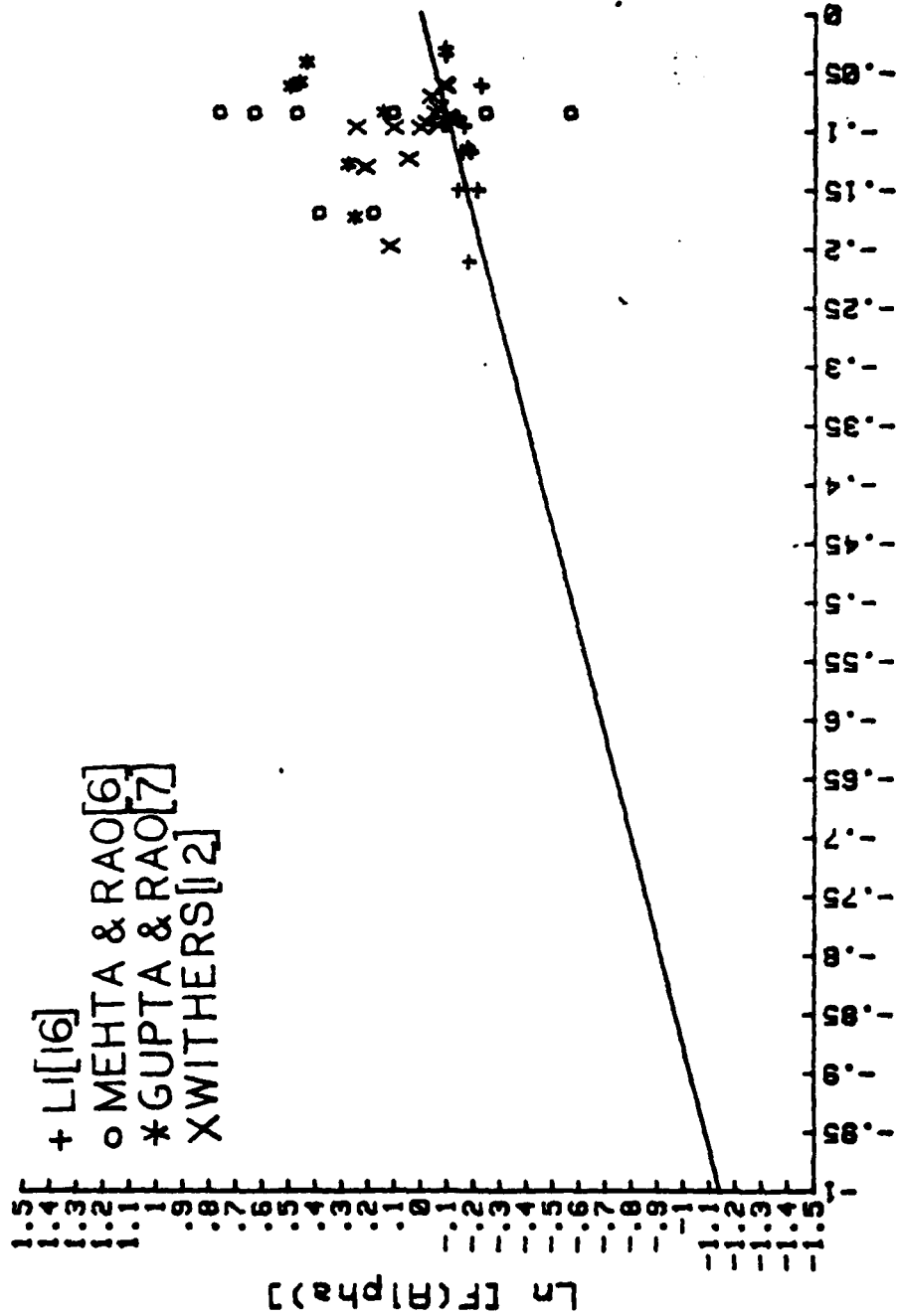


FIGURE 31 Comparisons of experimental data for single-start spirally corrugated tubes to equation (13).

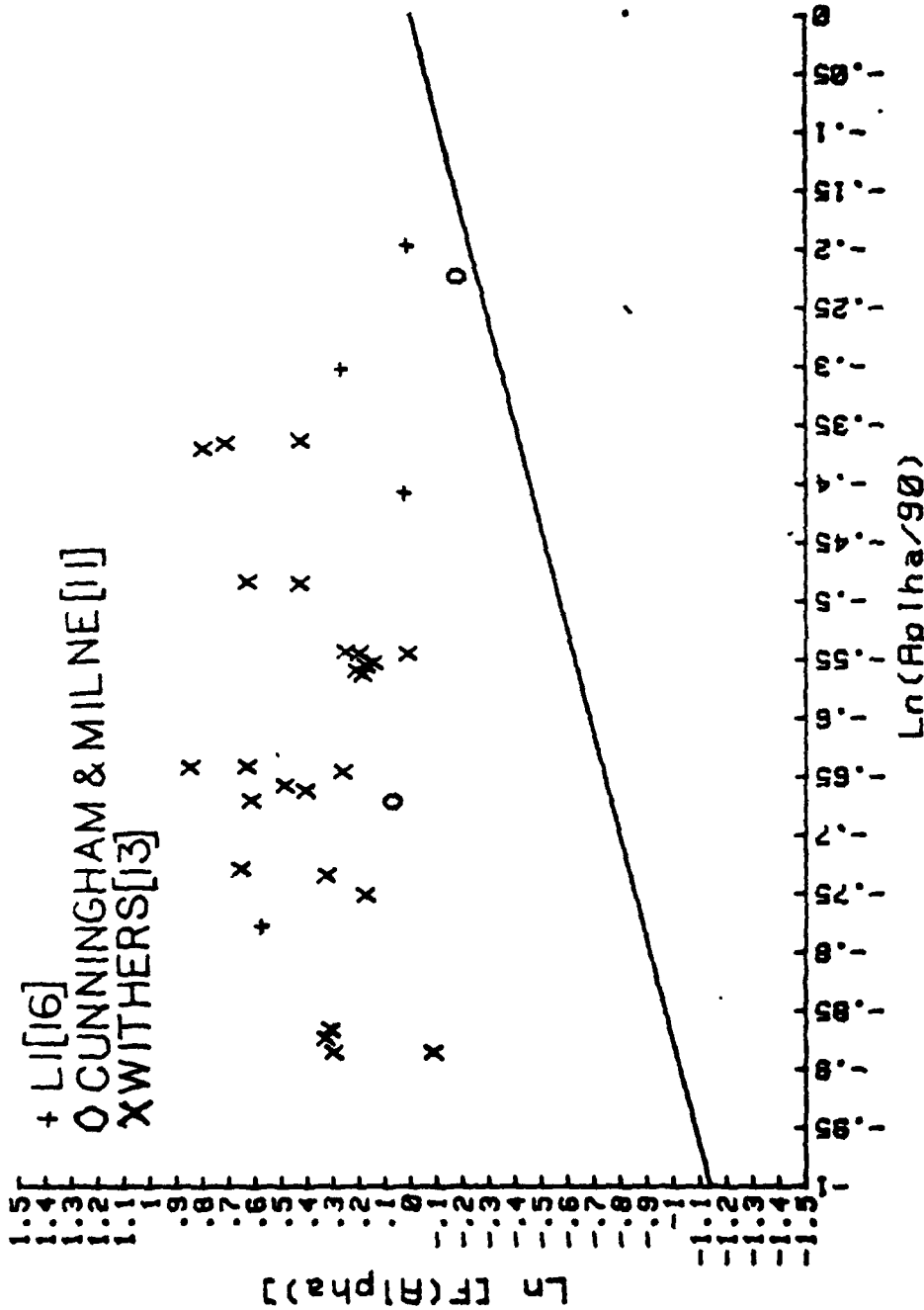


FIGURE 32 Comparisons of experimental data for multiple-start spirally corrugated and multiple-start ribbed tubes to equation (13)

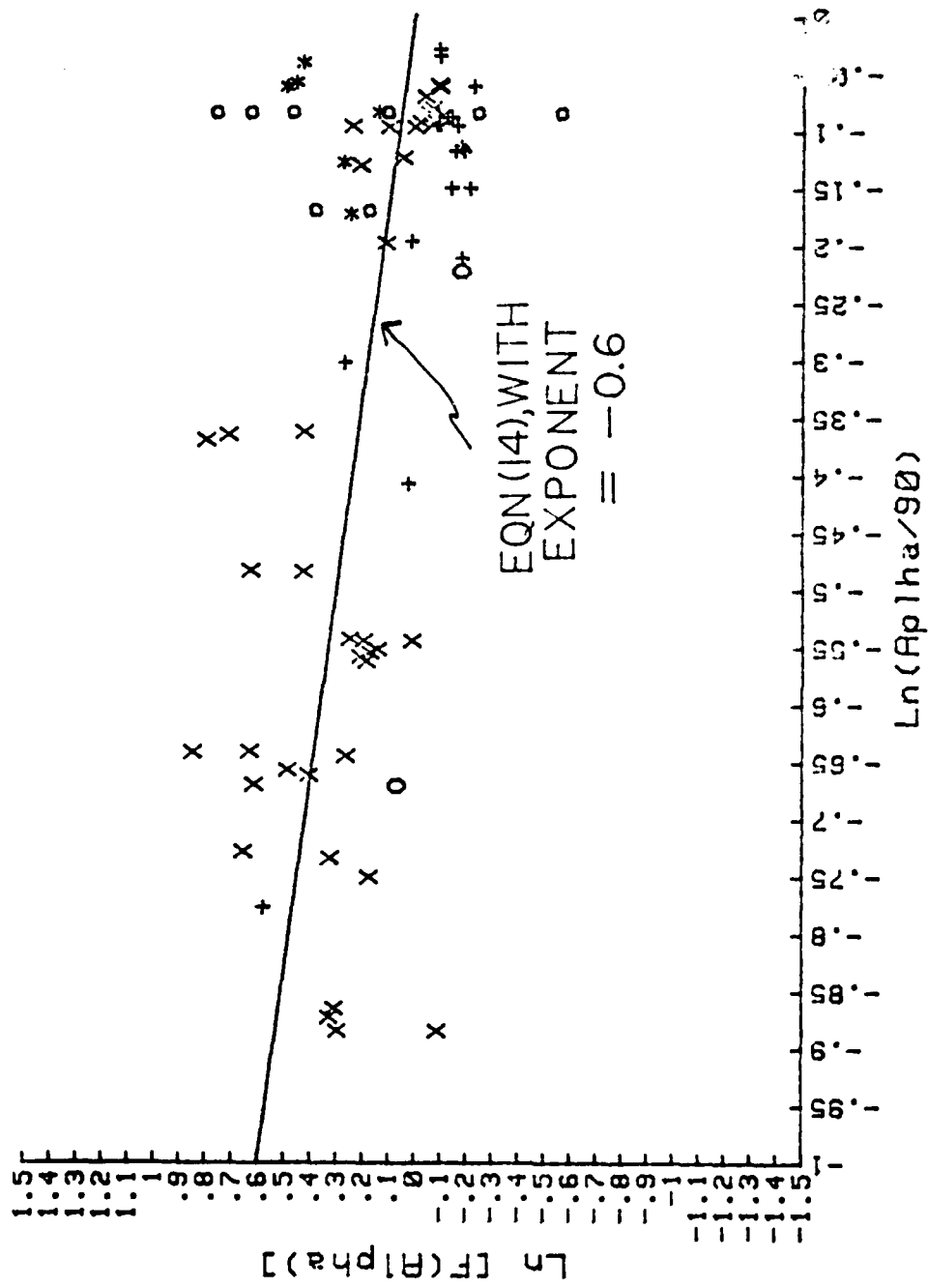


FIGURE 33 Experimental data for single-start and multiple-start tubes showing proposed exponent of - 0.6. Symbols are as in Figures 31 and 32.

Until more complete analysis of this data can be accomplished, equation (14) is proposed as the empirical relation for friction factor as a function of the tube geometric parameters for single-start and multiple-start spirally corrugated tubes:

$$\sqrt{2/f} = 3.42 \ln\left(\frac{D_i}{2e}\right) - 4.64 + 1.25\left(\frac{p}{e}\right)^{0.5} \left(\frac{e}{D_i}\right)^{-0.057} \\ \times \left(\frac{\alpha}{90}\right)^{-0.6} \exp\left[\frac{(\ln Re - 9.62)^2}{1000(p/e)^{-1.38}}\right] \quad (14)$$

The experimental data of Mehta and Rao [6], Gupta and Rao [7], Cunningham and Milne [11], Withers [12,13] and Li, et al [16] were compared to the predictions of equation (13). For 56 of the 63 tubes, equation (14) predicted the friction factor within 30%. The 63 tubes used for the comparison had dimensionless groove depths less than 0.05 and pitch-to-groove ratios greater than 10.

The reader will note that the multiple-start tubes of Withers [13] were considered in the section for internally ribbed tubes as well as this section for spirally corrugated tubes. The semi-circular profile of the ribs in the Turbo-chil tubes are considered similar in shape and characteristics to the spiral corrugated groove, thus allowing their study in both sections. The good correlation with the predictions of equation (14) substantiate the geometric similarity. (13 of the 14 Withers [13] multiple-start tubes correlated with equation (14) within 30%.)

### III. HEAT TRANSFER COEFFICIENT

#### A. GENERAL

##### 1. Analytical Basis

As will be shown, there are several empirical relations for heat transfer coefficient as a function of friction factor. For the purposes of the analysis of this chapter, examination of these several functions will be conducted on the premise that the friction factor used in any empirical relation has been accurately determined by either experimental means or by analytical methods. This premise will allow the various relations to be compared on a standard basis.

##### 2. Background Analysis

The Reynolds analogy is a widely known and well-publicized relation for the heat transfer coefficient (Stanton number) as a function of the friction factor for flow inside smooth tubes [20]:

$$St = \frac{Nu}{Re Pr} = \frac{f}{2} \quad (15)$$

The Reynolds analogy, however, is only applicable for cases in which the Prandtl number is unity and the velocity profile and temperature profiles are the same.

A logical extension to the Reynolds analogy was proposed by Prandtl [21] by including the velocity distribution in the laminar sublayer. The Prandtl analogy is presented in equation (16):

$$St = \frac{f/2}{1 + 5\sqrt{f/2} (Pr - 1)} \quad (16)$$

A more accurate relation was developed by Martinelli [22] who further suggested that the analogy between heat and momentum transfer might also apply to rough tubes:

$$St = \frac{\left(\frac{\epsilon_H}{\epsilon_m}\right) \left(\frac{T_w - T_c}{T_w - T_b}\right) \sqrt{f/2}}{5 \left[ \left(\frac{\epsilon_H}{\epsilon_m}\right) Pr + \ln(1 + 5 \frac{\epsilon_H}{\epsilon_m} Pr) + 0.5 F_1 \ln \left(\frac{Re}{60} \sqrt{f/2}\right) \right]} \quad (17)$$

For Pr near unity and Re = 40K [22], the correction factors  $\epsilon_H/\epsilon_m$ ,  $F_1$ , and  $T_w - T_c / T_w - T_b$  may be considered to be unity for the purposes of this work.

Dipprey and Sabersky [19], applying a heat transfer similarity analysis, similar in concept to the law of the wall analysis for friction factor, proposed a relationship that should be applicable to all types of roughness:

$$St = \frac{f/2}{1 + \sqrt{f/2} [A(e^+) + g(e^+, Pr)]} \quad (18)$$

The functions  $A(e^+)$  and  $g(e^+, Pr)$  must be established for a specified given family of tubes with similar geometric characteristics.

## B. INTERNALLY RIBBED TUBES

### 1. Empirical Relations

Webb et al [4], using a heat transfer similarity analysis in their investigation of repeated-rib roughened

tubes, with the helix angle fixed at 90 degrees, recommend equation (19) as an empirical relation for the heat transfer coefficient as a function of the friction factor, Prandtl number, pitch-to-groove ratio, and roughness Reynolds number:

$$St = \frac{f/2}{1 + \sqrt{f/2} [4.5(e^+)^{0.28} Pr^{0.57} - 0.95(p/e)^{0.53}]} \quad (19)$$

It is noted in equation (19) that the bracketed term in the denominator is the formulation for the corresponding term in equation (18) where  $A(e^+) = -0.95(p/e)^{0.53}$ , while  $g(e^+, Pr) = 4.5(e^+)^{0.28} Pr^{0.57}$ . Equation (19) is reported as valid for a Prandtl number range between 0.71 and 37.6. The reader is cautioned, however, that equation (19) is only reported as being valid for the fully rough region ( $e^+ > 35$ ), as was the case for equation (4) for the friction factor.

Gee and Webb [3] also proposed an empirical relation similar in form to equation (18) for internally, spirally ribbed tubes. The recommended relation includes not only the roughness Reynolds number and Prandtl number dependence, but also the effect of helix angle on the heat transfer coefficient:

$$St = \frac{f/2}{1 + \sqrt{f/2} [g(e^+, Pr, \alpha) (\alpha/50)^j - B(e^+, \alpha)]} \quad (20)$$

where:

$$j = -0.37 \quad \text{for } \alpha < 50^\circ,$$

$$j = 0.16 \quad \text{for } \alpha > 50^\circ, \text{ and}$$

$B(e^+, \alpha)$  is as defined in equation (6).

Equation (20) was derived as a result of studies conducted on the flow of air,  $Pr = 0.71$ . The function  $g(e^+, Pr, \alpha)$  is shown in Figure 34 using the experimental data from [3]. Upon examination of the data in Figure 34, it is easy to see that a value of 8.088 is valid for the function  $g(e^+, Pr, \alpha)$  for  $e^+ < 8$ . For  $e^+ > 8$ , a linear regression analysis produced the following relation (for  $Pr = 0.71$ ):

$$g(e^+, Pr) = 7.71 + 0.11(e^+) \quad (21)$$

Substitution of equation (21) into equation (20), with  $B(e^+, \alpha)$  assumed to be 8.26 (as previously determined), leads to equation (22):

$$St = \frac{f/2}{1 + \sqrt{f/2} [(7.71 + 0.11(e^+)) (\alpha/50)^j - 8.26]} \quad (22)$$

Carnavos [2] proposed an empirical relation for the heat transfer coefficient as a function of the geometric characteristics of the enhanced tube and the helix angle:

$$St = \frac{0.023 (A_{fa}/A_{fn})^{0.1} (A_n/A_a)^{0.5} (\sec \alpha)^3}{Re^{0.2} Pr^{0.6}} \quad (23)$$

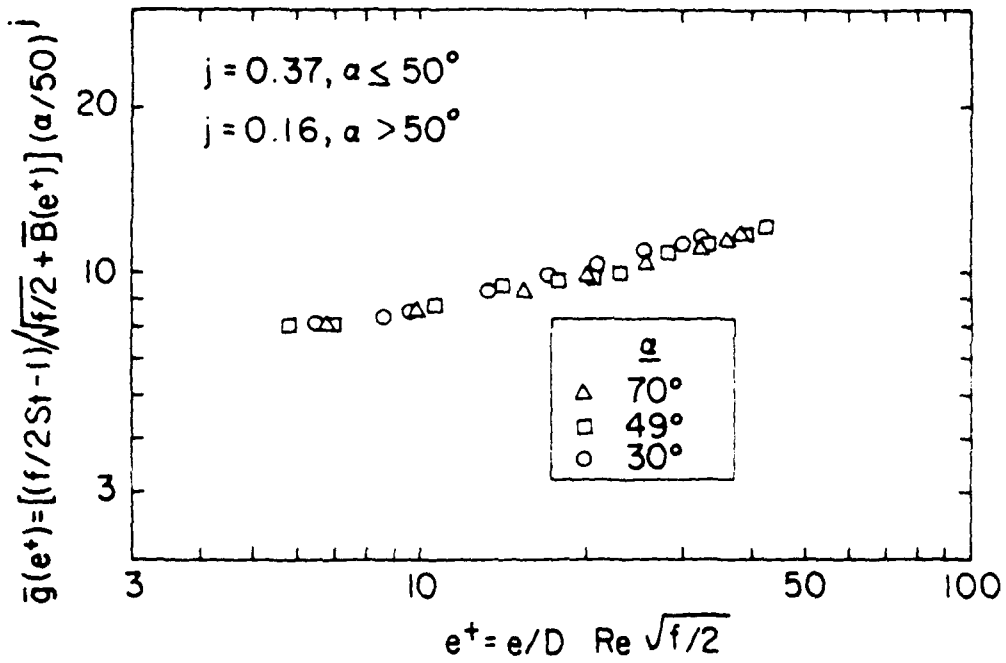


FIGURE 34 Correlation of heat transfer data using Dipprey and Sabersky's [19] heat transfer similarity law. From [3].

where  $A_n$  represents the nominal heat transfer area as if the ribs were not present, and  $A_a$  is the actual heat transfer area of the ribbed cube and  $A_{fa}$  and  $A_{fn}$  are as previously defined. Equation (23) was derived from experiments with various fluids in the Prandtl number range of  $0.7 \leq Pr \leq 30$ .

Withers [13] proposed an empirical relation for the heat transfer coefficient as a function of the pitch-to-groove ratio, roughness Reynolds number, dimensionless rib height, and Prandtl number:

$$St = \frac{\sqrt{f}/2}{[5.68(p.e)^{0.125} Pr^{0.5} (e^+)^{0.136} - 2.5 \ln(2e/D_i) - 3.75]} \quad (24)$$

The experiments of Withers [13] were conducted with water in the Prandtl number range of  $4 \leq Pr \leq 10$ . It is noted that although his experiments were conducted on ribbed tubes with helix angles from 37 to 62 degrees, (Table IV), no helix angle dependence is expressed in equation (24).

## 2. Determination of Effect of Relevant Parameters

The first determination to be made in the assessment of heat transfer coefficient for internally ribbed tubes is whether the increase in friction factor, as a result of the roughness, is sufficient to account for the increase in heat transfer coefficient through application of either equation (16), the Prandtl analogy, or equation (17), the Martinelli analogy.

Figure 35 shows the data of Carnavos [2] as data points compared to the predictions of equations (16) and (17), for  $Pr = 5$  and  $Re = 40,000$ . The data of Carnavos [2] do not correlate well with either of the analogies. Figure 36 compares equations (16) and (17) to the data of Webb, et al [4] for  $Pr = 5$  and  $Re = 40,000$ . The Prandtl analogy, equation (16), does not accurately predict the Stanton number of the repeated-rib roughened tubes whereas the Martinelli analogy approximates the data for 4 of the 5 tubes fairly well. Figure 37 shows the data of Withers [13] compared to the predictions of equations (16) and (17), again for  $Pr = 5$ , and  $Re = 40,000$ . For the Withers [13] data, the Prandtl analogy more accurately predicts the experimental data, but there is a nearly constant error of 15%. Figure 38 compares data of Gee and Webb [3] for air, at  $Pr = 0.71$  and  $Re = 40,000$  to equations (16) and (17). The data from the smooth tubes of [3] agrees very well with the Prandtl analogy, but a wide variation is seen for the internally ribbed tubes.

Examination of Figures 35 through 38 indicates that the increased friction factors for internally ribbed tubes do not sufficiently account for the observed increase in heat transfer coefficient when used with the analogies presented. It follows that the relation for heat transfer coefficient should itself explicitly be dependent upon the relevant geometric parameters of the enhanced tube.

Figure 39 shows data from Table VI for the repeated-rib roughened tubes of Webb, et al [4]. The data points in

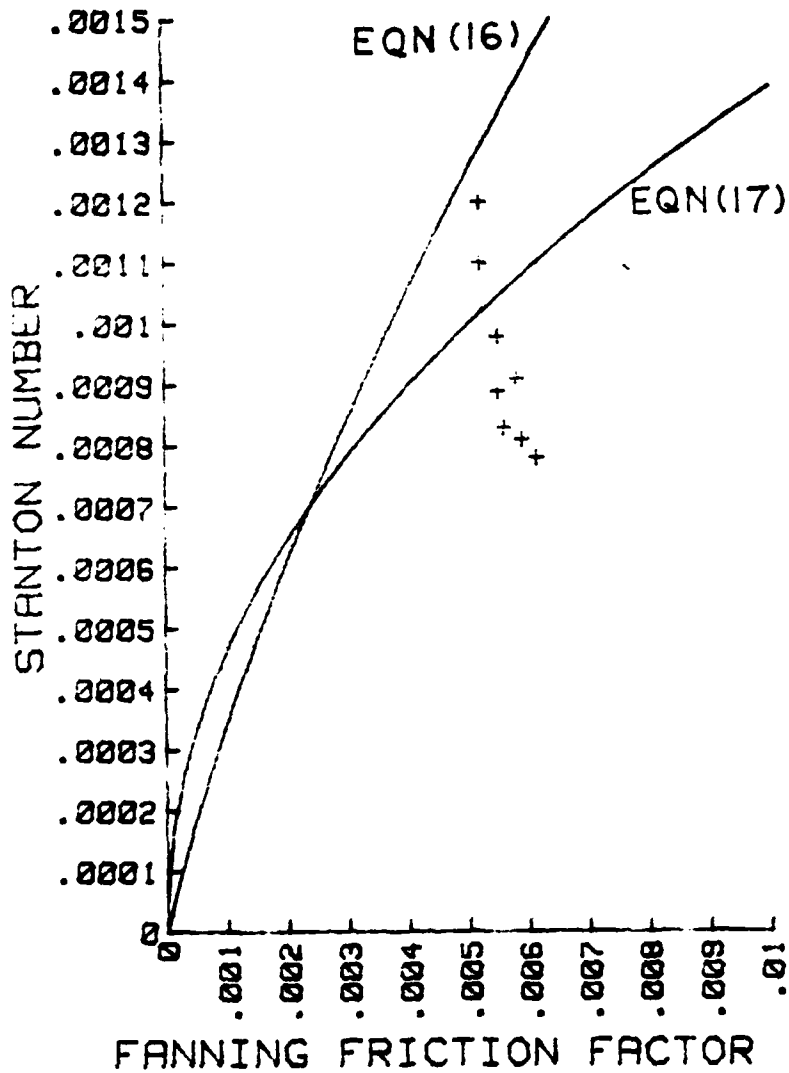


FIGURE 35 Experimental data of Carnavos [2] compared to equations (16) and (17) for  $Pr = 5$  and  $Re = 40K$ .

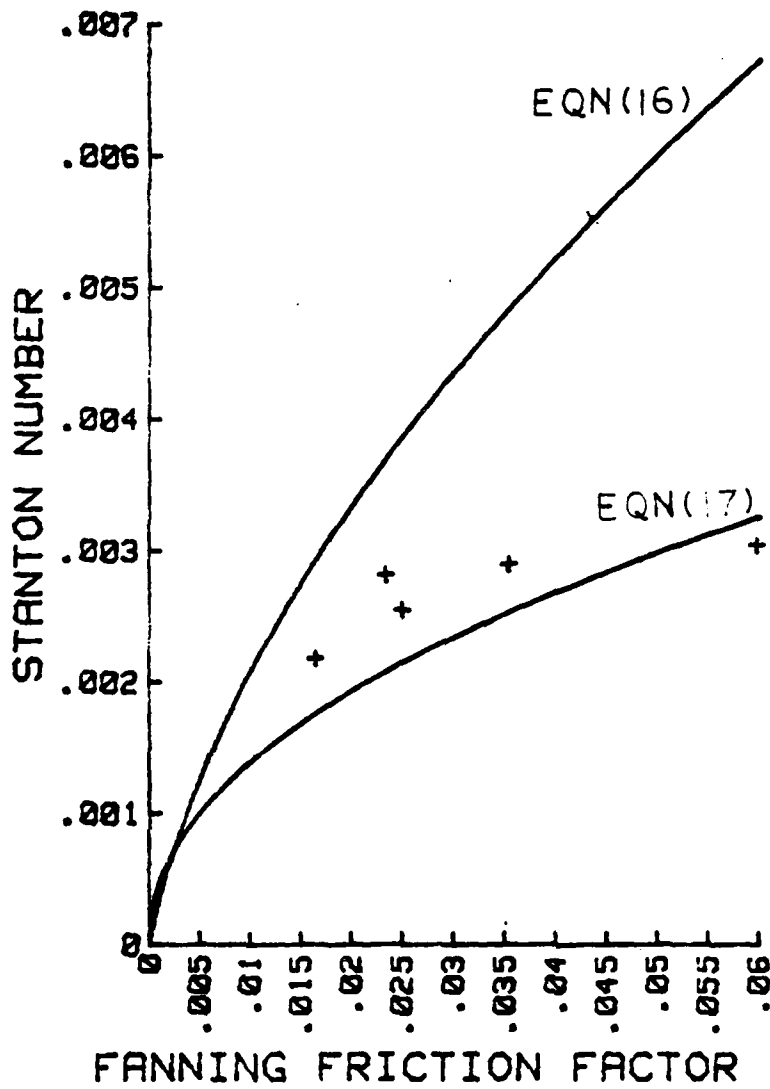
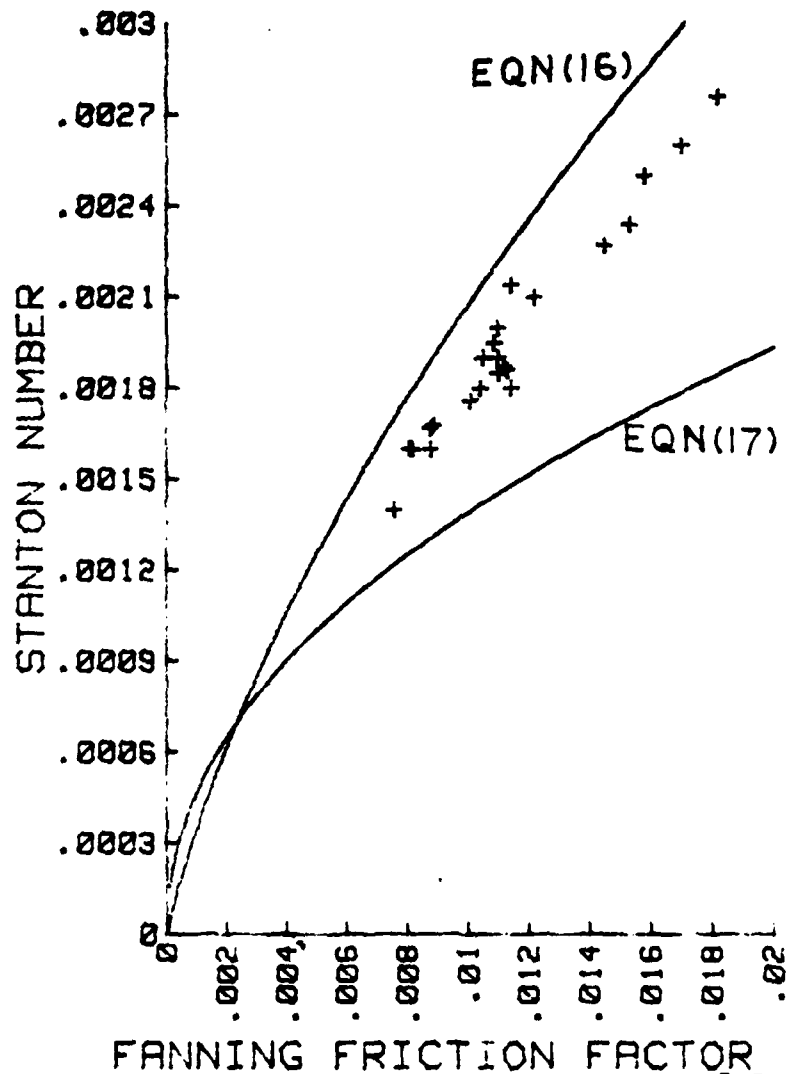
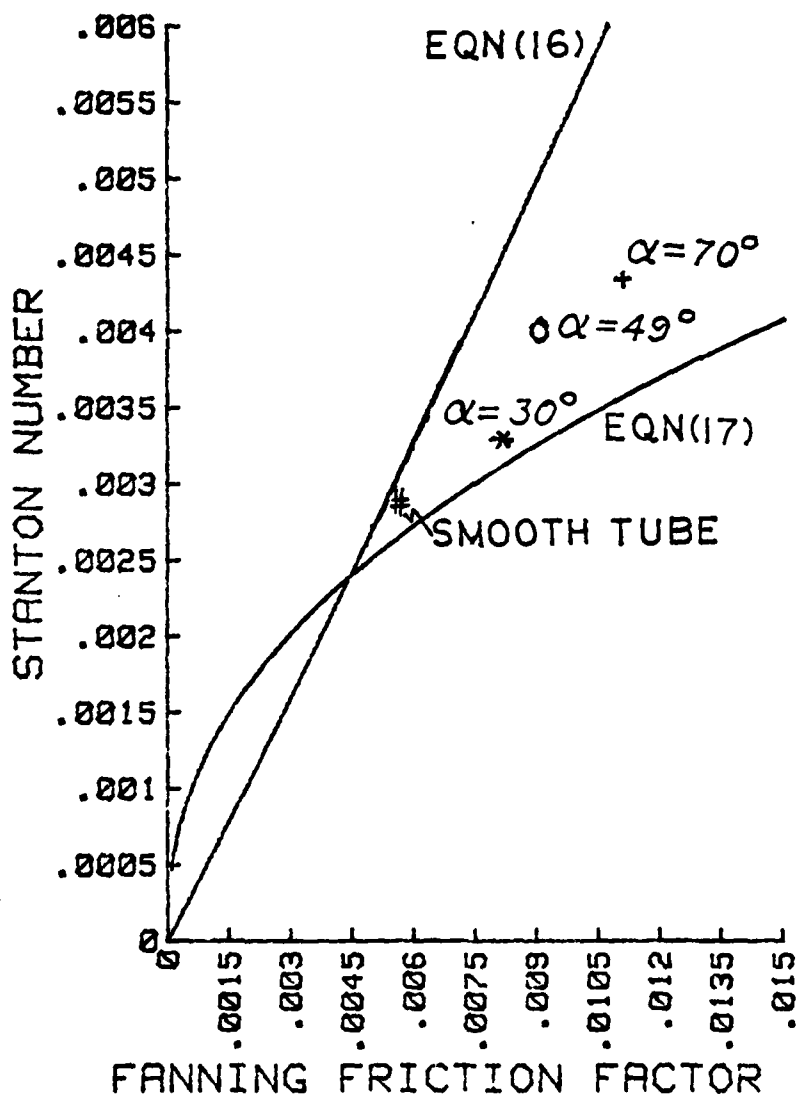


FIGURE 36 Experimental data of Webb, et al [4] compared to equations(16) and (17) for  $Pr = 5$  and  $Re = 40K$ .



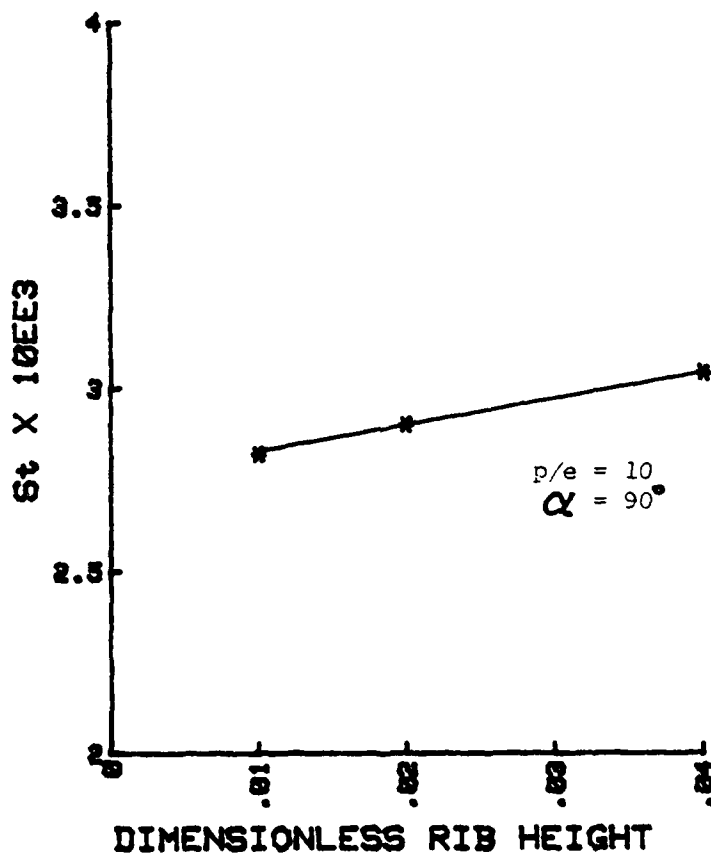
FANNING FRICTION FACTOR

FIGURE 37 Experimental data of Withers [13] compared to equations(16) and (17) for Pr = 5 and Re = 40K.



FANNING FRICTION FACTOR

FIGURE 38 Experimental data of Webb and Gee [3] compared to equations (16) and (17) for  $Pr = 0.71$  and  $Re = 40K$ .



**DIMENSIONLESS RIB HEIGHT**

FIGURE 39 Stanton number as a function of dimensionless rib height for a constant pitch-to-groove ratio and constant helix angle. From Webb, et al [4].

Figure 39 are for those tubes with a constant pitch-to-groove ratio of 10. Figure 39 clearly illustrates that the Stanton number increases with increasing dimensionless rib height. This increase is due to the increased heat transfer area that accompanies increased rib height and, more importantly, the effects of flow separation and increased turbulence that also accompanies increased rib height. Figure 40, also from Table VI, shows Stanton number as a function of the pitch-to-groove ratio for a constant dimensionless rib height of 0.02. Figure 40 illustrates the decrease in heat transfer as pitch-to-groove ratio increases. This decrease is due to the decreased surface area available for heat transfer and, more importantly, the decreased turbulence when the ribs are spaced further apart.

Figure 41 shows the data of Gee and Webb [3] from Table V. In Figure 41, Stanton number is plotted as a function of helix angle for a constant dimensionless rib height of 0.01 and a constant pitch-to-groove ratio of 15. Figure 41 illustrates the increase in heat transfer coefficient for the increase in helix angle. The increased helix angle increases the heat transfer of the ribbed tube by increasing the turbulence in the flow.

Figures 39, 40, and 41 indicate that any relation for heat transfer coefficient must contain explicit functional relationships for the relevant geometrical parameters (dimensionless rib height, pitch-to-groove ratio, helix angle).

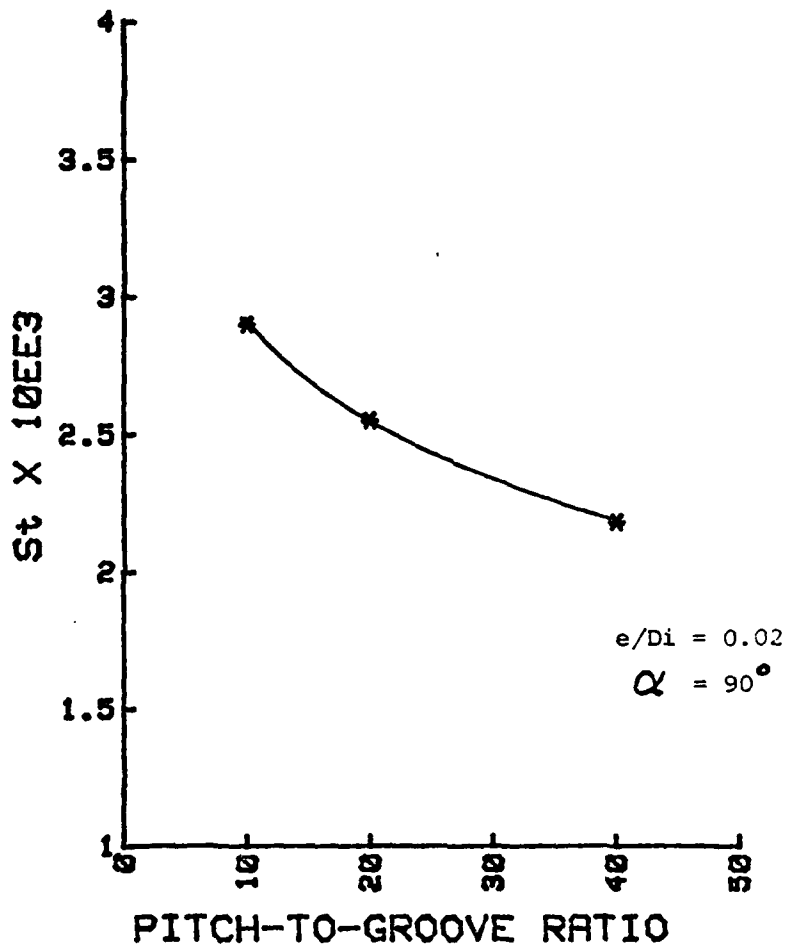


FIGURE 40 Stanton number as a function of pitch-to-groove ratio for constant dimensionless rib height and constant helix angle. From Webb, et al [4].

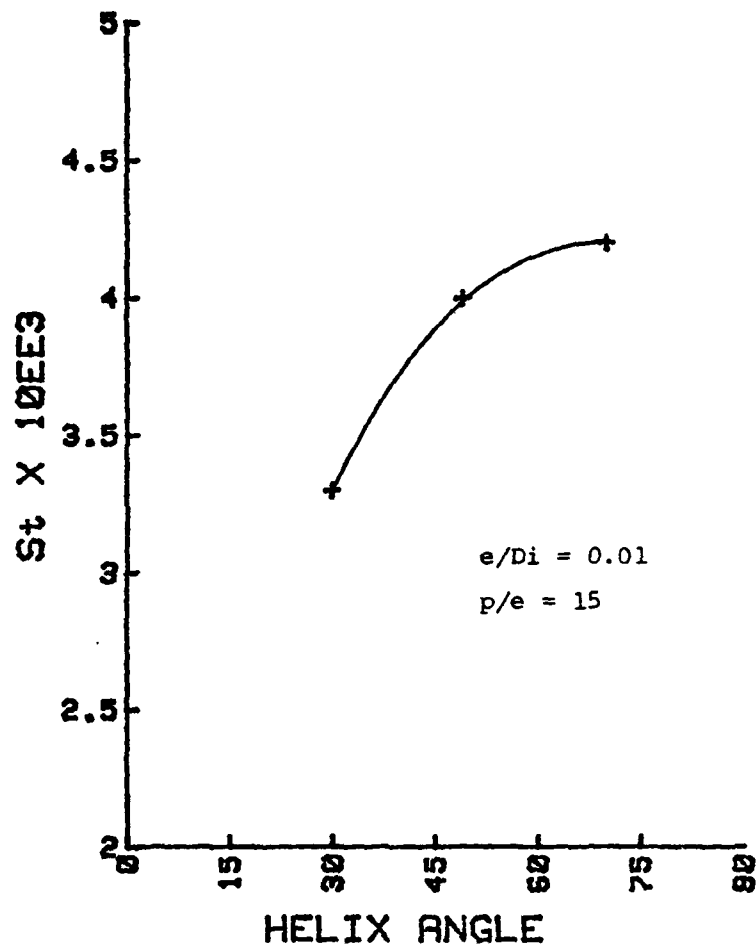


FIGURE 41 Stanton number as a function of helix angle for constant dimensionless rib height and constant pitch-to-groove ratio. From Webb and Gee [3].

### 3. Comparison of Empirical Relations to Existing Data

The comparisons of empirical relations to existing data for heat transfer coefficient are conducted on the previously stated premise that the friction factor is accurately known. For the analysis of this section, the friction factor used in the empirical relations for Stanton number is the experimentally obtained friction factor from the original author.

Equation (19) from Webb, et al [4] was used to calculate the Stanton number for the tubes studied by Gee and Webb [3], for  $Pr = 0.71$  and  $Re = 40K$ . Figure 42 shows the comparison of the experimental data to the predicted value. For the internally ribbed tubes of Gee and Webb [3], equation (19) predicts the heat transfer coefficient within 15%.

Figure 43 compares the experimental data of Carnavos [2] to the predictions of equation (19) at  $Pr = 5$  and  $Re = 40K$ . The error in predicted value of Stanton number for the Carnavos [2] tubes ranges from 0 to 40%. As seen in Figure 43 there is no discernible relation between the error of predicted value and experimental value attributable to dimensionless rib height. It should be noted that all the tubes studied by Carnavos [2] had either dimensionless rib heights greater than 0.05 or pitch-to-groove ratios less than 10.

Figure 44 compares the data of Withers [13] to the predictions of equation (19) for  $Pr = 5$  and  $Re = 40,000$ . For pitch-to-groove ratios less than 30, the error in predicted Stanton number varies from 15-40%, with the larger errors

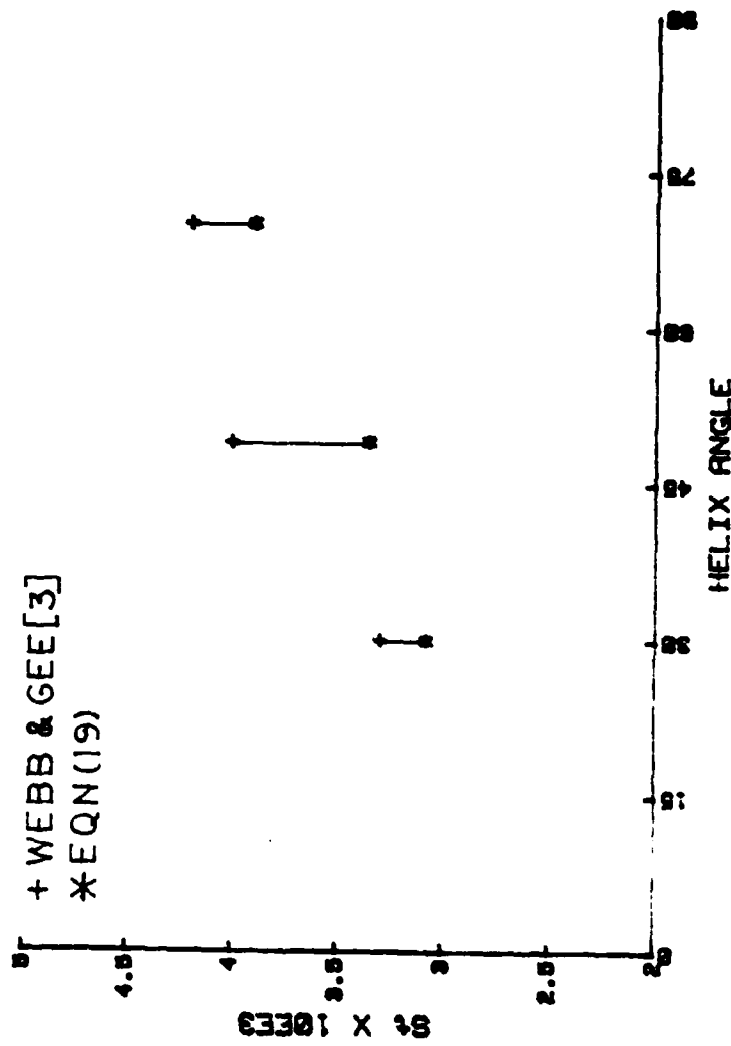


FIGURE 4. Experimental data of Webb and Gee [3] compared to predictions of equation (19).

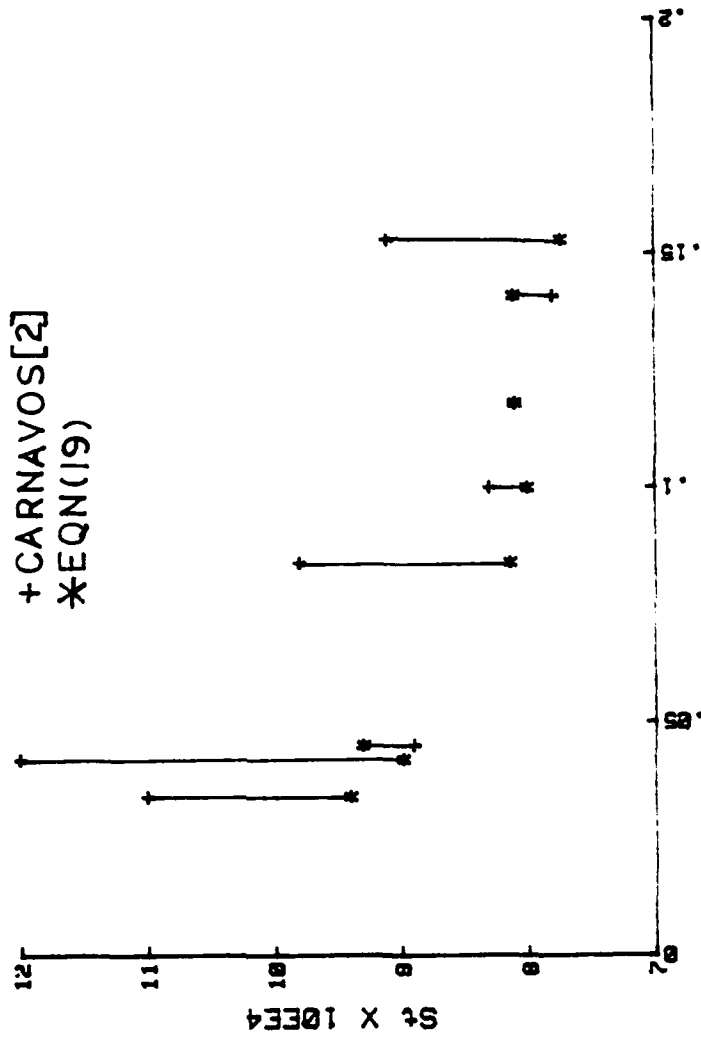


FIGURE 43 Experimental data of Carnavos [2] computed to the predictions of equation (19).

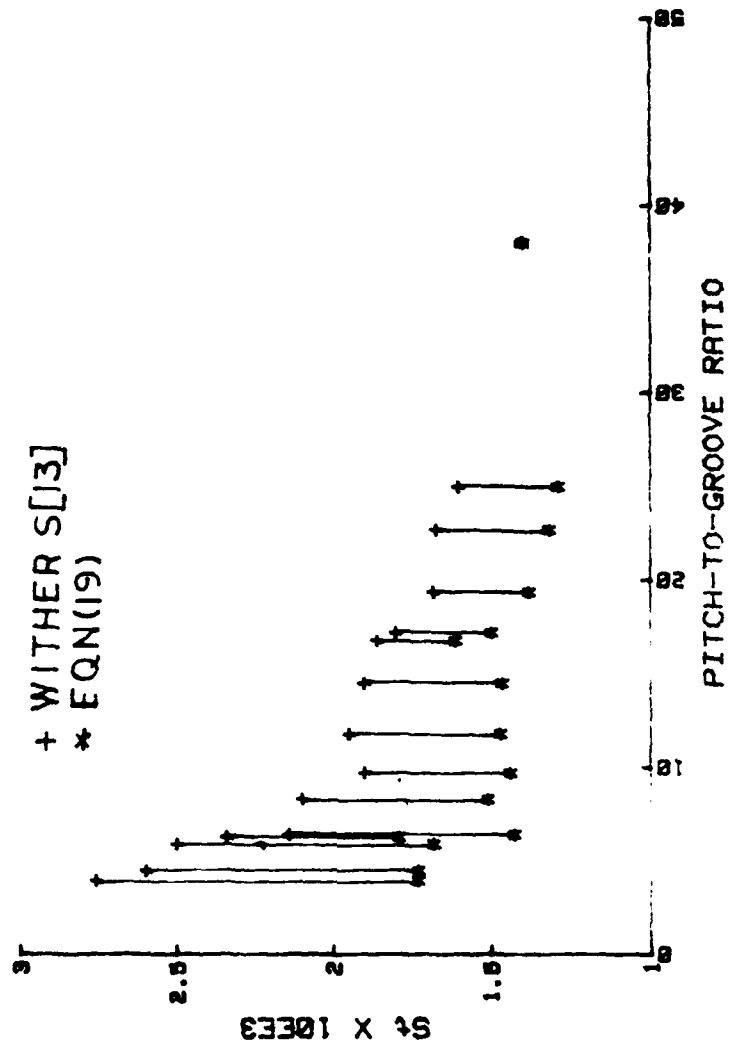
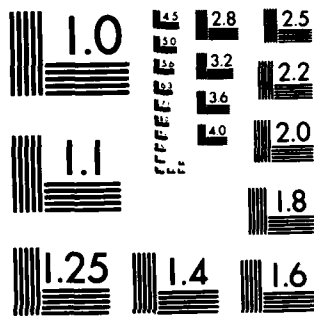


FIGURE 14. Experimental data of Withers [13] compared to the predictions of equation (19).





MICROCOPY RESOLUTION TEST CHART  
NATIONAL BUREAU OF STANDARDS-1963-A

associated with pitch-to-groove ratios less than 10. For pitch-to-groove ratios larger than 30, the error in predicted Stanton number is less than 10%.

Equation (22), derived from equation (20) and the experimental data of [3], was used to calculate heat transfer coefficients for comparison to the experimental data of Gee and Webb [3] at  $Pr = 0.71$  and  $Re = 40,000$ . Equation (22) correlated the Gee and Webb [3] data within 10%. Comparisons of the data of Carnavos [2], Webb et al [4] and Withers [13] to the predictions of equation (22) did not produce any correlation. The lack of correlation with the data of these other researchers is most probably due to equation (22) being derived from experimental data for air, and the subsequent loss of the explicit Prandtl number dependence, in deriving equation (22).

Equation (23) was not used for comparison purposes due to the lack of sufficient data to calculate  $Aa$  for the tubes of Gee and Webb [3], Webb et al [4], and Withers [13].

The data of Gee and Webb [3] from Table V was compared to the predictions of equation (24) from Withers [13] (see Figure 45). For  $Pr = 0.71$  and  $Re = 40,000$  the predictions of equation (24) are within 20% of the experimentally determined heat transfer coefficients. A comparison of the data of Webb et al [4] for a constant dimensionless rib height of 0.02 and a constant helix angle of 90 degrees with the predictions of equation (24) is shown in Figure 46. For a pitch-to-groove ratio of 10, the predictions of equation (24) are

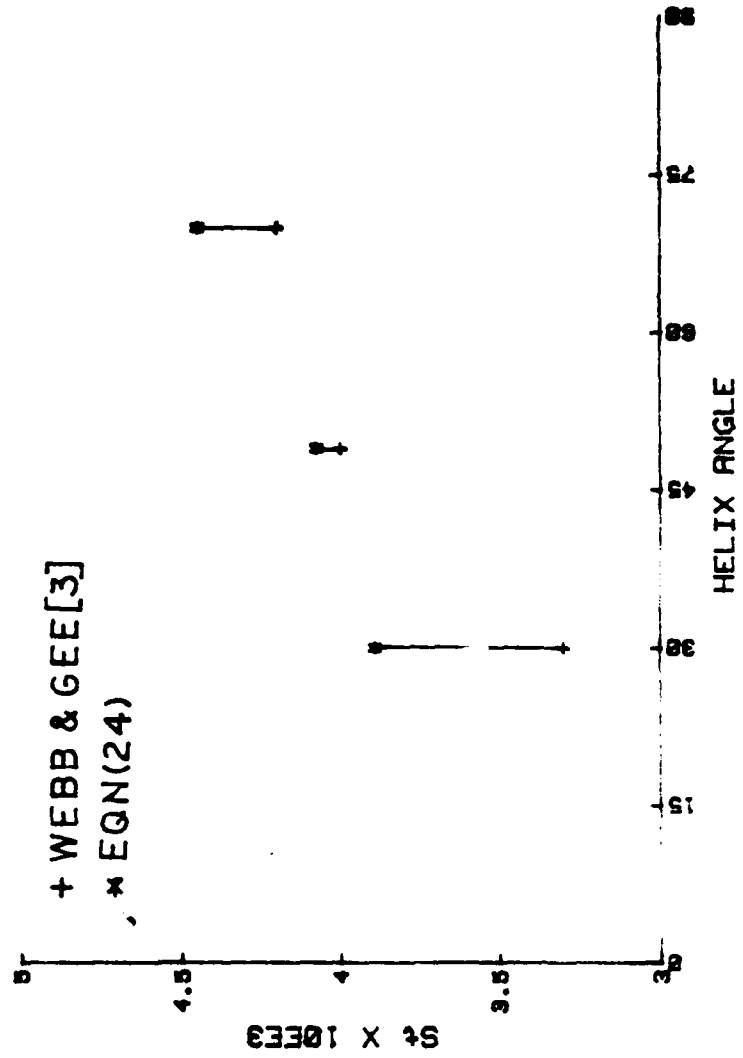


FIGURE 45. Experimental data of Webb and Gee [3] compared to  
 the predictions of equation (24).

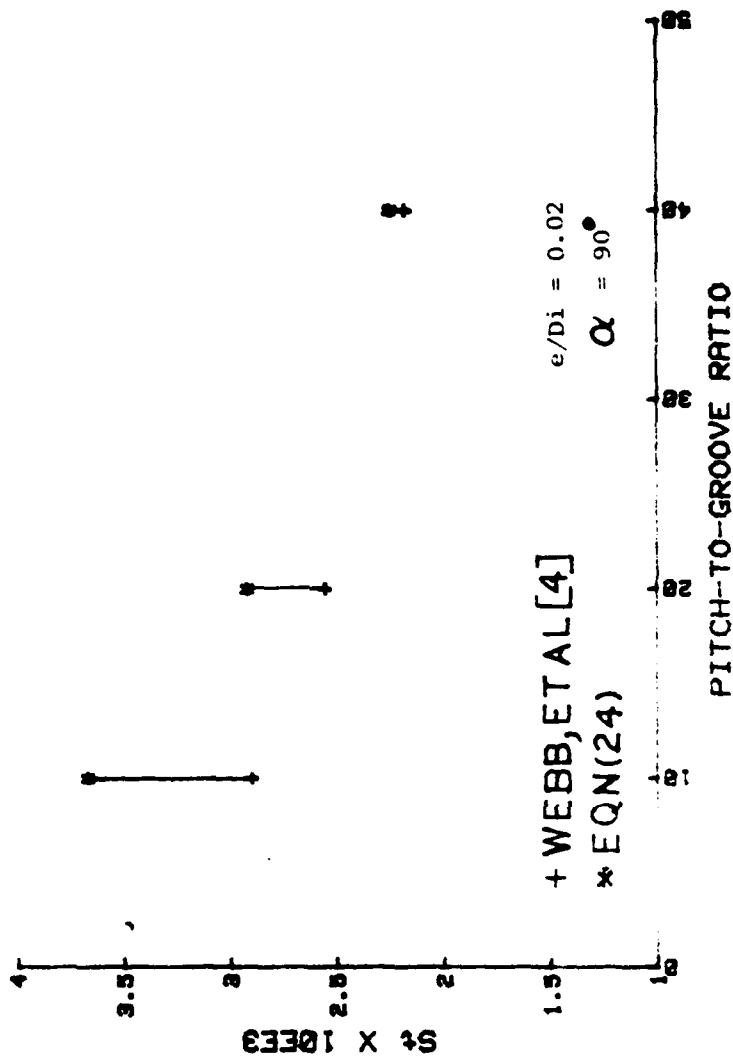


FIGURE 4. Experimental data of Webb, et al [4] compared to the predictions of equation (24).

approximately 25% high, but do improve for increasing pitch-to-groove ratios. For a constant pitch-to-groove ratio of 10, and a constant helix angle of 90 degrees, Figure 47 shows the data of Webb et al [4] for varying values of dimensionless rib height, compared to the predictions of equation (24). Figures 46 and 47 show that the error in heat transfer coefficient as predicted by equation (24) increases for increasing dimensionless rib height and decreasing pitch-to-groove ratio.

Comparison of the predictions of equation (24) to the data of Carnavos [2] showed large variations (as much as a factor of 3) and did not provide any further information.

#### 4. Summary

The application of a heat transfer similarity analysis, after Dipprey and Sabersky [19], is shown by several investigators to be a useful correlating method. The data of the individual investigators correlate well with the equations presented for their enhanced tubes. In some instances (see Figures 45 and 46), data from the studies of dissimilar tubes correlates well with the empirical relations of other investigators.

As was found in the application of the law of the wall analysis for friction factor, the heat transfer similarity analysis must include the effects of all the relevant parameters (dimensionless rib height, pitch-to-groove ratio, helix angle, and Prandtl number) to accurately predict the heat transfer coefficient for repeated-rib roughened tubes and internally, spirally ribbed tubes.

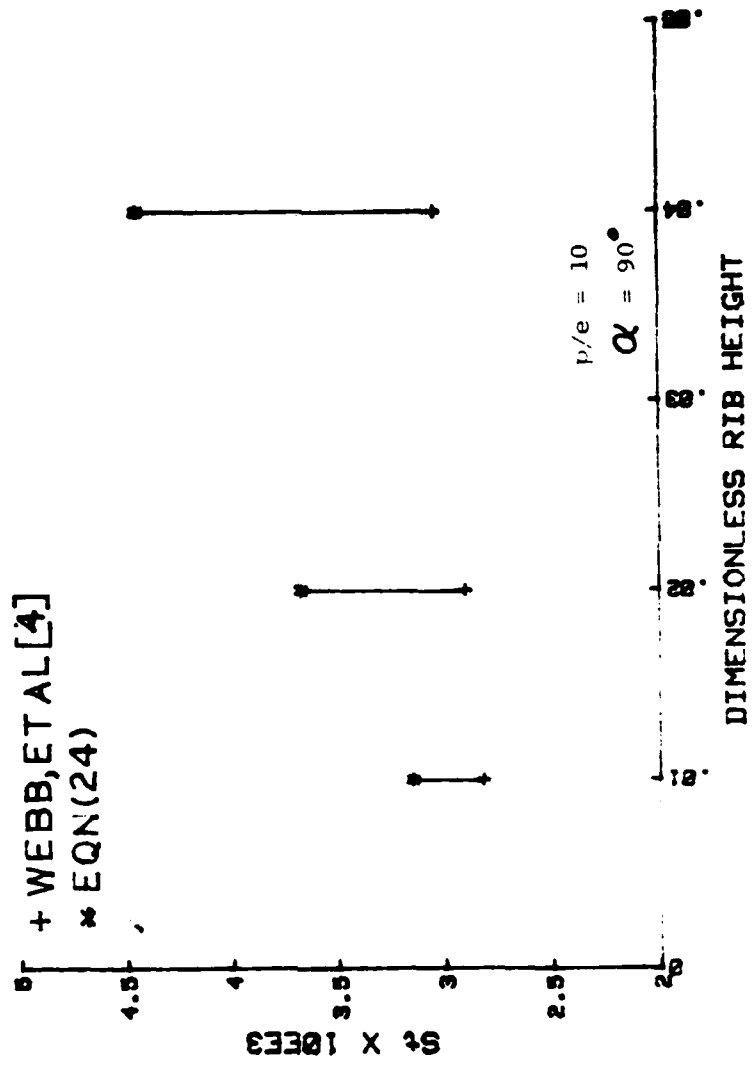


FIGURE 1. Experimental data of Webb, et al [4] compared to the predictions of equation (24).

Equation (22), derived for air ( $Pr = 0.71$ ), gives a very accurate prediction for the heat transfer coefficient with air as the working fluid. Its application to other Prandtl number fluids is still to be determined. Equation (20) from which equation (22) was formulated, could be of value if sufficient data were available to derive a relation similar to equation (22) for various tube geometries.

Equations (19) and (24) are limited in their application since neither contains all the relevant parameters affecting heat transfer performance. There is not sufficient data available for a given family of ribbed tubes to determine the effect of all the relevant parameters to allow modification of equations (19) and (22).

### C. SPIRALLY CORRUGATED TUBES

#### 1. Empirical Relations

Mehta and Rao [6] and Gupta and Rao [7] propose similar relations for the heat transfer coefficient as a function of the Prandtl number and the tube geometry.

$$Nu = 0.029e^{-16\theta} Re^{0.8} e^{25.5\theta} Pr^{0.4} \quad (25)$$

$$Nu = 0.029e^{-45\theta} Re^{0.8} e^{13\theta} Pr^{0.4} e^{13\theta} \quad (26)$$

Equation (25) from [6] and equation (26) from [7] both use the severity factor as the correlating parameter. The Prandtl number range for equation (25) was not specifically

stated, but it may be assumed to be representative of the Prandtl number range encountered in steam condensing applications with water as the tube-side fluid. The Prandtl number range for equation (26) is reported as  $5 < Pr < 82$ . This rather large range of Prandtl numbers is indicative of the variety of working fluids used in the experiments of Gupta and Rao [7].

For the single start, spirally corrugated tubes studied by Withers [12], the recommended empirical relation is:

$$St = \frac{\sqrt{f/2}}{7.22 (e/D_i)^{-1/3} (p/e)^{-1/3} Pr^{0.5} (e^+)^{0.127} - \gamma} \quad (27)$$

where:

$$\gamma = 2.5 \ln(2e/D_i) + 3.75$$

Comparison of equation (27) to equation (24) shows that the equations are the same in form, and use the same correlating parameters. The difference in the two equations is in the value of the constants and the exponents of the correlating parameters. These differences are to account for the two dissimilar geometries of the Korodense and Turbo-chil tubes. The Prandtl number range for equation (27) is reported as  $4 < Pr < 10$ .

Li, et al [16] propose an empirical relation for Stanton number as a function of the geometric parameters and physical parameters for the enhanced tube, including the helix angle dependence:

$$St = \frac{\sqrt{f/2}}{3.42 \ln(D_i/2e) - 4.64 + g^+} \quad (28)$$

where:

$$g^+ = 0.478(e/D_i)^{-0.621} (\alpha/90)^{-0.869} Pr^{0.57} (e^+) [0.641 + 0.105 \ln(e/D_i)]$$

The experiments of Li, et al [16] were conducted with water as the tube-side fluid ( $Pr = 5$ ).

It should be noted that equations (27) and (28), though not precisely of the form of equation (18), do reflect a dependency on  $e^+$  and the geometric characteristics of the corrugated tube.

## 2. Determination of the Effect of Relevant Parameters

Following the method of analysis used for ribbed tubes in Section III.B.2, the first determination to be made for spirally corrugated tubes is the applicability of the Prandtl analogy (equation (16)), and the Martinelli analogy (equation (17)).

Figures 48 and 49 compare the experimental data of Withers [12] and Li, et al [16] to both equations (16) and (17) for  $Pr = 5$  and  $Re = 40,000$ . In neither case do the experimental data correlate well with the analogies. A similar comparison to the data of Mehta and Rao [6] and Gupta and Rao [7] produced no correlation.

Figure 50 is a plot of data taken from Table XIV for the tubes studied by Li, et al [16] for single-start corrugated

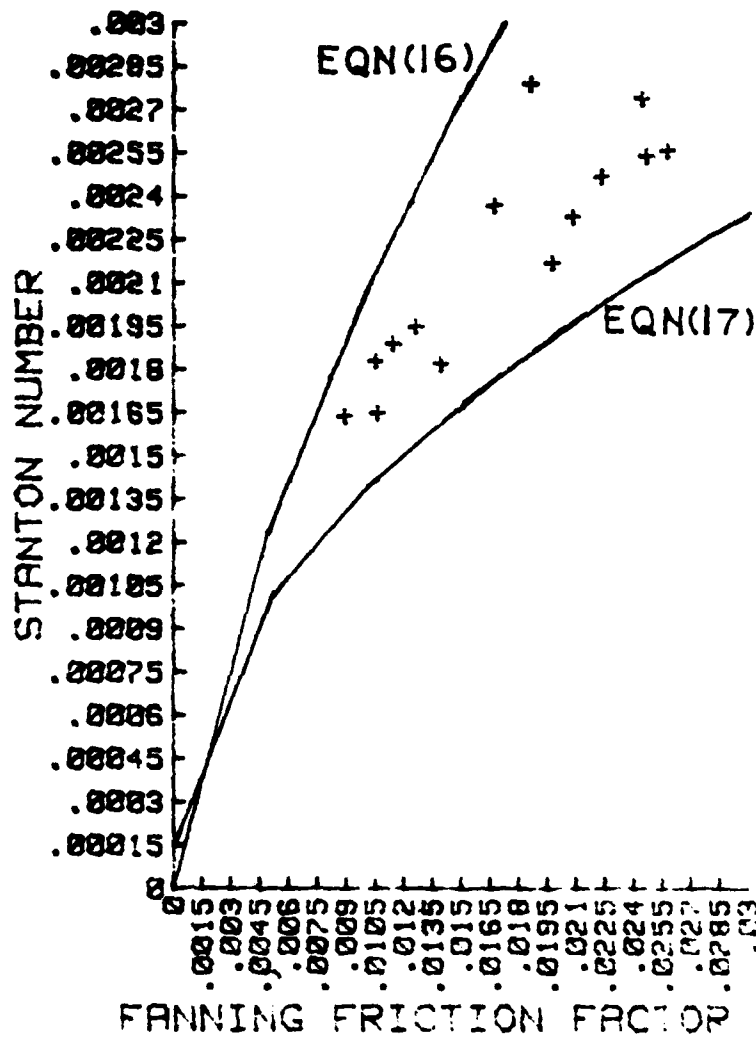


FIGURE 48 Experimental data of Withers [12] compared to equations (16) and (17) for  $Pr=5$  and  $Re = 40K$ .

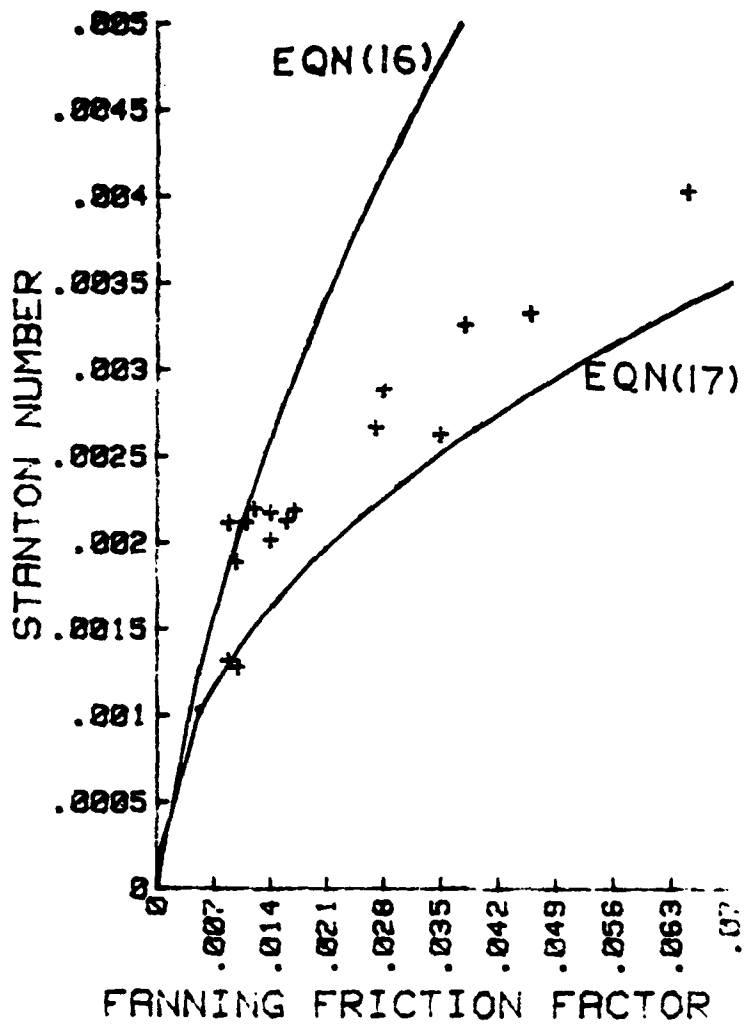


FIGURE 49 Experimental data of Li, et al [16] compared to equations (16) and (17) for  $Pr = 5$  and  $Re = 40K$ .

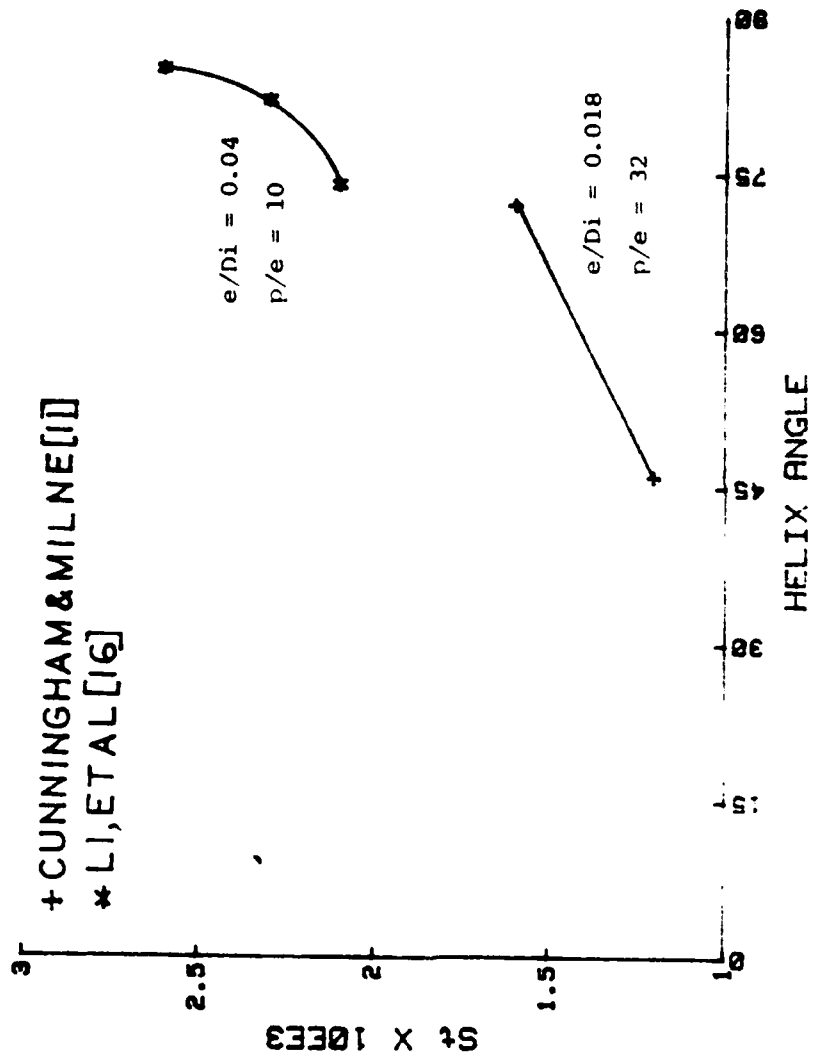


FIGURE 50 Stanton number as a function of helix angle for constant dimensionless groove depths and constant pitch-to-groove ratios.

tubes with pitch-to-groove ratios of 10 and dimensionless groove depths of 0.04, and data taken from Table XII for the tubes studied by Cunningham and Milne [11] for multiple-start corrugated tubes with pitch-to-groove ratios of 32 and dimensionless groove depths of 0.018. Figure 50 illustrates that for a constant pitch-to-groove ratio and a constant dimensionless groove depth, Stanton number increases with increasing helix angle. This increase in Stanton number may be attributed to the increased turbulence caused by the groove becoming closer to a transverse position to the flow.

Figure 51 plots data taken from Tables XII and XIII for single start tubes of Gupta and Rao [7] for a constant pitch-to-groove ratio of 20 and a helix angle that is essentially constant ( $80 \text{ degrees} \pm 3 \text{ degrees}$ ). Figure 51 illustrates the increase in Stanton number for increasing dimensionless groove depth. This increase in Stanton number is most likely due to the increased separation that occurs with an increase in groove depth(s).

For single-start tubes, insufficient data are available for a family of tubes to make an accurate determination of the effect of pitch-to-groove ratio on the heat transfer coefficient as a function of the pitch-to-groove ratio. By comparison of the semi-circular profile of the ribs of the Withers [13] tubes to the profile of a spirally corrugated tube groove, a representative comparison may be made, however. Using the data of Table XIII from Withers [13] for multiple-start

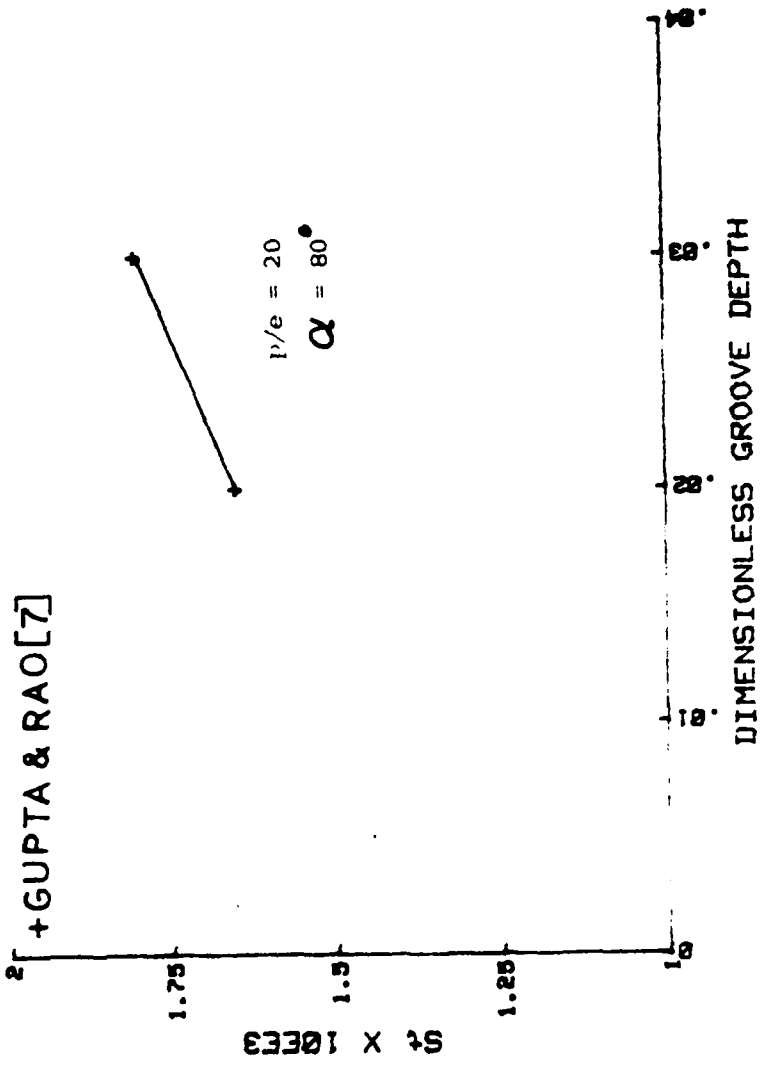


FIGURE 54. Relation number of a function of dimensionless groove depth for constant pitch-to-groove ratio and constant helix angle.

tubes (internally ribbed), Figure 52 shows a decrease in Stanton number for an increase in pitch-to-groove ratio, at a constant helix angle of approximately 45 degrees and a constant dimensionless groove depth of 0.03.

Examination of Figures 50, 51, and 52 show that the relevant parameters for spirally corrugated tubes are the same as the relevant parameters for the internally spirally ribbed tubes and the repeated-rib roughened tubes.

### 3. Comparison of Empirical Relations to Existing Data

The empirical relations of Mehta and Rao [6] and Gupta and Rao [7] were not used for comparison to the data of Withers [12] and Li, et al [16]. As was demonstrated in the thorough examination of the severity factor as a correlating parameter for friction factor, the use of the severity factor as the single correlating parameter is very limited in that the severity factor reflects an arbitrary combination of the dimensionless groove depth and pitch-to-groove ratio, and does not reflect the influence of the helix angle. Additionally, the severity factor is only marginally successful in correlating data in a very narrow range of values of severity factor.

The comparisons of empirical relations to existing data for spirally corrugated tubes will be conducted also on the basis that the friction factor is accurately known for use in the empirical relation.

Figure 53 compares the experimental data of Li, et al [16] to the predictions of equation (27) from Withers [12].

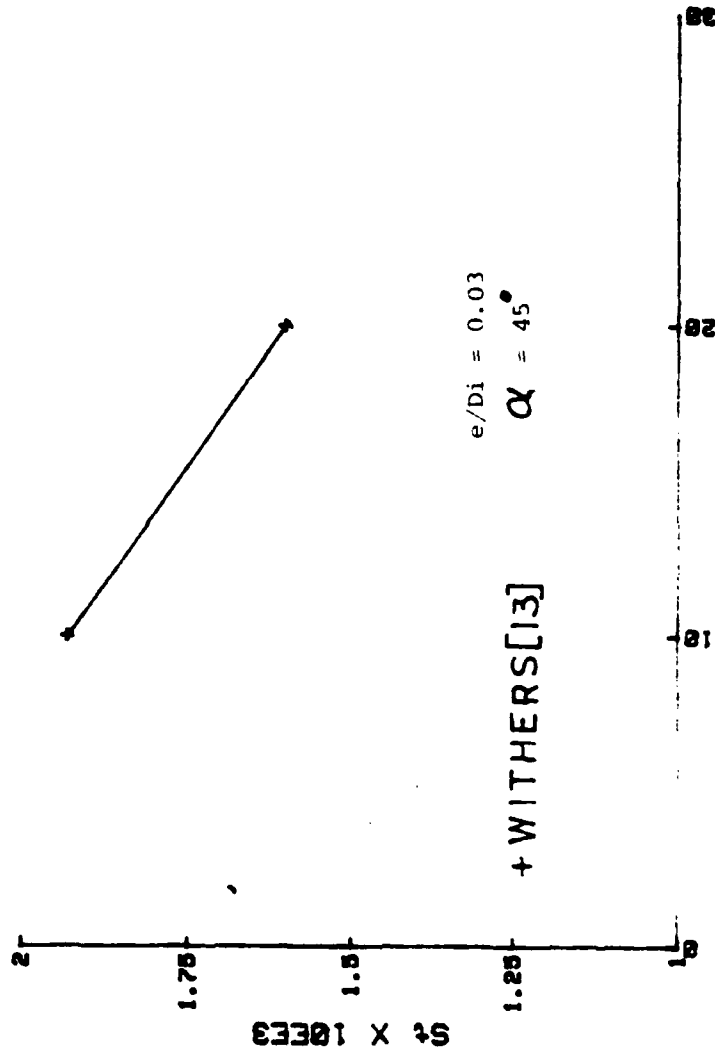


FIGURE 5. Stanton number as a function of pitch-to-groove ratio for constant helix angle and constant dimensionless groove depth.

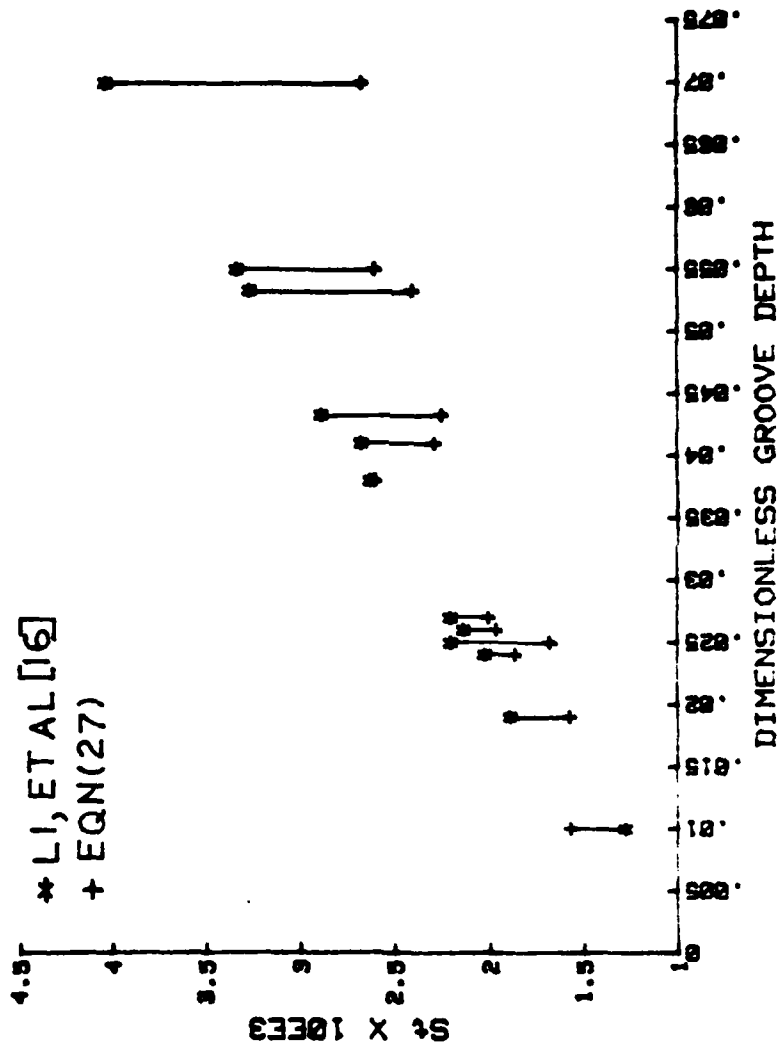


FIGURE 53 comparison of experimental data of Li, et al [16] to the predictions of equation (27) from Withers [12].

In Figure 53 the point-by-point comparison is plotted for Stanton number as a function of the dimensionless groove depth at  $Pr = 5$  and  $Re = 40K$ . As can be seen in Figure 53, for dimensionless groove depths less than 0.05, equation (27) predicts the heat transfer coefficient within 25%. It is noted that the dimensionless groove depths less than 0.05 correspond to tubes with pitch-to-groove ratios greater than 10. For dimensionless groove depths greater than 0.05 (corresponding to pitch-to-groove ratios less than 10) the error between predicted and observed values of heat transfer coefficient increases to approximately 50%. Note also that prediction errors decrease as the dimensionless groove depth decreases.

Figure 54 shows the data of Withers [12] compared to the predictions of equation (28) from Li, et al [16]. In Figure 54, 11 of the 14 data points correlate within 15%, with 9 of the 14 data points correlating within 10%. The 3 remaining data points correlate by 37%, 23%, and 20% for dimensionless groove depths of 0.052, 0.047, and 0.043 respectively.

#### 4. Summary

The heat transfer similarity analysis, after Dipprey and Sabersky [19], as applied by Withers [12] and Li, et al [16] produces very good correlation to experimental data. The reader is cautioned, however, that the data of Withers [12] and Li, et al [16] for single start corrugated tubes

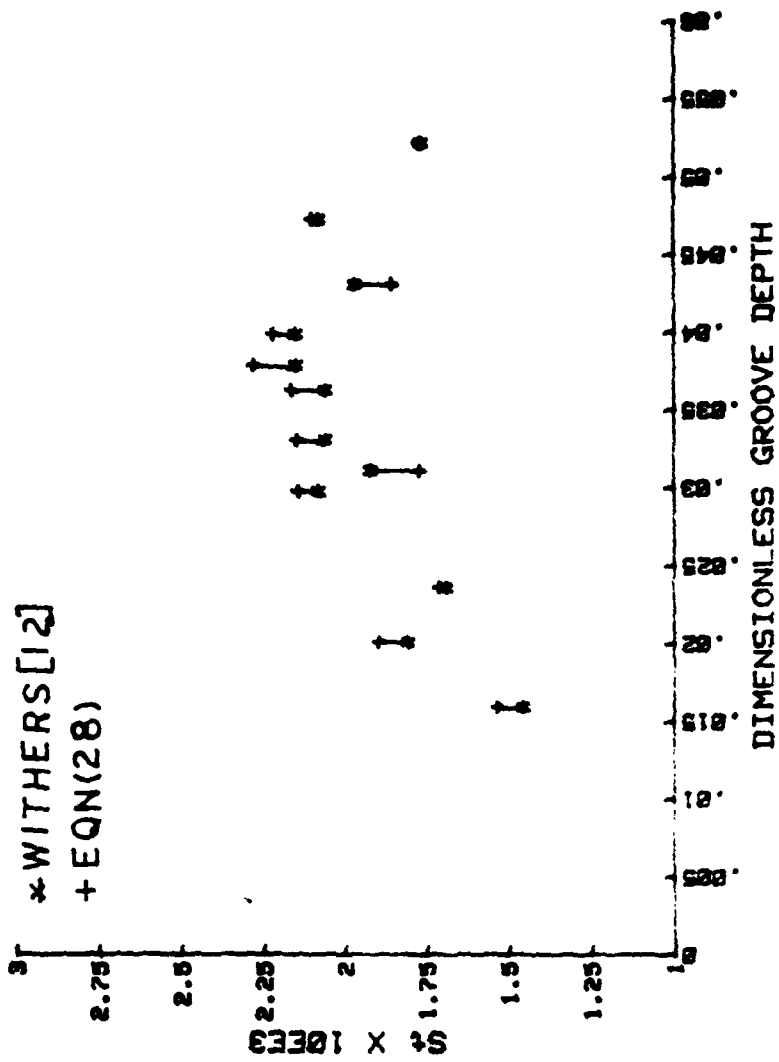


FIGURE 3. Comparison of the experimental data of Withers [12] to the predictions of equation (28) from Li, et al [16].

are within a somewhat narrow band of helix angles (see Tables IX and X ). The range of helix angles is  $72 < \alpha < 88$ .

Equation (27) correlates data from Li, et al [16] with some accuracy, but does not include a functional relation for the effects of helix angle. Equation (28) is more accurate in the prediction of heat transfer coefficient, and explicitly relates Stanton number to helix angle.

Equation (28) is recommended as an empirical relation for Stanton number as a function of the relevant physical parameters (Prandtl number, Reynolds number) and the relevant geometric parameters (dimensionless groove depth, pitch-to-groove ratio, helix angle). The reader is cautioned that equation (28) will not accurately predict the heat transfer coefficient for dimensionless groove depths greater than 0.05 and/or pitch-to-groove ratios less than 10.

#### IV. CONCLUSION AND RECOMMENDATIONS

##### A. CONCLUSION

Equation (14) for friction factor was substituted into equation (28) for Stanton number and the resulting relation was used to calculate Stanton number for single-start and multiple-start spirally corrugated tubes. Figure 55 plots the Stanton number as calculated by equation (28) vs. the experimentally obtained Stanton number. The dashed lines represent  $\pm 15\%$  of the experimentally obtained Stanton number. As seen in Figure 55, all the predicted Stanton numbers with the exception of those for the Cunningham and Milne [11] tubes are within  $\pm 15\%$  of the experimental values.

The data points shown in Figure 55 are for those tubes with pitch-to-groove ratios greater than 10 and dimensionless groove depths less than 0.05. The calculated Stanton numbers for the spirally corrugated tubes and the internally ribbed tubes with geometric parameters outside these stated limits did not correlate.

Figure 56 from [4] provides a graphic illustration of the influence of the pitch-to-groove ratio on the fluid flow pattern in a repeated-rib roughened tube. For pitch-to-groove ratios greater than 10, the boundary layer disturbed by the rib becomes re-attached to the tube wall, thereby increasing heat transfer with the increased turbulence. For

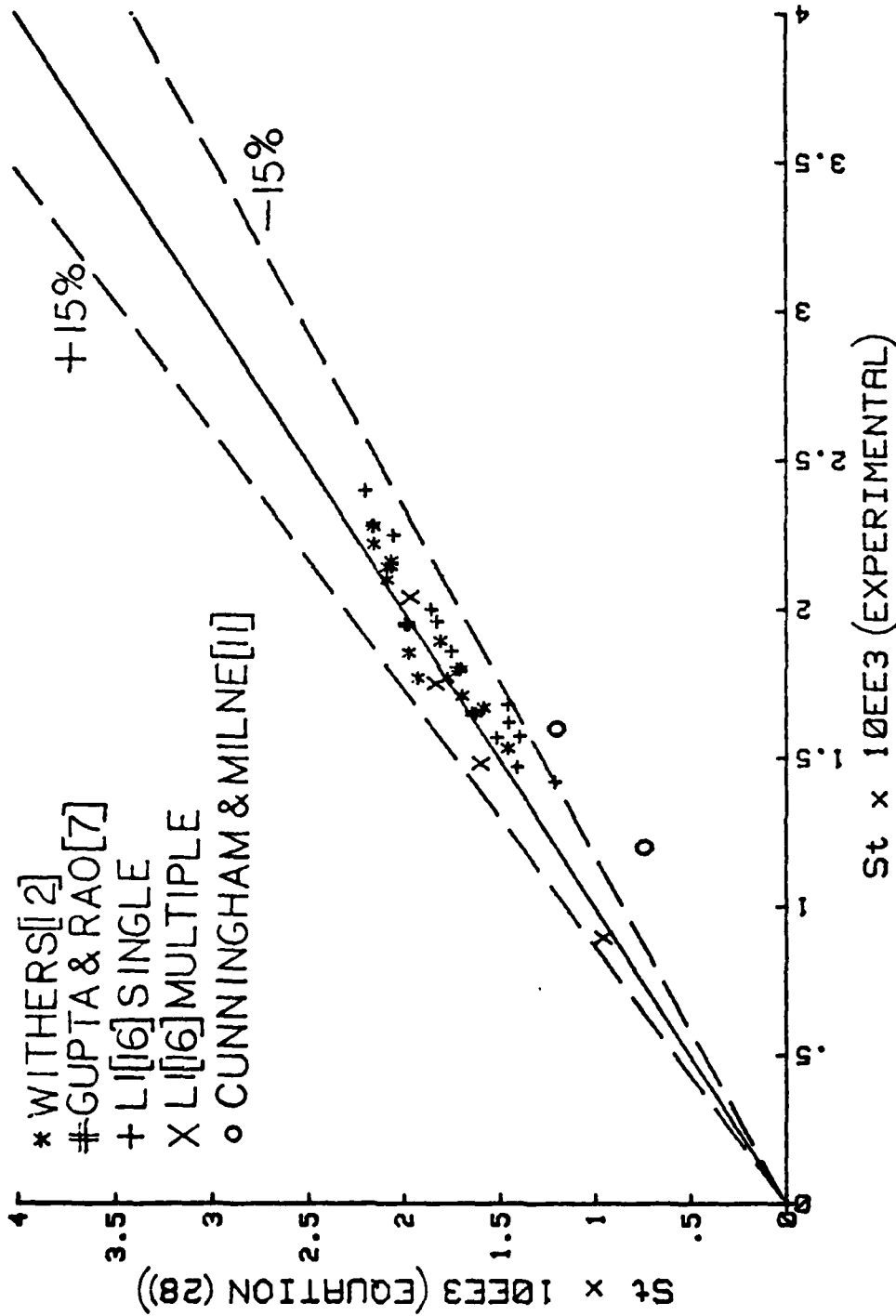


FIGURE 55 Stanton number as calculated from equation (28) compared to experimental data for single-start and multiple-start spirally corrugated tubes.

Ref	$p/e$	Flow pattern
[15]	$\rightarrow \infty$	
[16]	10	
[6]	8	
[6] [7]	5	
[6] [7]	2	
[6] [8]	0.75- 1.25	

FIGURE 56 Flow patterns as a function of pitch-to-groove ratio. From [4]. Bracketed reference numbers refer to references contained in [4].

pitch-to-groove ratios less than 8, boundary layer re-attachment is inhibited, decreasing heat transfer [4].

#### B. RECOMMENDATIONS

Equations (14) and (28) are recommended as empirical relations for the friction factor and Stanton number for single-start and multiple-start spirally corrugated tubes for the following conditions:

- 1)  $e/D_i < 0.05$ ,
- 2)  $p/e > 10$ ,
- 3)  $10,000 \leq Re \leq 80,000$ ,
- 4)  $0.71 \leq Pr \leq 10$ , and
- 5)  $35 \leq \alpha \leq 85$ .

What remains to be accomplished is two-fold:

- 1) More experimental data are needed for specific families of tubes. An experimental program must be well-planned to include a family of tubes with the pitch-to-groove ratio and the dimensionless groove depth constant for the family while the helix angle is varied by varying the number of groove starts. An additional family of tubes that are geometrically similar to the first family must then be investigated with the helix angle held constant and the pitch-to-groove ratio constant, while varying the dimensionless groove depth. The third set of data must be from another family of geometrically similar tubes with the helix angle held constant, the dimensionless groove depth constant,

while varying the pitch-to-groove ratio. This complete set of experimental data for geometrically similar families of tubes will allow more thorough examination of the exponent for the helix angle term in equation (28) and the refinement of the constants and exponents of the functional relationship terms for pitch-to-groove ratio and dimensionless groove depth in equation (28).

2) Equations (14) and (28) must be applied to an optimization routine to determine the best condenser tube. The optimization must be concerned with one of the three design criteria [4]:

- a) for a constant heat load and constant pumping power, minimize surface area, or
- b) for a constant heat load and constant surface area, minimize pumping power, or
- c) for a constant pumping power and constant surface area, maximize heat transfer.

An additional research area that must accompany the ongoing research in the tube-side performance characteristics is research into the enhancement benefits on the shell-side of the condenser, as may be found with the Turbo-chil tube (Figure 6.b).

### LIST OF REFERENCES

1. Bergles, A.E., Bibliography on Augmentation of Convective Heat and Mass Transfer, Report HTL-19 ISU-ERI-AMES-79206, DOE Contract EG-78-S-02-4649, 1979.
2. Carnavos, T.C., "Heat Transfer Performance of Internally Finned Tubes in Turbulent Flow," Advances in Heat Transfer, ASME, New York, 1979.
3. Gee, D.L., and Webb, R.L., "Forced Convection in Helically Rib-roughened Tubes," Int. Journal of Heat and Mass Transfer, Vol. 23, pp. 1127-1136, 1980.
4. Webb, R.L., et al., "Heat Transfer and Friction in Tubes with Repeated-rib Roughness," Int. Journal of Heat and Mass Transfer, Vol. 14, pp. 601-617, 1971.
5. Han, J.C., et al., "An Investigation of Heat Transfer and Friction for Rib-roughened Surfaces," Int. Journal of Heat and Mass Transfer, Vol. 21, pp. 1143-1156, 1978.
6. Mehta, M.H. and Rao, M.R., "Heat Transfer and Frictional Characteristics of Spirally Enhanced Tubes for Horizontal Condensers," Advances in Heat Transfer, ASME, New York, 1979.
7. Gupta, P.K. and Rao, M.R., "Heat Transfer and Friction Characteristics of Newtonian and Power-law Type of Non-Newtonian Fluids in Smooth and Spirally Corrugated Tubes," Advances in Heat Transfer, ASME, New York, 1979.
8. Le Rue, J.C., et al., Fluid Mechanics and Heat Transfer, Spirally Fluted Tubing, ONR CA-A16541, Contract N00014-79-C-0773, General Atomic Company, 1981.
9. Catchpole, J.P., and Drew, B.C.H., "Evaluation of Some Shaped Tubes for Steam Condensers," Steam Turbine Condenser, NEL Report 619, pp. 66-82, 1976.
10. Bergles, A.E., Heat Transfer Characteristics of Turbotec Tubing, HTL-24, ISU-ERI-AMES-81018, Project 1477, Iowa State University, Ames, Iowa, 1980.
11. Cunningham, J. and Milne, H.K., "The Effect of Helix Angle on the Performance of Roped Tubes," Proceedings of the Sixth International Heat Transfer Conference, Vol. 2, Toronto, 1978.

12. Withers, J.G., "Tube-side Heat Transfer and Pressure Drop for Tubes Having Internal Helical Ridging with Turbulent/Transitional Flow of Single-phase Fluid: Part 1--Single-helix Ridging," Heat Transfer Engineering, Vol. 2, No. 1, 1980.
13. Withers, J.G., "Tube-side Heat Transfer and Pressure Drop for Tubes Having Helical Internal Ridging with Turbulent/Transitional Flow of Single-phase Fluid: Part 2--Multiple-helix Ridging," Heat Transfer Engineering, Vol. 2, No. 2, 1980.
14. Marto, P.J., et al, "An Experimental Comparison of Enhanced Heat Transfer Condenser Tubing," Advances in Heat Transfer, ASME, New York, 1979.
15. Newson, I.H. and Hodgson, T.K., "The Development of Enhanced Heat Transfer Condenser Tubing," Fourth International Symposium on Fresh Water from the Sea, Vol. 1, pp. 69-94, Athens, 1973.
16. Li, H.M., et al, "Investigation on Tube-side Flow Visualization, Friction Factors, and Heat Transfer Characteristics of Helical Ridging Tubes," Seventh International Heat Transfer Conference, Munich, 1982.
17. Nikuradse, J., "Laws of Flow in Rough Pipes," VDI Forsch., 361 (1933). English Translation NACA TM-1292, 1965.
18. Schlichting, H., Boundary Layer Theory, Seventh Edition, McGraw-Hill, 1979.
19. Dipprey, D.F. and Sabersky, R.H., "Heat and Momentum Transfer in Smooth and Rough Tubes at Various Prandtl Numbers," Int. Journal of Heat and Mass Transfer, Vol. 6, pp. 329-353, 1963.
20. Reynolds, O., Transactions of The Royal Society, 174A:935, London, 1883.
21. Prandtl, L., Physik, 11:1072 (1910).
22. Martinelli, R.C., "Heat Transfer to Molten Metals," Trans. ASME, 69, 947, 1947.
23. Carnavos, T.C., "Some Recent Developments in Augmented Heat Exchanger Elements," Heat Exchangers: Design and Theory Sourcebook, N. Afgan and E.U. Schlunder eds., McGraw-Hill, 1974.
24. Withers, J.G., et al, United States Patent No. 3,847,212, Nov. 12, 1974.

25. Withers, J.G., United States Patent No. 4,007,774,  
February 15, 1977.

INITIAL DISTRIBUTION LIST

	No. Copies
1. Defense Technical Information Center Cameron Station Alexandria, Virginia 22314	2
2. Library, Code 0142 Naval Postgraduate School Monterey, California 93940	2
3. Department Chairman, Code 69 Department of Mechanical Engineering Naval Postgraduate School Monterey, California 93940	1
4. Professor Paul J. Marto, Code 69Mx Department of Mechanical Engineering Naval Postgraduate School Monterey, California 93940	5
5. Professor R.H. Nunn, Code 69Nn Department of Mechanical Engineering Naval Postgraduate School Monterey, California 93940	1
6. Professor M.D. Kelleher, Code 69Kk Department of Mechanical Engineering Naval Postgraduate School Monterey, California 93940	1
7. Mr. R.W. Kornbau Code 2721 David Taylor Naval Ship Research and Development Center Bethesda, Maryland 20084	1
8. Dr. D. Knauss Code 2721 David Taylor Naval Ship Research and Development Center Bethesda, Maryland 20084	1
9. LCDR R.K. Alexander 3710 Heather Ct. Alexandria, Virginia 22310	2
10. Mr. M. Keith Ellingsworth Materials and Mechanics Branch Office of Naval Research Arlington, Virginia 22217	1

**DAT  
FILM**